AD NUMBER

ADB096851

LIMITATION CHANGES

TO:

Approved for public release; distribution is unlimited.

FROM:

**Distribution authorized to U.S. Gov't. agencies and their contractors;
Administrative/Operational Use; NOV 1985. Other requests shall be referred to Arnold Engineering Development Center, Arnold AFB, TN.**

AUTHORITY

AEDC/DO ltr dtd 6 Sep 1994

AEDC-TR-85-31

Spray Characteristics of Pyrophoric Flare Nozzles

W. K. McGregor and D. W. Roberds
Sverdrup Technology, Inc.

November 1985

Final Report for Period November 1982 – May 1983

ARNOLD ENGINEERING DEVELOPMENT CENTER
ARNOLD AIR FORCE STATION, TENNESSEE
AIR FORCE SYSTEMS COMMAND
UNITED STATES AIR FORCE

NOTICES

When U. S. Government drawings, specifications, or other data are used for any purpose other than a definitely related Government procurement operation, the Government thereby incurs no responsibility nor any obligation whatsoever, and the fact that the government may have formulated, furnished, or in any way supplied the said drawings, specifications, or other data, is not to be regarded by implication or otherwise, or in any manner licensing the holder or any other person or corporation, or conveying any rights or permission to manufacture, use, or sell any patented invention that may in any way be related thereto.

Qualified users may obtain copies of this report from the Defense Technical Information Center.

References to named commercial products in this report are not to be considered in any sense as an endorsement of the product by the United States Air Force or the Government.

APPROVAL STATEMENT

This report has been reviewed and approved.

Frank T. Tanji

FRANK T. TANJI, Captain, USAF
Directorate of Technology
Deputy for Operations

Approved for publication:

FOR THE COMMANDER

Lowell C. Keel

LOWELL C. KEEL, Lt Colonel, USAF
Director of Technology
Deputy for Operations

UNCLASSIFIED

SECURITY CLASSIFICATION OF THIS PAGE

REPORT DOCUMENTATION PAGE

1a. REPORT SECURITY CLASSIFICATION Unclassified	1b. RESTRICTIVE MARKINGS
2a. SECURITY CLASSIFICATION AUTHORITY	3. DISTRIBUTION/AVAILABILITY OF REPORT Distribution limited to U.S. Government agencies and their contractors; critical technology; November 1985.
2b. DECLASSIFICATION/DOWNGRADING SCHEDULE	
4. PERFORMING ORGANIZATION REPORT NUMBER(S) AEDC-TR-85-31	5. MONITORING ORGANIZATION REPORT NUMBER(S)
6a. NAME OF PERFORMING ORGANIZATION Arnold Engineering Development Center 6b. OFFICE SYMBOL (If applicable) DOP	7a. NAME OF MONITORING ORGANIZATION
6c. ADDRESS (City, State and ZIP Code) Air Force Systems Command Arnold Air Force Station, TN 37389-5000	7b. ADDRESS (City, State and ZIP Code)
8a. NAME OF FUNDING/SPONSORING ORGANIZATION Aeronautical Systems Div. 8b. OFFICE SYMBOL (If applicable) RWWS	9. PROCUREMENT INSTRUMENT IDENTIFICATION NUMBER
8c. ADDRESS (City, State and ZIP Code) Wright-Patterson Air Force Base, OH 45433	10 SOURCE OF FUNDING NOS PROGRAM ELEMENT NO: PROJECT NO: DA52EW TASK NO: WORK UNIT NO:
11. TITLE (Include Security Classification) Spray Characteristics of Pyrophoric	
12. PERSONAL AUTHOR(S) McGregor, W.K., and Roberds, D.W., Sverdrup Technology, Inc., AEDC Group	
13a. TYPE OF REPORT Final 13b. TIME COVERED FROM 11/82 TO 5/83	14 DATE OF REPORT (Yr., Mo., Day) 15. PAGE COUNT 87
16. SUPPLEMENTARY NOTATION Available in Defense Technical Information Center (DTIC).	

17. COSATI CODES		
FIELD	GROUP	SUB. GR
19	01	
17	05	

18. SUBJECT TERMS (Continue on reverse if necessary and identify by block number)
pyrophoric flares droplet size distributions
nozzle sprays
atomizers

19. ABSTRACT (Continue on reverse if necessary and identify by block number)

Liquid spray behavior was studied in a wind tunnel using a non-burning fuel simulant for a number of different types of nozzles suitable for use with air-dropped, pyrophoric flares. Droplet size distribution and the shape and spread rate of the nozzle spray were recorded under a range of flight speed, altitude, and nozzle parameters such as orifice size, fuel pressure and flow rate, and atomizing gas pressure and flow rate. A pulsed laser camera system was used to record photographs of the spray. The superiority of gas-atomizing (pneumatic) nozzles in producing fine droplets was confirmed, while no purely hydraulic nozzle stood out as offering special potential for engineering application.

20. DISTRIBUTION/AVAILABILITY OF ABSTRACT UNCLASSIFIED/UNLIMITED ☐ SAME AS RPT ☒ DTIC USERS ☐	21 ABSTRACT SECURITY CLASSIFICATION Unclassified
22a. NAME OF RESPONSIBLE INDIVIDUAL W.O. Cole	22b TELEPHONE NUMBER (Include Area Code) (615) 454-7813 22c OFFICE SYMBOL DOS

DD FORM 1473, 83 APR EDITION OF 1 JAN 73 IS OBSOLETE

UNCLASSIFIED

SECURITY CLASSIFICATION OF THIS PAGE

3. DISTRIBUTION/AVAILABILITY OF REPORT. Concluded.
Other requests for this document shall be referred to Arnold Engineering Development Center/DOS, Arnold Air Force Station, TN 37389-5000.

11. TITLE. Concluded.
Flare Nozzles

PREFACE

The work reported herein was conducted by the Arnold Engineering Development Center (AEDC), Air Force Systems Command (AFSC), from November 1982 through May 1983, at the request of the Aeronautical Systems Division (ASD/RWWS), Wright-Patterson AFB, Ohio. The results of the research were obtained by Sverdrup Technology, Inc., AEDC Group, operating contractor for propulsion testing at AEDC, AFSC, Arnold Air Force Station, Tennessee, under Project No. DA52EW. The AEDC/DOT project manager was Captain K. H. Leners. The manuscript was submitted for publication on March 25, 1985.

Those on the project team responsible for obtaining the data were R. A. Belz, D. B. Van Dyke, C. W. Brasier, H. C. Walker, D. G. Gardner, and V. A. Zaccardi.

CONTENTS

ILLUSTRATIONS

Figure Page

Figure Page

TABLES

APPENDIX

1.0 INTRODUCTION AND BACKGROUND

An experimental and analytical program to further the development of pyrophoric flares designed to be dropped from aircraft has been in progress since 1981 at Arnold Engineering Development Center (AEDC). Wind tunnel testing of flares at AEDC has included mapping the regions of flight conditions and flare fuel flow and temperature where spontaneous ignition of the fuel occurs when it is sprayed into the atmosphere through various types of nozzles. The fuel used has generally been 60/40 and 50/50 mixtures, by weight, of trimethylaluminum (TMA) and triethylaluminum (TEA). Where ignition occurred, the radiant intensity and spectral signatures were measured and recorded. The effect of different flare orientations with respect to the airstream was also observed.

The objective of the AEDC work has been to gain a basic understanding of the operation of pyrophoric flares to establish criteria to aid in their development. Analytical work has proceeded in developing a computer model of the combustion and radiation from the flare's wake.

It was found experimentally when using a simple, circular orifice nozzle that ignition occurred at higher altitudes when fuel temperature or air speed was increased, while increases in fuel flow rate or air temperature appeared to have only a secondary effect in improving ignition. Ignition was also improved when the fuel was finely atomized upon ejection from the flare by a "gas atomizing", (i.e., pneumatic) nozzle, one which uses gas pressure to break up the liquid flow.

The preliminary analytical model explains the observed effects of the various parameters on ignition. According to the model, ignition depends on the fuel being warmed enough to raise the vapor pressure and evaporate a sufficient amount of fuel into the vapor state. The vaporized fuel then produces a reacting mixture of fuel and oxygen having a combustion temperature high enough to produce a flame. The fuel may be pre-warmed in the flare canister, or it may be warmed by a surface reaction with oxygen after ejection from the flare body. If a surface reaction is to provide the fuel warming, it must be made as efficient as possible by having the fuel atomized into very fine droplets having a high surface area-to-volume ratio.

The model explains the occurrence of ignition of cold fuel in terms of at least some of the fuel being atomized into very fine droplets, either by the dynamic pressure of the airstream (greatest at low altitudes and high air speeds) or by nozzle gas pressure when a gas atomizing nozzle is used. Failure of ignition at high altitudes or low air velocities is attributed to insufficient atomization of the fuel.

An assumption made by the model in predicting ignition is that for the cases where airstream dynamic pressure must be relied upon to atomize the fuel, i.e., for simple hydraulic nozzles, droplet diameters are inversely proportional to ϱv^2, where ϱ is the air density and v is the free-stream velocity. By appropriately choosing values of certain constants, researchers can use the model to predict quite well whether or not ignition will occur for a given set of conditions. It has proved especially useful in providing a physical understanding of the process.

One of the recommendations resulting from the work at AEDC was that a study be made of nozzle injection phenomenology. Design criteria for an optimum nozzle had not been established. In tests, pneumatic nozzles failed to produce ignition under certain conditions and it was not clear why. Further, it was believed that a study of hydraulic nozzles might result in a design capable of providing the desired ignition of cold fuel at high altitude without resorting to a more complicated pneumatic atomizing nozzle. Different orifice sizes, fuel pressures, and flow rates to various nozzle types had not been investigated. One type of widely used hydraulic nozzle which had not been tested is the impinging jets nozzle, which uses liquid jets which impinge on each other just after exiting the nozzle to effect droplet break-up. Furthermore, it was desirable to test the analytical model's assumption that for hydraulic nozzles, the spray droplet diameters are inversely proportional to the dynamic airstream pressure, ϱv^2.

A study was undertaken in two phases for the Aeronautical Systems Division of Air Force Systems Command. In the first phase, conducted from February 9 to March 14, 1983 and covered by this report, n-butyl alcohol was used as a fuel simulant in non-burning studies of nozzle spray characteristics. N-butyl alcohol has a density, surface tension, and viscosity which closely approximate the values reported for mixtures of TMA and TEA (Ref. 1). Liquid droplet injection behavior was studied under a range of flight speed, altitude, and nozzle parameters such as orifice size, fuel pressure and flow rate, and atomizing gas pressure and flow rate.

The second phase, conducted from April 11 to 21, 1983, consisted of combustion testing of the best candidate nozzles using mixtures of TMA and TEA; the results are reported separately.

2.0 TEST FACILITY AND HARDWARE

2.1 TEST CELL AND FUEL INJECTION STRUT

The T-6 wind tunnel at AEDC (Fig. 1) was used to produce the flight velocities and simulated altitudes for these studies. It is capable of simulating altitudes as high as 50,000 ft

with refrigerated air at high subsonic velocities. The tunnel test section is 18 ft long and approximately 3 ft in diameter. A fuel injection strut shown in Fig. 2 carried the fuel (alcohol for the non-burning studies) to a candidate nozzle mounted in a simulated flare canister located on centerline of the tunnel, where fuel injection was normally pointed downstream in the same direction as the tunnel air flow. The strut could also be disconnected at the tunnel wall and turned so that the flare canister and nozzle could be pointed 90-deg to the tunnel air flow, as shown. The nozzle could also be mounted in the canister facing upstream so that fuel injection was 180 deg from the air flow direction.

A fuel delivery and conditioning system shown in simplified form in Fig. 3 pre-cooled the alcohol to approximately −20°C to increase its viscosity to a handbook value of approximately 10 centipoise, which represents the viscosity of the TMA/TEA mixtures at −55°C. The alcohol was injected under pressure of up to 500 psi in shots lasting up to 150 sec.

Wind tunnel total air temperature was set at about −20°C to prevent evaporation of the alcohol droplets. Computer calculations using a droplet evaporation model developed for spray coolers (Ref. 2) indicated evaporation would be significant at ambient air temperature but minimal if the air was kept cold. Experimental testing at warm (+15°) and then cold (−20°) temperatures verified the need for using cold air, with the single particle sizers counting a lower total number of droplets when the same flow rate of warm air was used, due to droplet evaporation.

2.2 NOZZLES

The following is a list and description of the candidate nozzles which were tested. Pressurized nitrogen was used as the atomizing gas in the pneumatic nozzles.

1. Single orifice, 0.025-in.-diam, 4.21 orifice length-to-diameter (ℓ/d) ratio. Figure 4 shows routing of fuel to this and the other single orifice nozzles.

2. Single orifice, 0.045-in.-diam, 4.21 ℓ/d.

3. Single orifice, 0.045-in.-diam, reduced ℓ/d ("sharp edge").

4. Single orifice, 0.089-in.-diam, 4.21 ℓ/d.

5. Impinging jets nozzle, 2 orifices of 0.045-in.-diam shown in Fig. 5. The jets impinge on each other at approximately a 30-deg angle.

6. Gas atomizer, multihole transverse. As shown in Fig. 6, fuel is routed to a central tube and then admitted through twelve 0.016-in. holes transversely (radially outward) into a coaxially flowing gas stream. The gas flows through an annulus of 0.310 in. outer diameter and 0.175 in. inner diameter. The closest ring of fuel holes is approximately 0.6 in. from the nozzle exit.

7. Gas atomizer, single-hole transverse. As shown in Fig. 7, fuel is admitted transversely (radially inward) through a single 0.125-in.-diam orifice into a central tube of flowing gas. The fuel orifice is located approximately 2.5 in. from the nozzle exit. The gas flows through a tube of 0.25 in. diam.

8. Gas atomizer, flush coaxial. As shown in Fig. 8, fuel is routed to a central tube inside a gas stream flowing coaxially in an outer annulus. The fuel is kept separate from the gas to the nozzle exit where fuel and gas are ejected together and then mixed. The fuel tube has an inner diameter of approximately 0.08 in. and the tip is flush at the nozzle exit with the gas annulus; i.e., has the same length as the gas annulus.

9. Gas atomizer, recessed coaxial. This nozzle is like the preceding one except the fuel tube is of approximately 0.06 in. inner diameter and is recessed about 0.25 in. inside the gas annulus at the exit, i.e., is shorter than the gas annulus.

3.0 FUEL SIMULANT: N-BUTYL ALCOHOL

In 1981 Battelle Columbus Laboratories, Columbus, Ohio, measured certain physical properties of mixtures of TMA and TEA, including the temperature dependence of the density, viscosity, and surface tension. As part of this work, Battelle was asked to recommend a non-pyrophoric liquid which would simulate the density, viscosity, and surface tension of the TMA/TEA mixtures for non-burning studies of flare spray characteristics (Ref. 1). Battelle's recommendation for the most suitable simulant was n-butyl alcohol (n-butanol, or 1-butanol). Table 1 shows a comparison of the selected properties of n-butyl alcohol and TMA/TEA mixtures at 20°C. Data sources are Refs. 1 and 3.

Graphs of the temperature dependence of the viscosity and surface tension for TMA/TEA and n-butyl alcohol are shown in Figs. 9 and 10. The temperature dependence of the density of n-butyl alcohol was not available, but the density increase of TMA/TEA as reported in Ref. 1 is only about 6 percent for a temperature decrease from +20° to −55°C. The surface tension of the TMA/TEA mixtures increases about 30 percent over the same temperature range while the surface tension of the alcohol appears somewhat less sensitive.

The parameter most sensitive to temperature is the viscosity, which for TMA/TEA increases by more than 600 percent for a temperature change from +20°C (1/T = 0.00341) to −55°C (1/T = 0.00458), and for the alcohol, increases more than an order of magnitude.

A temperature for the n-butyl alcohol was chosen to give a viscosity to match that of the TMA/TEA at the desired TMA/TEA temperature. An alcohol temperature of −20°C (1/T = 0.00395) was selected to give a viscosity of approximately 10 centipoise, which represents the viscosity of TMA/TEA after it has been cooled at high altitude to −55°C.

4.0 INSTRUMENTATION

4.1 GENERAL

In this investigation of nozzle performance, one of the most significant characteristics of the spray is the droplet size distribution, since it is related to fuel ignition. Size distributions can be measured without disturbing the flow by using various types of optical instrumentation. Another characteristic of the liquid spray in the coaxial airstream is the fuel/air ratio, which can be measured with mass sampling techniques. Pulsed laser holography/photography can provide pictures of the droplet formation at the nozzle exit. The shape and spread rate of the spray can be tracked using laser beams and mass sampling.

A series of window ports located at about 3-ft intervals along the tunnel test section permitted mounting of instrumentation for observation of the fuel spray in the wake behind the flare canister. Table 2 lists the various instruments used and their locations in feet downstream of the flare nozzle. Unlike the other instruments, which were mounted outside the tunnel, the Particle Measuring Systems, Inc., Model FSSP single particle sizer was mounted inside the tunnel at the far end of the test section. The fuel mass sampling probes could be extended into the tunnel by hydraulic cylinders to take measurement samples from the flow.

4.2 DROPLET SIZING INSTRUMENTATION

4.2.1 PMS, Inc., Model FSSP Forward Scatter Spectrometer Probe

The Forward Scatter Spectrometer Probe (FSSP) built by Particle Measuring Systems, Inc., is designed to measure droplet size distributions in the diameter range of 0.5 to 48 μm. The design principle is based on measuring the absolute intensity of small forward angle light scattering by single particles. The optics and detector are housed within a probe which was mounted at Station 6 in the test cell. The installation in Test Cell T-6 is shown schematically in Fig. 11.

The FSSP was interfaced to an Apple II computer and associated printer/plotter. The system was programmed to plot size distribution histograms and calculate parameters of the distribution. Four ranges of particle sizes could be selected:

Size Range	Range (μm)	Bin Size (μm)
3	0.5–8	0.5
2	1–16	1
1	2–32	2
0	2–47	3

Any of these ranges could be selected independently, or the system could be made to step through them sequentially. A sampling time could also be selected. After some experimentation with different procedures and sampling times, the sequential mode was selected so that all 4 ranges were obtained automatically for a given test point, and a standardized sampling time of 20 sec was chosen. Example histograms produced by the FSSP are included in Section 5.0.

The Model FSSP measured and recorded the instrument activity, defined as the percentage of the total run time during which the instrument was engaged in measuring and processing data. During the processing time, the instrument was effectively "off-line" and was unresponsive to any droplets which may have passed through the measurement volume. High activities attributable to high droplet concentrations would indicate significant loss in total count rate as well as increased probability for more than one droplet appearing at a time in the measurement volume. Low activities in the range of 2 to 6 percent, as were usual during this testing, should indicate little loss in total counts, and negligible effect on the measured relative distribution of droplet diameters.

The electronic frequency response of the FSSP is specified by PMS to extend to 100 KHz, with the note that for particle velocities greater than 100 m/sec, (328 ft/sec) corrections should be made to the histogram bin size and size range. The correction to be applied is a multiplying factor given by the curve of Fig. 12, which was supplied by PMS. For example, for a velocity of 150 m/sec, the sizes bounding the histogram bins should all be multiplied by 1.05; e.g., the Range 0 (2-47 μm) bin interval size would be $3 \times 1.05 = 3.15$ μm; Bin 1 would be from $2\,(1.05) = 2.10$ to $5\,(1.05) = 5.25$ μm; Bin 2 would be from 5.25 to 8.40 μm, etc. Velocity corrections were necessary for only a few of the histograms.

4.2.2 Fiber Optics Particle Sizing System (FOS)

The Fiber Optics System (FOS) developed at AEDC (Ref. 4) was used to measure droplet size distributions in the range of 3 to 90 μm. In the technique employed, a magnified shadow image of a particle passing through the laser beam is focused onto a linear array consisting of 32 optical fibers. The passage of a particle image across the array triggers a number of photo-detector modules, corresponding to the number of fibers covered by the shadow, thus recording the relative size of the particle. If either of the end fibers is shadowed, an error signal is generated to indicate the image was not adequately centered or was too large for the array. A schematic of the system as installed at Station 5 in the test cell is shown in Fig. 13.

The data processor was interfaced with a Tektronix 4051 computer and associated printer. The system was programmed to provide on-line data reduction and printouts of the droplet size distribution in tabulated and histogram form, along with a table of calculated distribution parameters.

4.3 FUEL MASS SAMPLING

The mass concentration of the n-butyl alcohol simulant in the spray was measured as a function of radius at axial stations 2 and 4, located 2.5 and 8.5 ft downstream, respectively. Sampling probes, consisting of 0.25-in. stainless steel tubing (Fig. 14) were jacketed with steam lines to maintain 121°C, a temperature above the vaporization temperature of the alcohol, which is 117.7°C at 1 atm (Ref. 3). The sample transfer line, valving, and pump were wrapped with electrical heat tape and also maintained at about 121°C. Analysis of the air/alcohol mixture was accomplished using a Beckman Model 402 hydrocarbon analyzer, which uses the flame ionization method of detection. The system schematic is shown in Fig. 15. The probes were actuated by hydraulic cylinders which could be stopped at fixed positions.

The Beckman Model 402 was calibrated using a mixture of 1.5-percent methane in air. The preliminary mass flow measurements were calculated as volume percent of methane and later converted to weight percent of n-butyl alcohol. Methane was selected as the calibration gas rather than the alcohol because of the difficulty in preparing gaseous alcohol calibration mixtures.

Prior to testing, the instrument was calibrated by introducing the 1.5-percent methane directly into the analyzer inlet. Next the calibration gas mixture was introduced at Stations 2 and 4 probe inlets with the sample vacuum pump on, to confirm the integrity of the sampling system. A post-test calibration was also done to verify that the instrument sensitivity had not changed during the test.

The mass flow sampling measurement procedure was as follows:

1. Select the required probe (Station 2 or 4)

2. Position the probe to the outermost mass flow boundary. It became evident early in the test that the traverse range for Station 4 should be centerline to 14 in. and for Station 2, centerline to 7 in.

3. As soon as alcohol flow is established, traverse the probe to the centerline and back, stopping at discrete radial locations.

The probe position and instrument response were recorded on the test facility digital data acquisition system for off-line computer analysis, and on a strip chart recorder for on-line verification and quick-look data.

The following calculations were used to determine the mass concentration of n-butyl alcohol (n-butanol):

$$\% \text{ n-butanol (vol)} \quad R \times \frac{1}{K} \times \frac{MW_{C_4H_{10}}}{MW_{CH_4}}$$

where

R = Instrument response as methane

K = Relative response ratio by weight $\frac{C_4H_{10}}{CH_4}$ (Ref. 5)

$= 1.469$ gm C_4H_{10}/gm CH_4

$MW_{C_4H_{10}}$ = Molecular weight n-butanol

$= 74.0$ gm/mole

MW_{CH_4} = Molecular weight Methane

$= 16.0$ gm/mole

Therefore,

$$\% \text{ n-butanol (vol)} = R \times \frac{1}{1.469} \times \frac{74}{16}$$

$$= R \times 3.148$$

To convert the alcohol from volume percent to weight percent, the following equations were used:

$$\%\ C_4H_{10}\ (wt) = \%\ C_4H_{10}\ (vol) \times \frac{MW_{C_4H_{10}}}{MW_{sample}}$$

where

$$MW_{sample} = (\text{mole fraction } C_4H_{10} \times MW_{C_4H_{10}}) + (\text{mole fraction }_{Air} \times MW_{Air})$$

where

$$MW_{Air} = \text{molecular weight of air}$$

4.4 LASER PHOTOGRAPHY

A pulsed laser camera system, Fig. 16, was used to photograph the spray at the nozzle exit. The system consisted of a 15-nsec pulse, ruby laser having an output energy of one joule, associated collimating and collecting optics, and a 70-mm camera. A HeNe alignment laser was also part of the system. The laser was pulsed during each shot at 5, 30, 60, and 88 sec after the start of fluid injection. The pulse repetition rate was limited by the time to charge the high voltage power supply, approximately 15 sec. Figures 17 and 18 give dimensions of two fields of view used during the tests. Some of the photographs show the flare can exit, while in other cases the can was out of the field of view. The photographs, some of which are of holographic quality, are useful for qualitative assessment of performance, although there was no attempt to obtain holograms or quantitative data from them.

5.0 RESULTS

5.1 DEFINITIONS: DROPLET SIZE DISTRIBUTION MEANS

Examples of particle size distributions in the form of histograms recorded by the FSSP and FOS droplet sizers are included in this section. Various mean sizes can be defined for a distribution (Ref. 6).

For example, the mean of a number distribution such as any of the histograms in this report is given by

$$d_{10} = \Sigma\, d_i N_i / N \qquad (1)$$

where N_i is the number of droplets counted in the ith histogram bin, d_i is the diameter of the droplets counted in the ith bin, and N is the total number of droplets counted in all the bins, i.e., $N = \Sigma N_i$. The diameter d_{10} is the arithmetic average diameter.

The volumetric or mass mean d_{30} is defined as

$$d_{30} = \left(\Sigma d_i^3 N_i / N\right)^{1/3} \tag{2}$$

If the spray had the same total number of droplets, but each droplet had the diameter d_{30}, the spray would contain the same total volume (or mass) of liquid as does the actual spray; i.e., the arithmetic average mass is contained in a droplet of diameter d_{30}.

It is straightforward to show that the number (n) of droplets per gram of liquid in the spray is related to d_{30} as:

$$n = \frac{6}{\varrho_\lambda \pi d_{30}^3} \text{ droplets/gm} \tag{3}$$

where ϱ_λ is the liquid mass density.

The Sauter mean d_{32} is defined as

$$d_{32} = \Sigma d_i^3 N_i / \Sigma d_i^2 N_i \tag{4}$$

If all the droplets had the same diameter d_{32}, the spray would have the same liquid surface-to-volume ratio as does the actual spray. The Sauter mean is significant in this study because of its relation to the total liquid surface area (a) per gram of liquid in the spray:

$$a = \frac{6}{\varrho_\lambda d_{32}} \text{ cm}^2/\text{gm} \tag{5}$$

5.2 TEST AND DATA POINT SUMMARY

Table 3 lists each experimental test shot as a test and data point number, giving the significant flight and fuel nozzle conditions. These values are averages of data obtained over approximately a 50-sec time period during each metered fuel (alcohol) shot. Data points are grouped in the table to show where conditions were maintained relatively constant, usually to permit the taking of mass sampling data. The mass concentration samples and sizing instrument samples were taken sequentially in time, rather than simultaneously, to avoid

perturbing data taken downstream of a sample probe inserted in the flow. Different data point numbers were then assigned each sampling.

Where data are of good quality, Table 3 includes listing of the mass mean d_{30} and Sauter mean d_{32} for the fuel spray droplet size distribution measured by the Model FSSP sizer, and also a listing of the fuel spray widths in the flare can wake as determined by the mass concentration profiles at Stations 2 and 4. The width listed is that measured where the mass concentration has fallen off to one-half its peak value. Examples of mass concentration plots are included under Section 5.5, below.

Recorded nozzle gas pressures in Table 3 can be seen to vary between different nozzles for the same gas flow rate. One reason is that for the single-hole transverse atomizer the pressure was measured at the back of the nozzle where pressure is high, while for other nozzles, it was measured where the pressure is lower near the nozzle exit. For the recessed coaxial nozzle, the measurement location was probably beyond the nozzle choke point, where the pressure would normally be low.

5.3 NOZZLE COMPARISONS

Table 4 compares mean sizes produced by the different nozzles under similar operating conditions at relatively low tunnel airstream dynamic pressure, ϱv^2. Under such low air velocity conditions, the advantage possessed by the gas atomizers over the hydraulic orifice nozzles in producing smaller droplets is immediately evident. The mean diameters d_{30} and d_{32} are from distributions recorded by the FSSP droplet sizer.

Example size distributions recorded by the FSSP under low ϱv^2 conditions for the 0.025-in. orifice, the impinging jets, and two coaxial nozzles are shown in Fig. 19.

Table 5 compares mean sizes produced by the different nozzles under conditions of relatively high airstream dynamic pressures. In these cases, the airstream atomizes the fuel, and all nozzles produce comparably small droplets. Example size distributions for the 0.045 orifice and the single-hole transverse nozzles under high air velocity conditions are shown in Fig. 20.

Example photographs of sprays from different nozzles and for different conditions, taken with the pulsed laser system, are shown in Appendix A. Figures A-1 through A-4 show photographs corresponding to the histograms of Fig. 19. Figure A-5 shows a photograph corresponding to data point 2.15 of Fig. 20.

5.4 NOZZLE GAS FLOW RATE EFFECTS IN PNEUMATIC NOZZLES

Figure 21 plots effects of the nozzle gas flow rate on mean sizes produced by various pneumatic nozzles, as measured by the FSSP sizer. The numbers on the graphs represent test and data point numbers. Solid lines connect data points where a given nozzle was operated under approximately the same conditions, except that the parameter of interest was varied.

In Fig. 21a, data points 4.16, 4.11, and 4.8 at the upper left are for the single-hole transverse nozzle under low ρv^2 conditions. For these three data points, as would be expected, the mean sizes decrease with increasing atomizing gas flow. Photographs illustrating data points 4.16 and 4.8 are shown in Appendix A, Figs. A-6 and A-7, respectively, and histograms are shown in Fig. 22.

The effect of increasing gas flow to the single-hole transverse nozzle under high airstream dynamic pressure is shown in Fig. 21a, data points 4.18, 4.20, and 4.25. Here there is little change in mean size with increasing gas flow, since the airstream dynamic pressure alone is capable of finely atomizing the fuel.

The means for the various nozzles show generally little further decrease for gas flow rates above about 10 gm/sec. Experience in flare combustion testing has shown that a nozzle gas flow of 7 gm/sec is usually adequate to cause ignition, and this may, then, represent a limiting operation where increases in gas flow do not appreciably decrease the smallest sizes in the spray. (But see Section 5.5.)

5.5 CONSISTENCY OF DATA: NOZZLE GAS FLOW RATE EFFECTS

The spray photographs, contrary to the FSSP measurements, seem to show continually finer atomization with nozzle gas flows increasing above 10 gm/sec. For example, Figs. A-8, A-9, and A-10 in Appendix A are photographs of the spray from the multihole transverse nozzle for data points 5.18, 5.16, and 5.14, respectively, which are plotted in Fig. 21a. Qualitative examination of the photos indicates finer atomization as gas flow is increased, although in contrast, the calculated means measured by the FSSP increase slightly.

Figure 23 shows the size distributions for these three data points as measured by the FSSP at Station 6. Figure 24 shows the raw count size distributions for these same data points as measured by the FOS particle sizer at Station 5, and these distributions agree qualitatively with the FSSP measurements, including the slight increase in the mean size d_{30}.

A second indication besides the photographs, however, that finer atomization is actually occurring with increased gas flow is that both the FSSP and FOS droplet count rates are

considerably larger at the higher gas flows. The total droplet counts by the FSSP in 20 sec for data points 5.18, 5.16, and 5.14 were 30,216, 85,238, and 103,312, respectively. As given in Section 5.1, the number of droplets (n) per gram of liquid in the spray is related to d_{30} as:

$$n = \frac{6}{\varrho_\lambda \pi d_{30}^3} \text{ droplets/gm} \tag{3}$$

The fuel flow rate for the 3 data points under consideration varied only slightly from 50 gm/sec. It would be expected, then, that since the mass in the spray remained approximately constant, an increasing count (n) of droplets would indicate a decreasing d_{30}, not an increase as shown by the recorded size distributions. (An exception would be if the count at the instrument location was not proportional to the count in the spray as a whole; as, for example, if a larger percentage of the total spray droplets were being directed along centerline at the higher gas flow rates.)

An explanation for the apparent discrepancy between the distributions measured by the sizers and the evidence of the photos and sizer count rates could be that the larger droplets seen in the spray photographs at the lower gas flows represent a second mode in the distribution, above the range of sizes covered by the FSSP and FOS sizers. Suppose, for example, the instrument count rates are indeed proportional to the total count in the spray as a whole, and further assume that $d_{30} = 16.4$ μm measured by the FSSP for the high gas flow rate (data point 5.14) is correct for the total spray (no large droplets in this case above the range of the instrument). The count rates may be used to calculate what d_{30} for the spray of data point 5.18 should be. Since, for constant fuel flow, the count (n) is inversely proportional to d_{30}^3, the volumetric mean for point 5.18 should be

$$d_{30}^3 = (16.4)^3 \, 103{,}312/30{,}216$$

$$d_{30} = 24.7 \ \mu\text{m}$$

This is a reasonable answer if there are a few large droplets above the size range covered by the sizers. For example, if there were 450 droplets with a diameter of 100 μm in the spray of data point 5.18 (less than the number in the 26-29 μm bin), the mean would increase from the measured 14.9 μm to 26.2 μm, consistent with the decreased count rate.

If such an explanation does account for the evident discrepancy between the photographs and the histograms, then the sizer data can still be considered reliable in measurement of that part of the size distribution which is within the sizer sensitive range.

As a partial check on the assumption that count rates at the sizer's location are proportional to the count in the spray as a whole, reference can be made to the fuel mass sampling results. Alcohol mass concentration was measured versus radial distance at axial

Stations 2 and 4, in percent (by weight) of the total tunnel flow. The results give the radial spread of the alcohol flow as it travels down the tunnel.

The question of interest here is whether the measurements give any reason to suspect that the increasing count in the data point sequence 5.18, 5.16, 5.14 is attributable not to finer atomization, but rather to change in flow pattern that could increase the number of alcohol droplets on centerline where the sizer takes its sample.

Figure 25 gives results of mass concentration measurements at Stations 2 and 4, data points 5.20 and 5.19, respectively, for approximately the same conditions as data point 5.18. The two curves show the dispersion of the flow which occurs between Stations 2 and 4, located 2.5 and 8.5 ft downstream of the nozzle, respectively.

The data of particular interest are plotted in Fig. 26, which gives the mass concentration profiles for data points 5.19 and 5.15, corresponding to the conditions of 5.18 and 5.14, respectively, at Station 4. (The profile for data point 5.16 lies intermediate between these two.) The alcohol flow pattern is more concentrated near the centerline for data point 5.19 (low nozzle gas pressure) than for data point 5.15, just opposite to what might cause an increased droplet count at the higher gas pressure. Therefore, these data do not contradict the assumption that the increased count is attributable to finer atomization.

5.6 FUEL FLOW RATE EFFECTS

Figure 27 plots effects of nozzle fuel flow rate on the mean droplet diameter d_{30} as measured by the FSSP sizer. The plots show that mean sizes tend to increase somewhat in most instances with increasing fuel flow, although the effect seems to be of secondary importance.

5.7 AIRSTREAM EFFECTS

For hydraulic nozzles, an assumption made in formulating droplet size inputs to the analytical flare model is that the airstream atomizes the fuel upon ejection from the flare nozzle. The finer atomization which results from higher airstream dynamic pressures is well illustrated by the data here. The effect is illustrated in the spray photographs in Appendix A, Figs. A-11 – A-14, which show spray from the 0.25-in. orifice nozzle under varying airstream conditions. The assumption made for the model that droplet size for hydraulic nozzles is inversely proportional to the dynamic pressure ρv^2 enabled the model to predict quite successfully under what conditions flare ignition would occur.

Although experimental data taken during these tests show the decrease in drop size which accompanies increased dynamic pressure, the specific inverse proportionality assumed for the model was not obtained. Fig. 28 plots the variation of ln d_{30} with ln (ϱv^2). Assuming a relationship of the form

$$d_{30} = k/(\varrho v^2)^q \tag{6}$$

where k is a constant of proportionality, the number q is the (negative) slope of the linear relationship between ln d_{30} and ln (ϱv^2).

The plot of Fig. 28 shows that the data correlate reasonably well with a least-squares fit. The slope of the dashed line is q = 0.15, not q = 1 as assumed for the model.

In the data of Fig. 28, velocity was held approximately constant (400 ± 30 ft/sec), and altitude, i.e., density ϱ, was varied to change the dynamic pressure. Referring to Eq. (6), then, in this case where velocity was constant, d_{30} varied inversely as $\varrho^{0.15}$.

In Fig. 29, the log of the arithmetic mean, ln d_{10}, for the same data is plotted versus ln (ϱv^2). The slope of the linear least-squares fit in this case is q = 0.20.

Figure 30 plots experimental data of the log of the mass mean, ln d_{30} versus ln (ϱv^2), at an altitude of approximately 5,000 ft. The density ϱ in this case was approximately constant, equal to 1.18 ± 0/0.02 mg/cm^3. The data correlate quite well linearly with a slope of q = 0.255. Thus, d_{30} was observed here, where density was constant, to vary inversely as approximately the fourth root of the dynamic pressure; i.e., as approximately the square root of the velocity.

It might be argued that what should be plotted is the dynamic pressure of the airstream relative to the fuel injection velocity, rather than relative to the flare canister. Table 6 lists airstream velocities, fuel injection velocities, and their differences for a number of the same data points plotted in Fig. 30. The fuel velocity v_λ was calculated from the equation

$$\dot{m} = \varrho_\lambda A v_\lambda \tag{7}$$

where $\dot{m}$ was the fuel mass flow rate, ϱ_λ the fuel density, and A the area of the nozzle fuel ejection orifice.

Figure 31 plots ln d_{30} versus ln$(\varrho v_r)^2$, where $v_r = (v - v_\lambda)$, for the data points listed in Table 6, with the exception of those three data points where the relative velocity was negative; i.e., where the fuel injection velocity was actually greater than the tunnel air flow velocity.

The data do not correlate as well in Fig. 31, plotted versus relative air/fuel dynamic pressure, as the same data do in Fig. 30, plotted simply against the tunnel airstream dynamic pressure. This is probably because the basic interaction is not between a fuel stream and a moving air mass into which it is injected, but rather between a fuel stream and the recirculating, turbulent wake immediately behind a flare canister.

5.8 FLARE ORIENTATION EFFECTS

Data were taken for the impinging jets and 0.45-in. sharp edge hydraulic nozzles with the nozzle pointed 90 deg (perpendicular) and 180 deg (upstream) relative to the tunnel air flow. High and low fuel flow rates were used. The results are shown in Table 7. No dramatic effect attributable to flare orientation is evident, although there seems to be a tendency for the mean diameters to decrease slightly when the nozzle is pointed upstream.

6.0 CONCLUSIONS

Liquid droplet injection behavior was studied using a non-burning fuel simulant for a number of different types of nozzles suitable for use with air-dropped pyrophoric flares. Characteristics such as droplet size distribution and the shape and spread rate of the nozzle spray were recorded under a range of flight speed, altitude, and nozzle parameters such as orifice size, fuel pressure and flow rate, and atomizing gas pressure and flow rate.

Although it was hoped that a purely hydraulic nozzle might be found which would atomize the fuel as well as a pneumatic gas atomizer under all conditions, no parameter such as orifice size or fuel flow rate which might be exploited in nozzle design had a strong influence on droplet size. The device of impinging two liquid jets on each other likewise offered little advantage. The superiority of gas atomizing nozzles in producing fine drops was immediately evident in the droplet size distributions when the fuel was injected into low velocity tunnel airstream conditions.

As was anticipated, the dynamic pressure (ρv^2) of high tunnel air velocities and densities was observed to produce as fine an atomization of the fuel after injection from hydraulic nozzles as was provided by pneumatic nozzles.

The volumetric mean d_{30} of the spray size distributions was observed to vary inversely as $(\rho v^2)^{0.15}$ when velocity was held constant (i.e., as $\rho^{0.15}$) and to vary inversely as $(\rho v^2)^{0.25}$ when density was held constant (i.e., as $v^{0.5}$). Better correlation of the data was found when d_{30} was plotted versus the dynamic pressure relative to the flare canister rather than relative

to the fuel injection velocity. It is believed this is because the basic interaction is not between a fuel jet and a moving air mass into which it is injected, but between a fuel jet and the recirculating, turbulent wake behind the canister.

No dramatic effect was observed attributable to flare orientation with respect to the airstream, although there seems to be a tendency for the mean size to decrease somewhat when the nozzle is pointed upstream into the air flow.

The results of the testing seem to be as significant in what they do not show as what they do. By systematically examining spray characteristics for different nozzle types under different operating conditions, it was seen that the gas atomizers held a distinct advantage in producing finer drops, while no simple hydraulic orifice stood out as offering special potential for engineering application. The test data add to the volume of information to be drawn upon to understand flare ignition and combustion phenomena.

REFERENCES

1. Mezey, E. J., Coutant, R. W., Zamejc, E. R., and Mohler, P. S. "Physical Properties and Combustion Kinetics of TMA/TEA and TMA/TEA/DEAH Mixtures, Phase I: Key Physical Property Measurements." AEDC-TR-82-18 (AD-B071955L), March 1983.

2. Willbanks, C. E., and Schulz, R. J. "Analytical Study of Icing Simulation for Turbine Engines in Altitude Test Cells." AEDC-TR-73-144 (AD770069), November 1973.

3. Weast, Robert C., ed. *CRC Handbook of Chemistry and Physics.* CRC Press, Boca Raton, Florida, 1969 (50th Edition).

4. Bentley, H. T. "Fiber Optics Particle-Sizing System." AEDC-TR-73-111 (AD-766647), September 1973.

5. McNair, H. M., and Bonelli, E. J. *Basic Gas Chromatography.* Varian Aerograph, March 1969 (5th Edition).

6. Allen, T. *Particle Size Measurement.* Chapman and Hall, London, 1975.

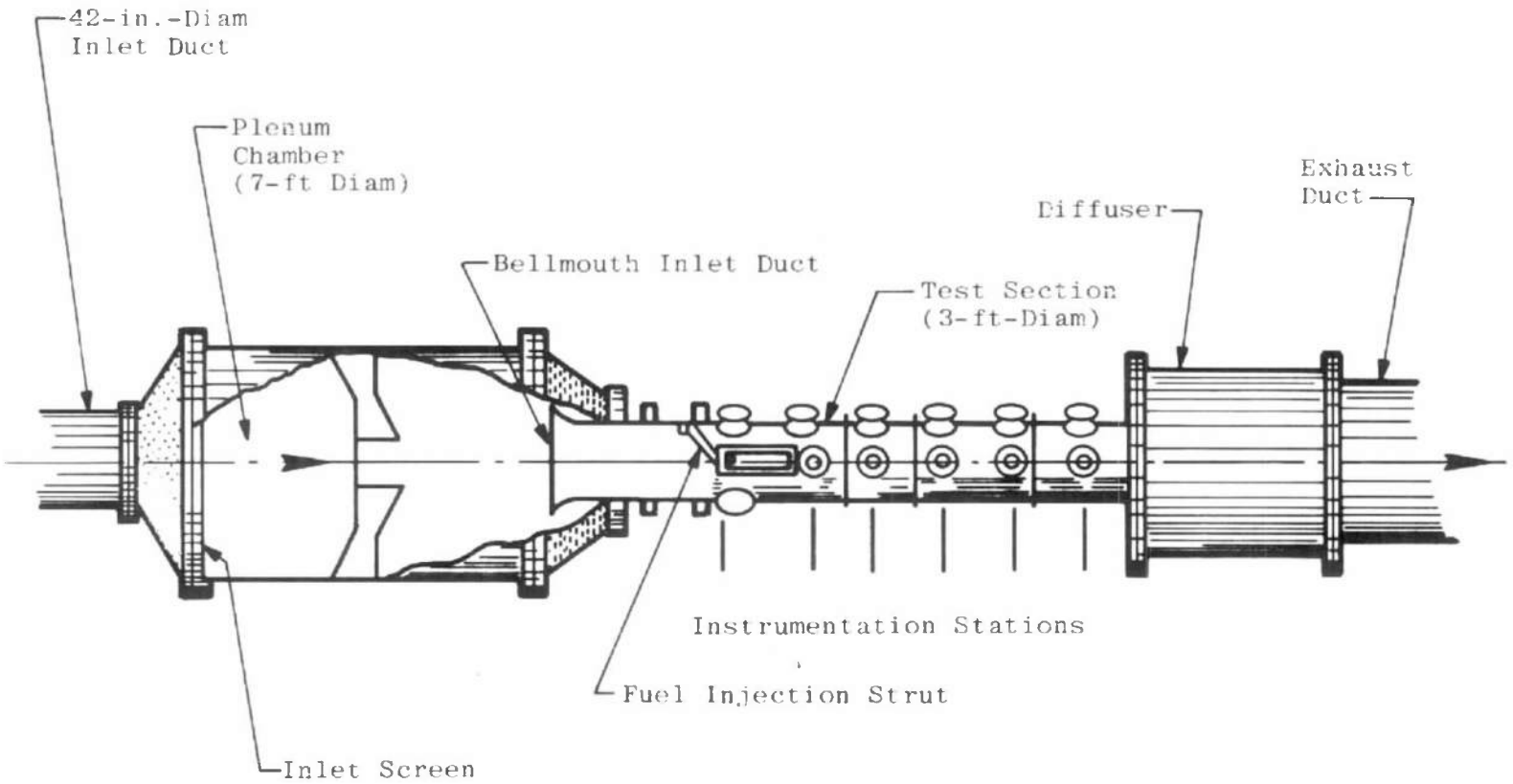

Figure 1. Research Cell T-6.

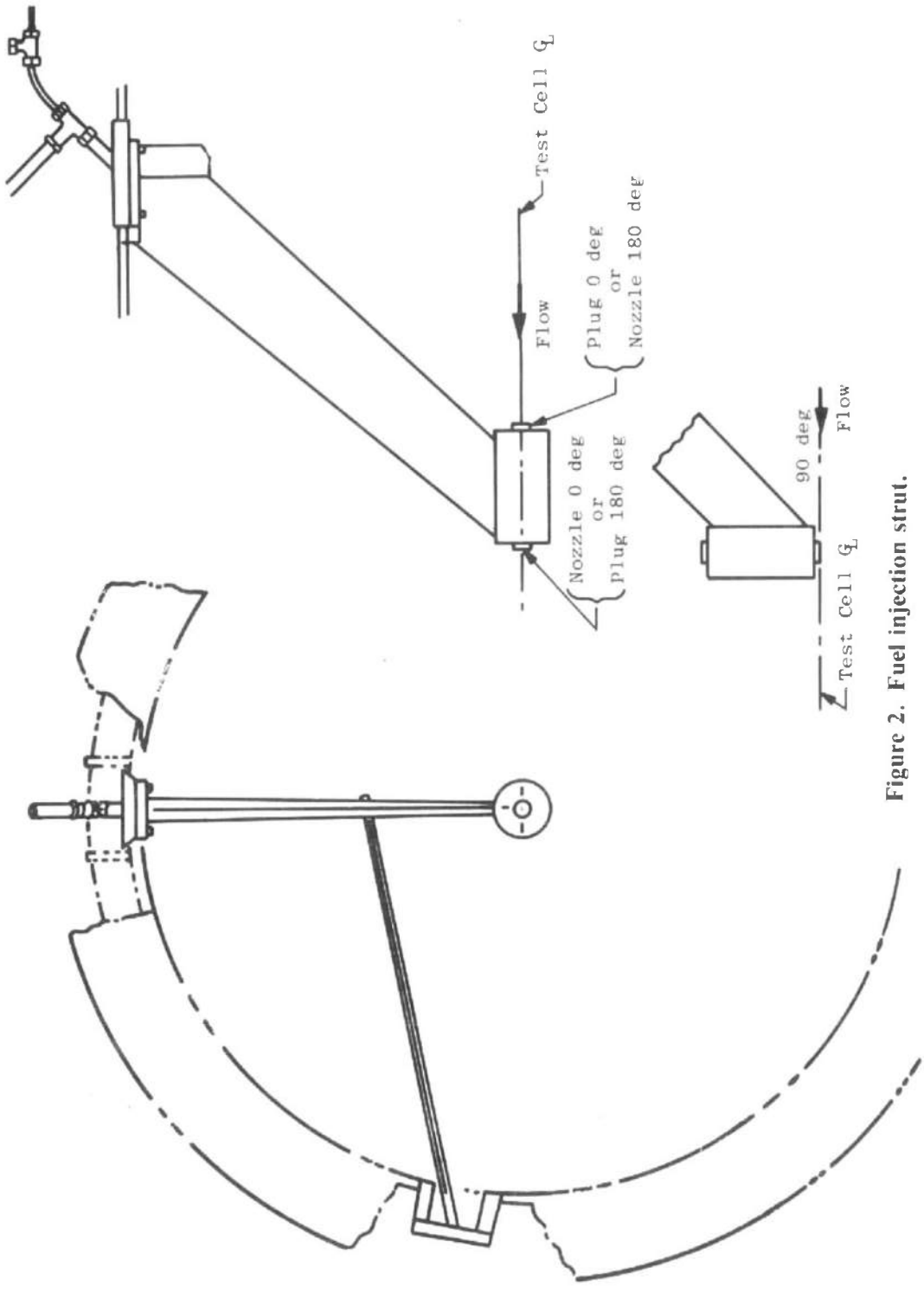

Figure 2. Fuel injection strut.

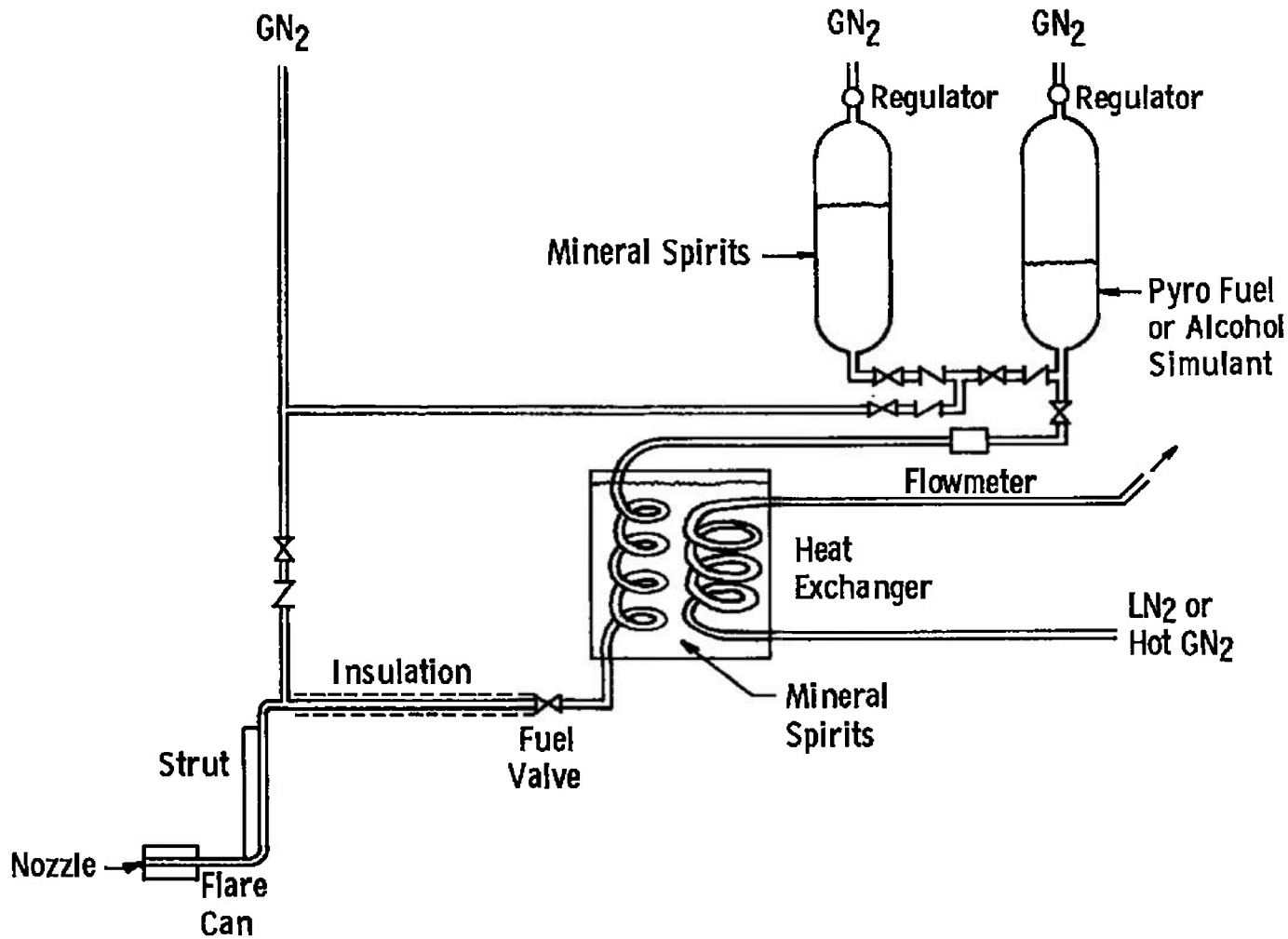

Figure 3. Fuel delivery and conditioning system, simplified schematic.

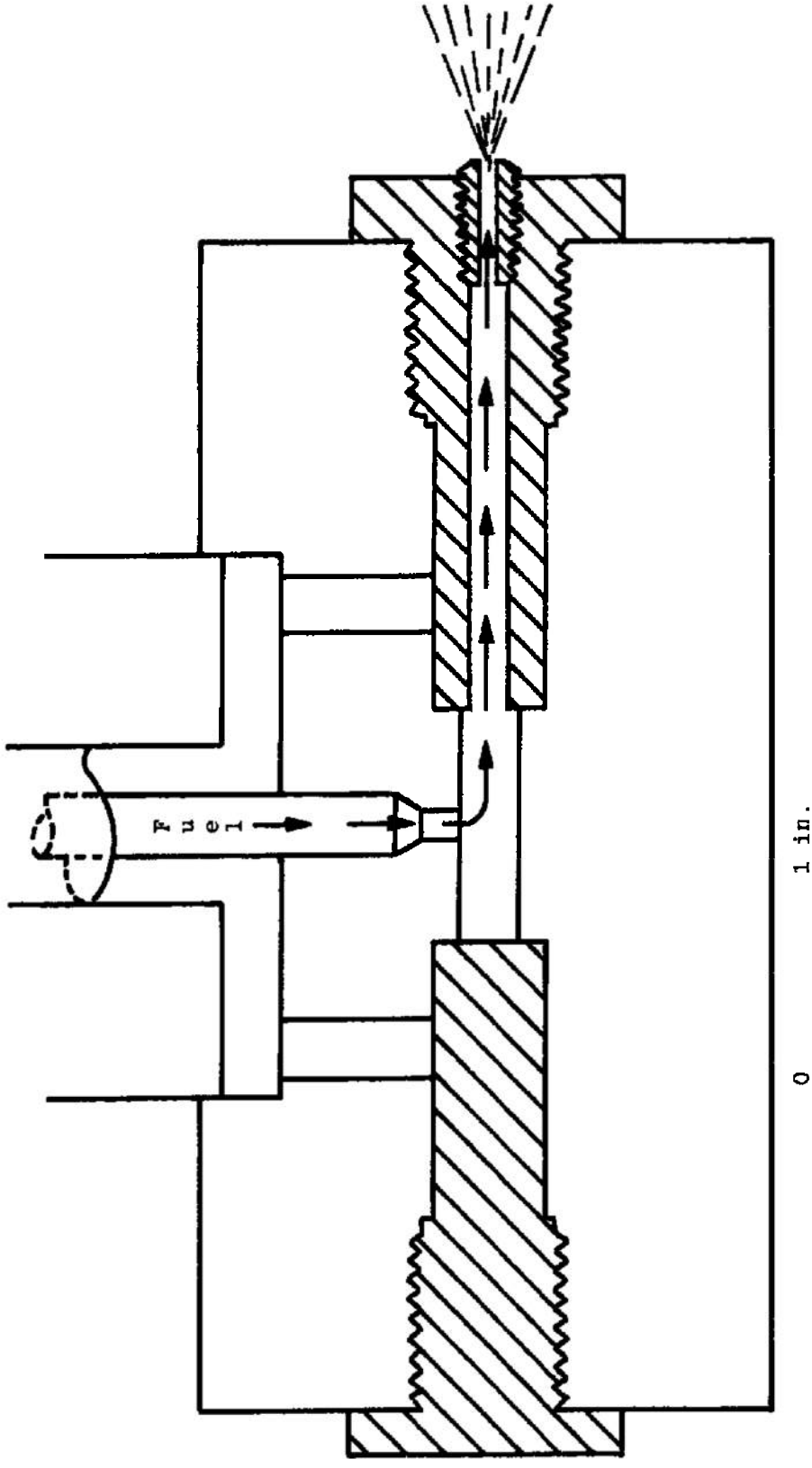

Figure 4. Hydraulic single orifice nozzle.

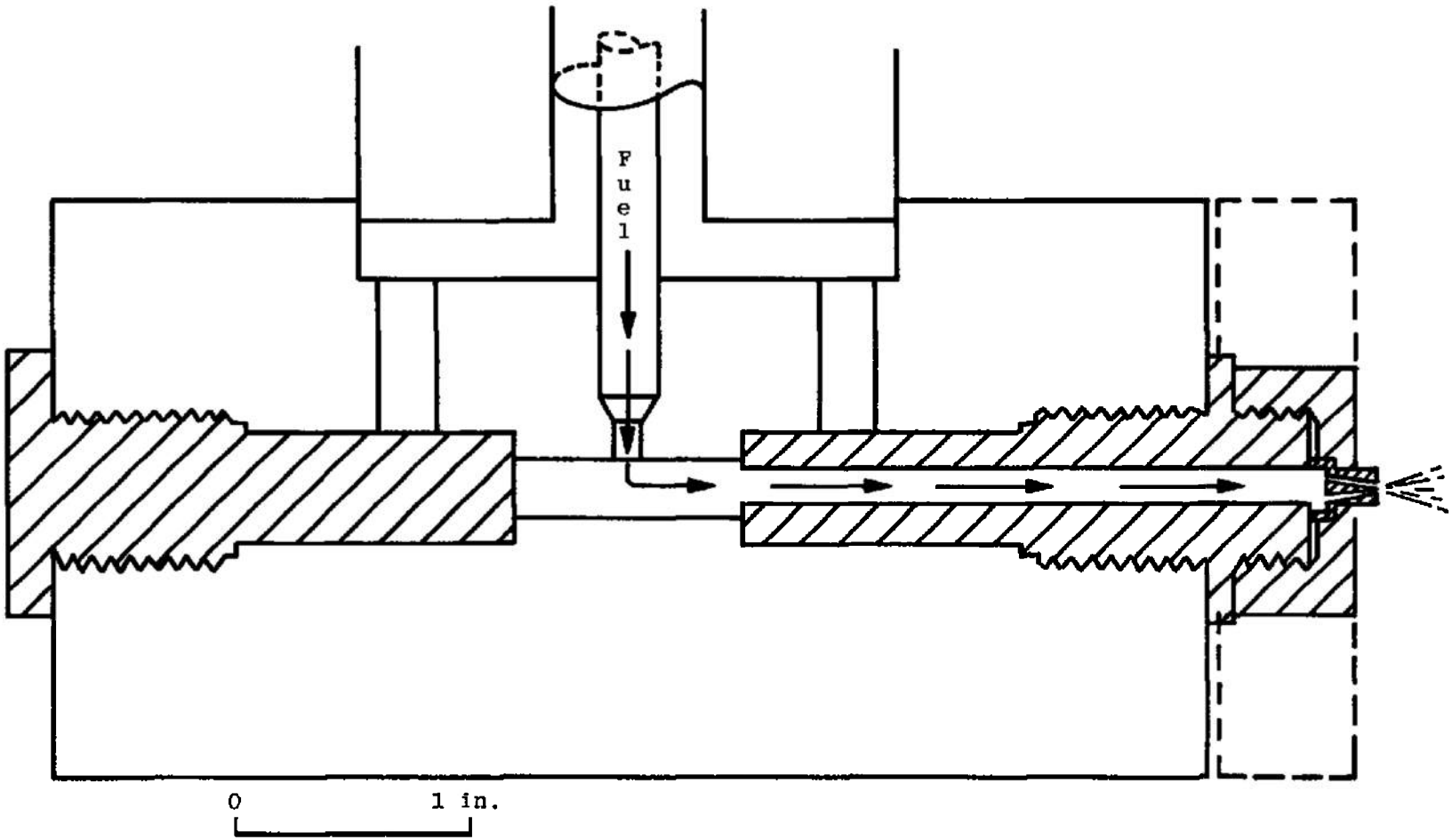

Figure 5. Hydraulic impinging jets nozzle.

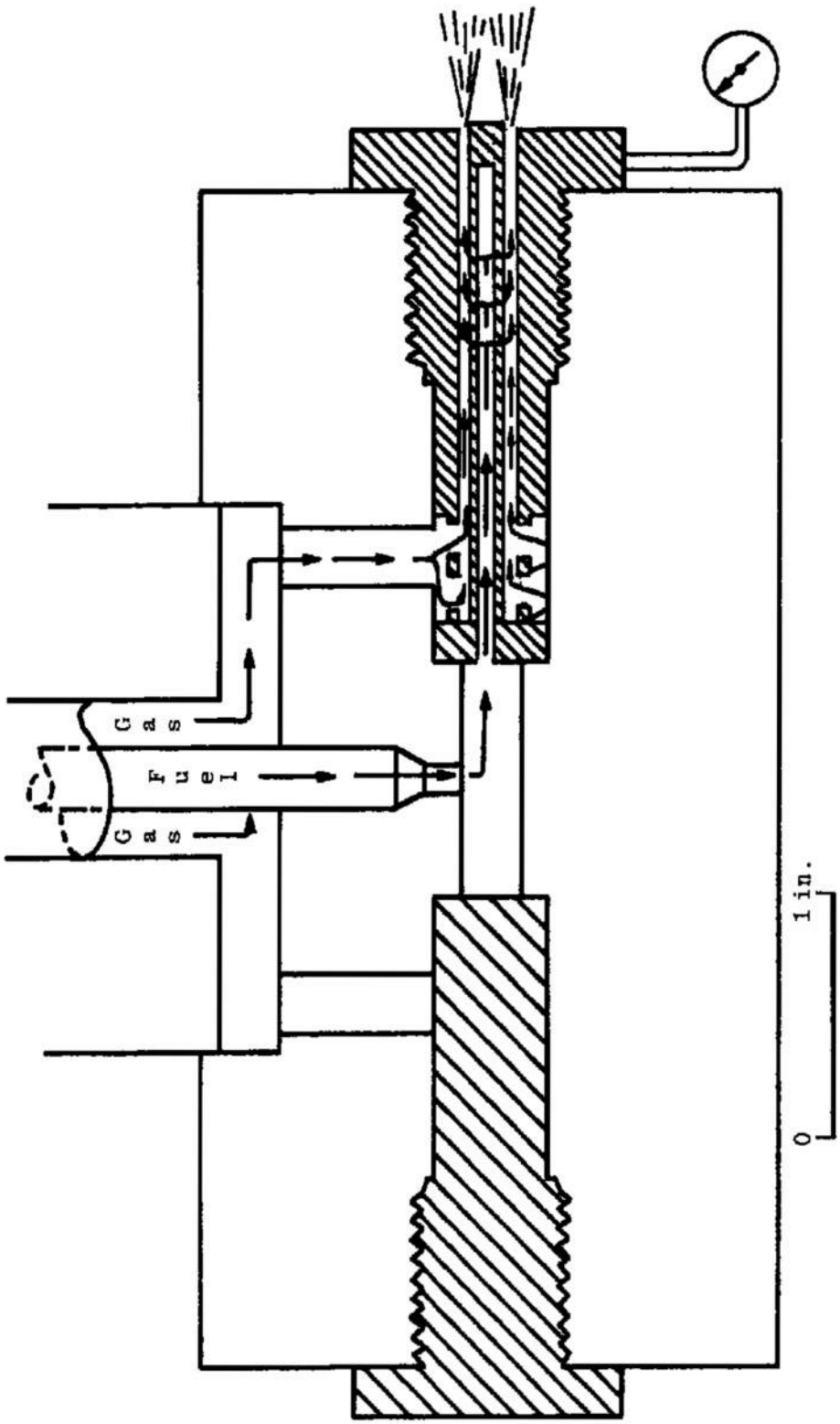

Figure 6. Gas atomizing nozzle, multihole transverse.

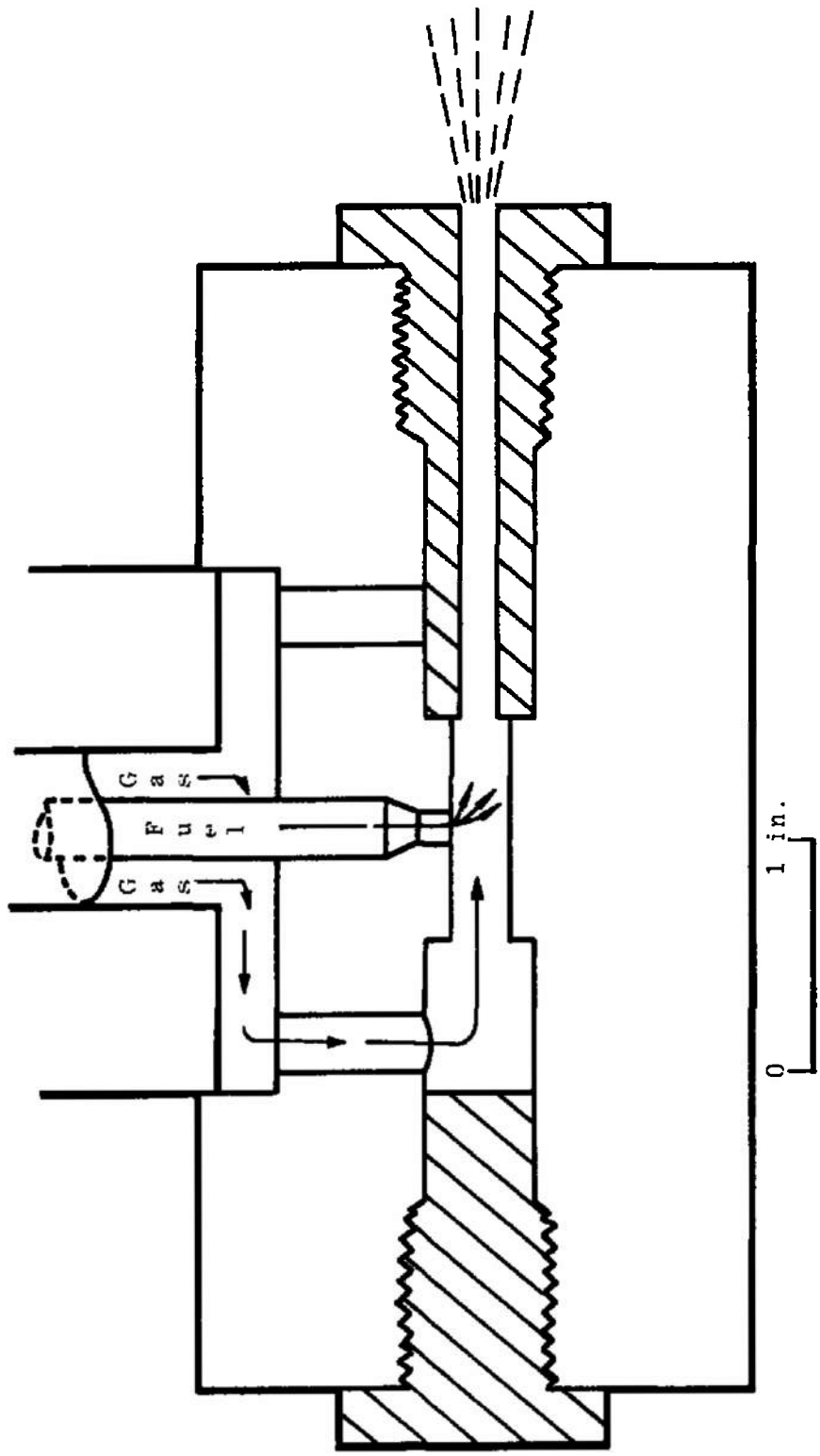

Figure 7. Gas atomizing nozzle, single-hole transverse.

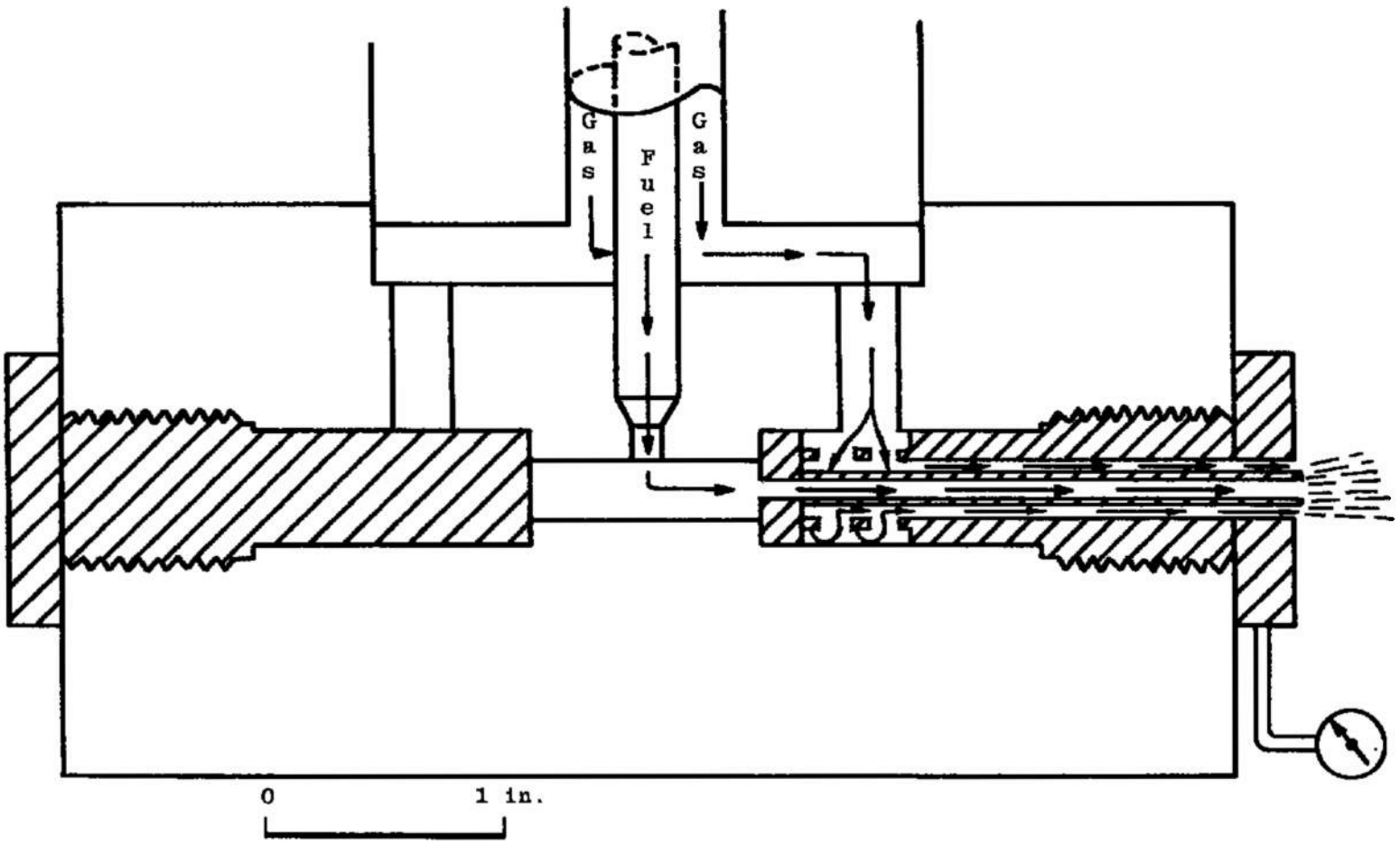

Figure 8. Gas atomizing nozzle, coaxial.

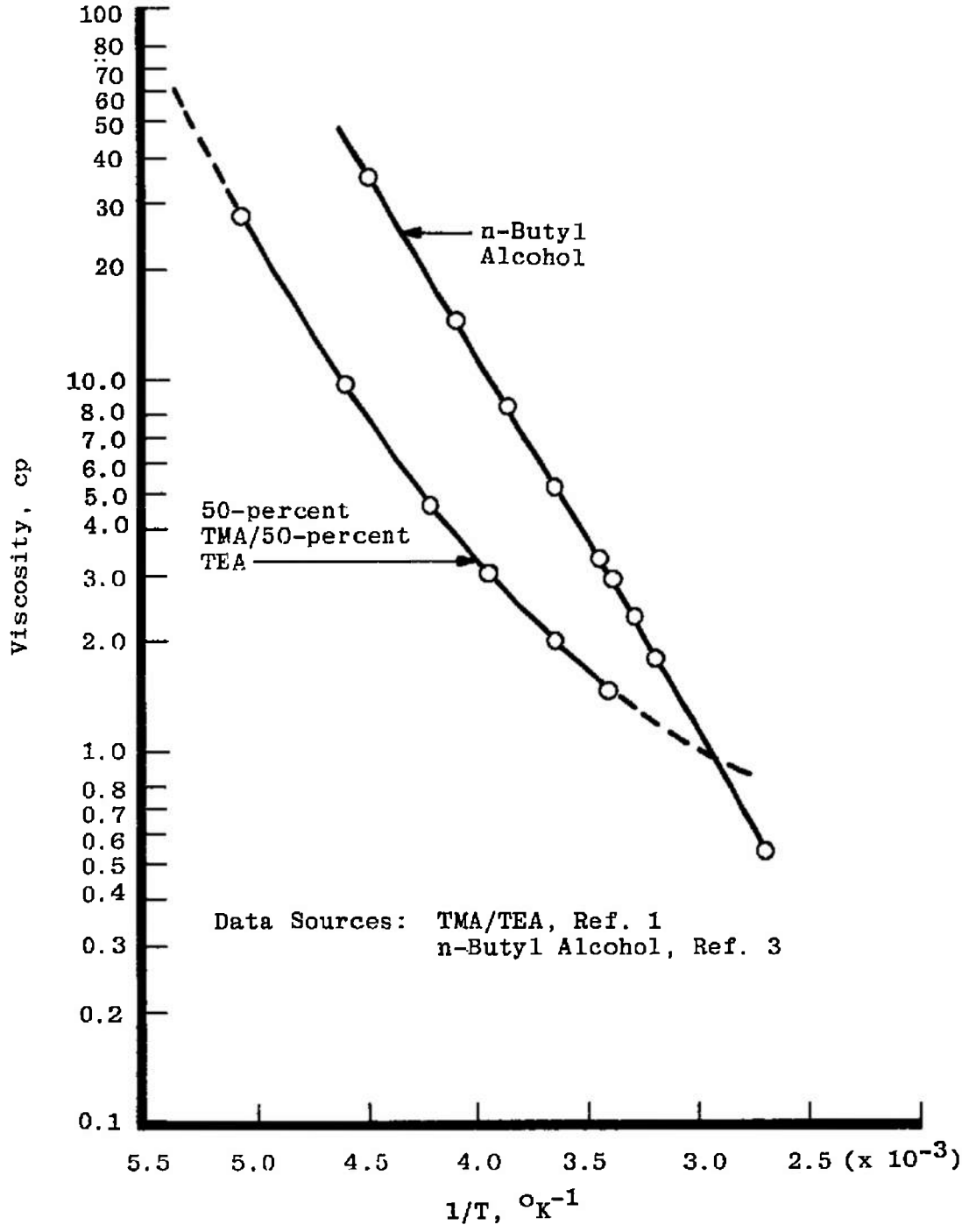

Figure 9. Viscosity of n-butyl alcohol and a 50/50 TMA/TEA mixture as a function of the reciprocal of the absolute temperature.

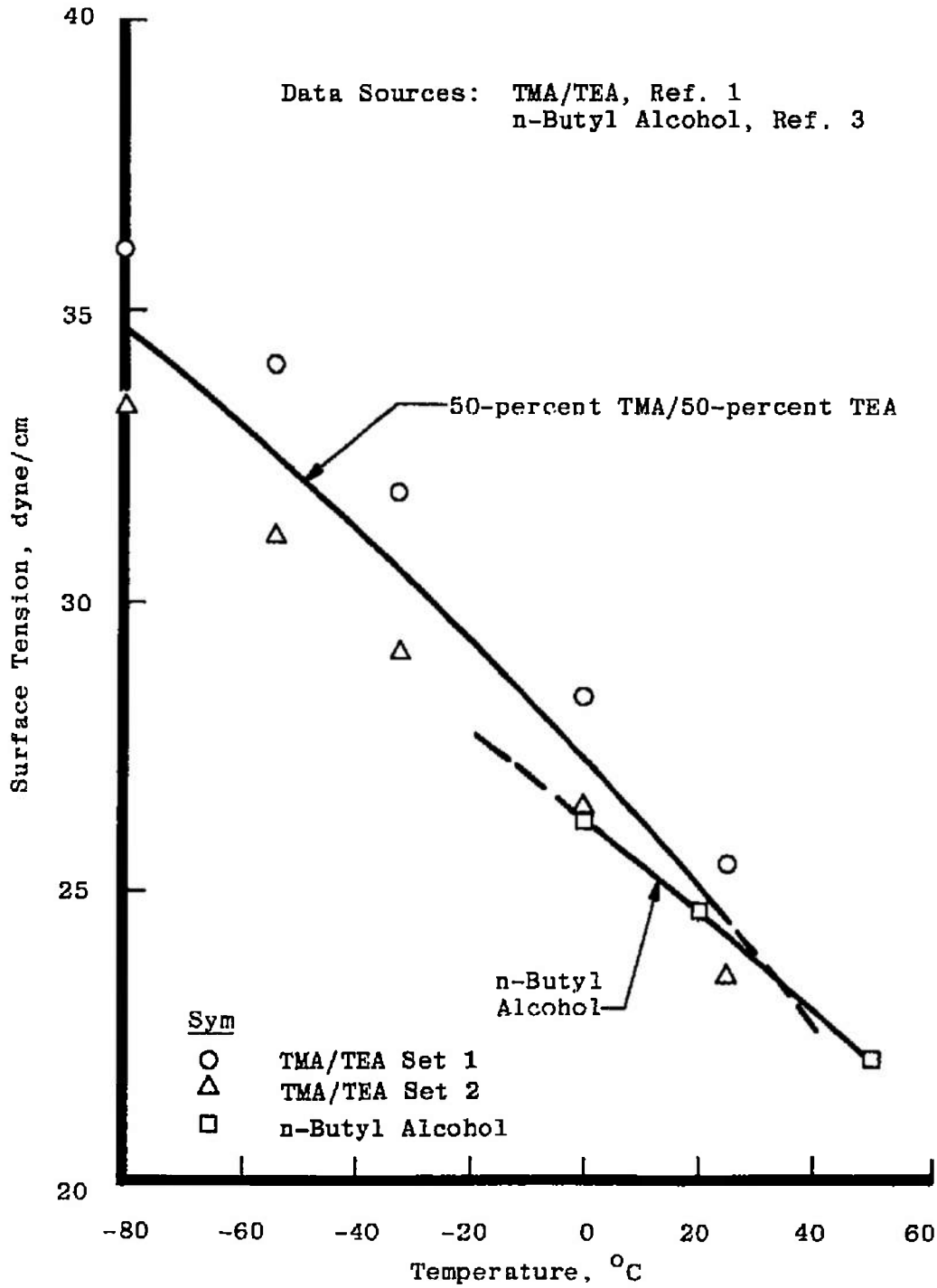

Figure 10. Surface tension of n-butyl alcohol and a 50/50 TMA/TEA mixture as a function of temperature.

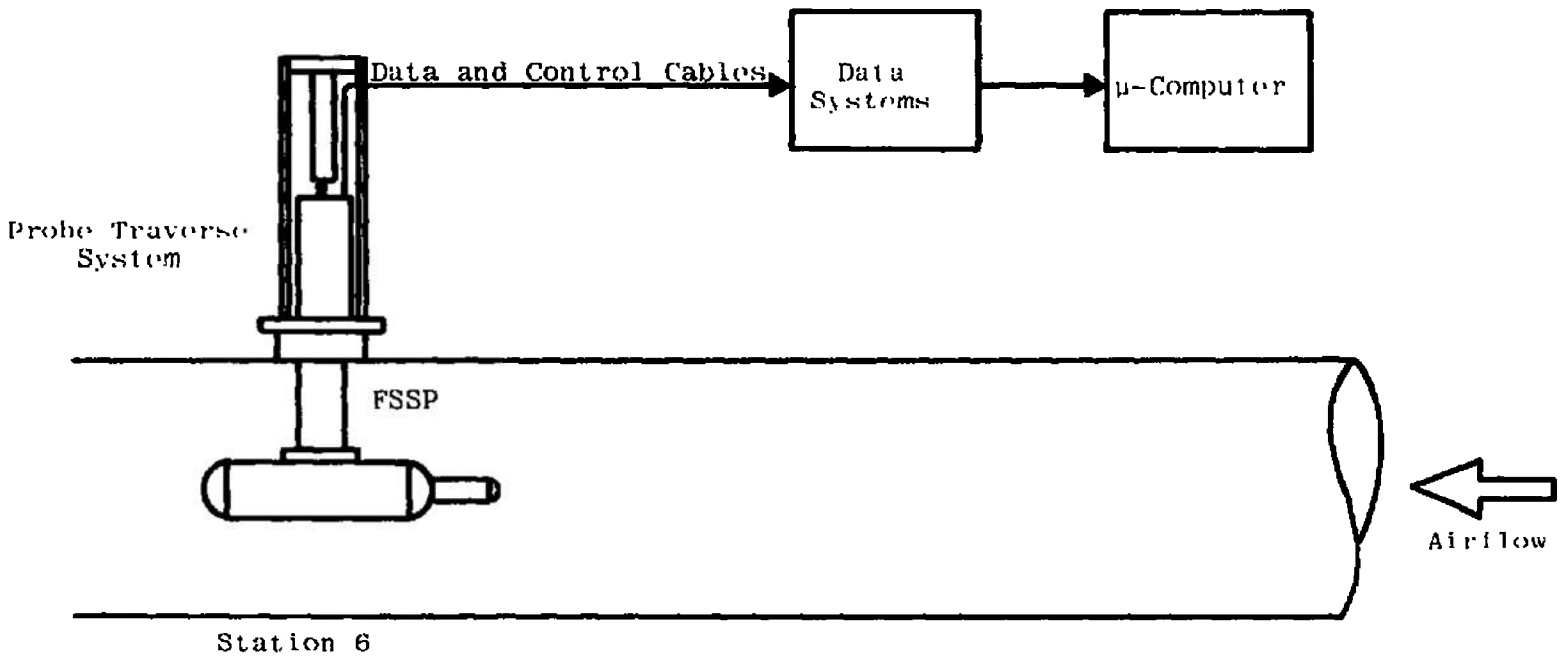

Figure 11. Model FSSP particle sizer installation.

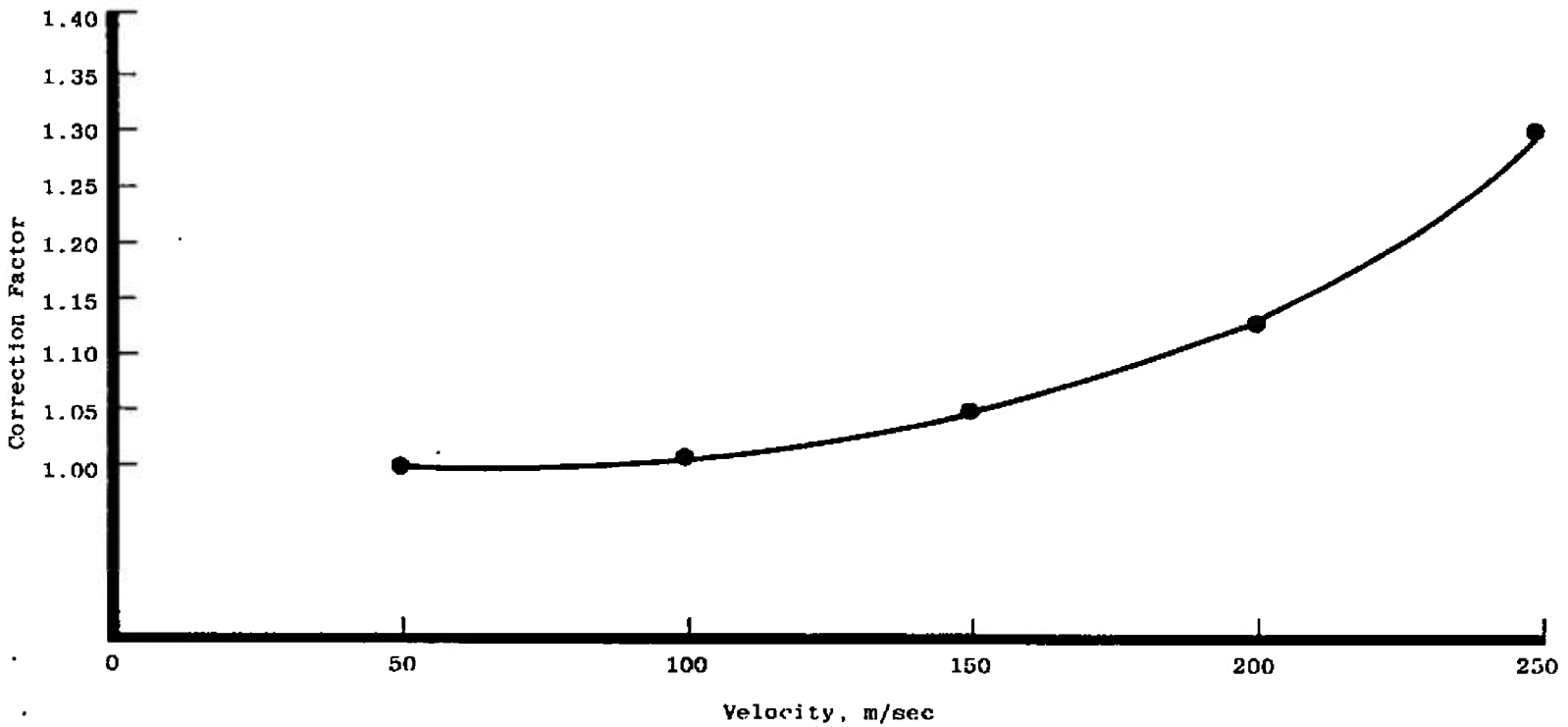

Figure 12. Model FSSP velocity correction factor curve.

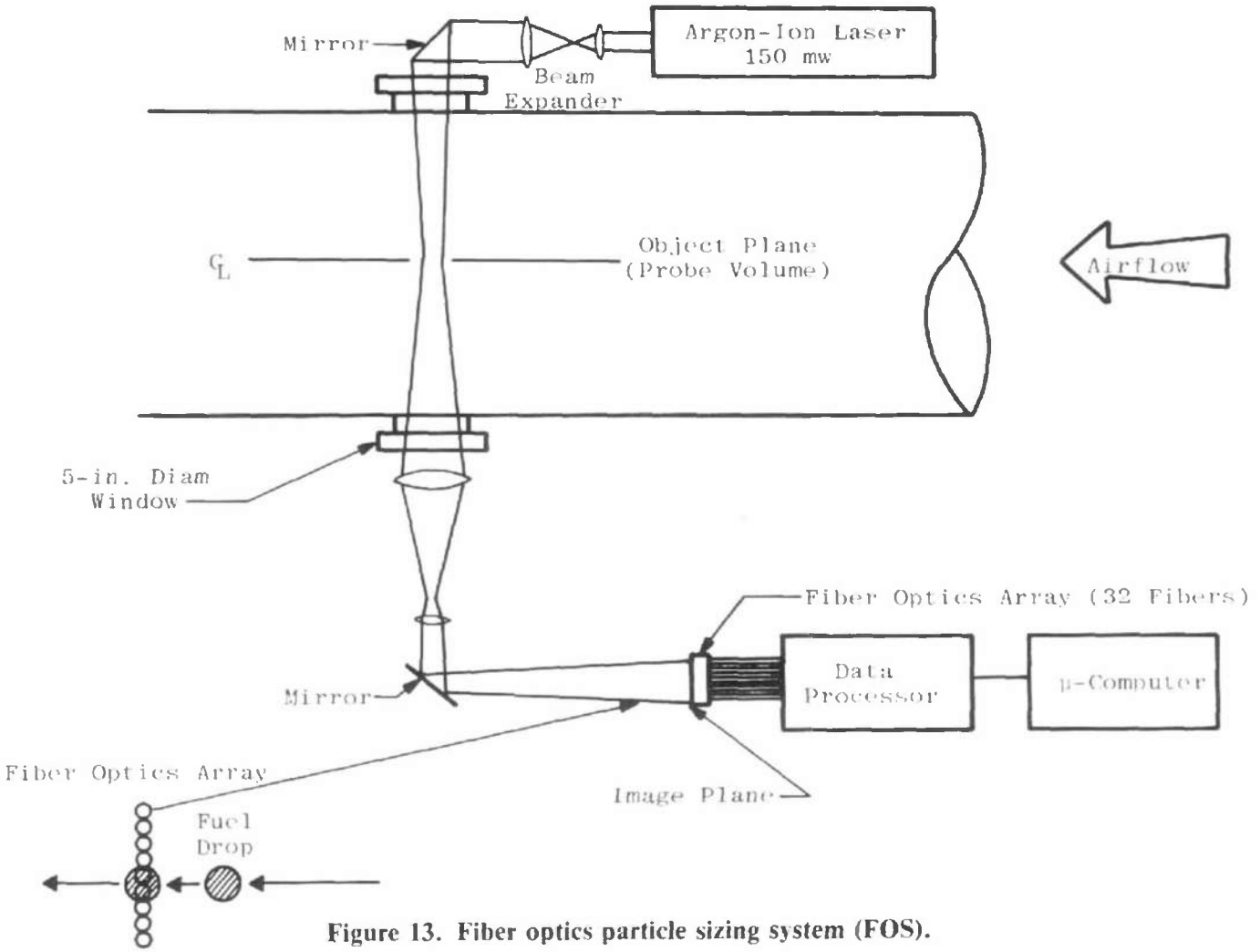

Figure 13. Fiber optics particle sizing system (FOS).

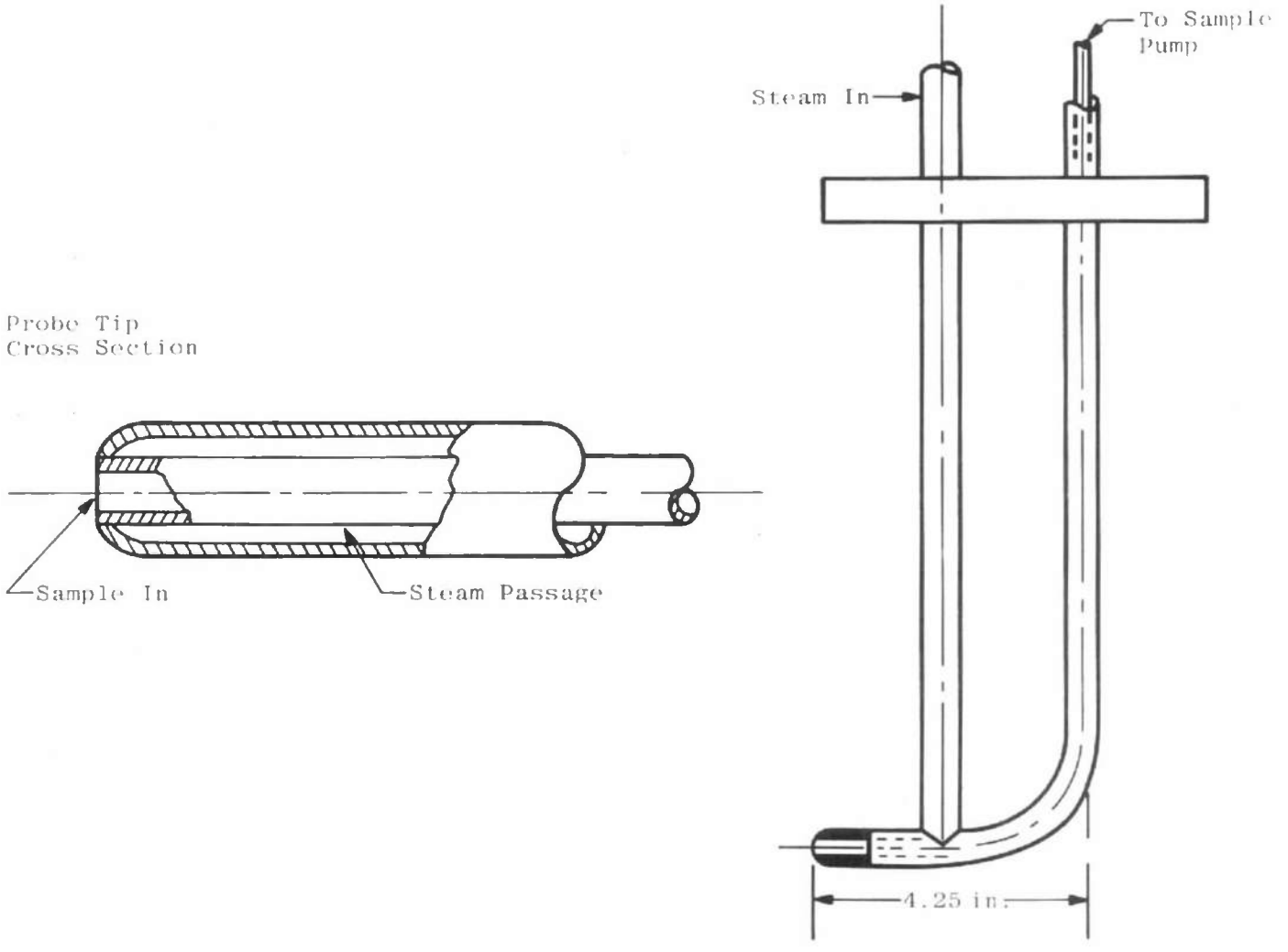

Figure 14. Fuel mass sampling probe.

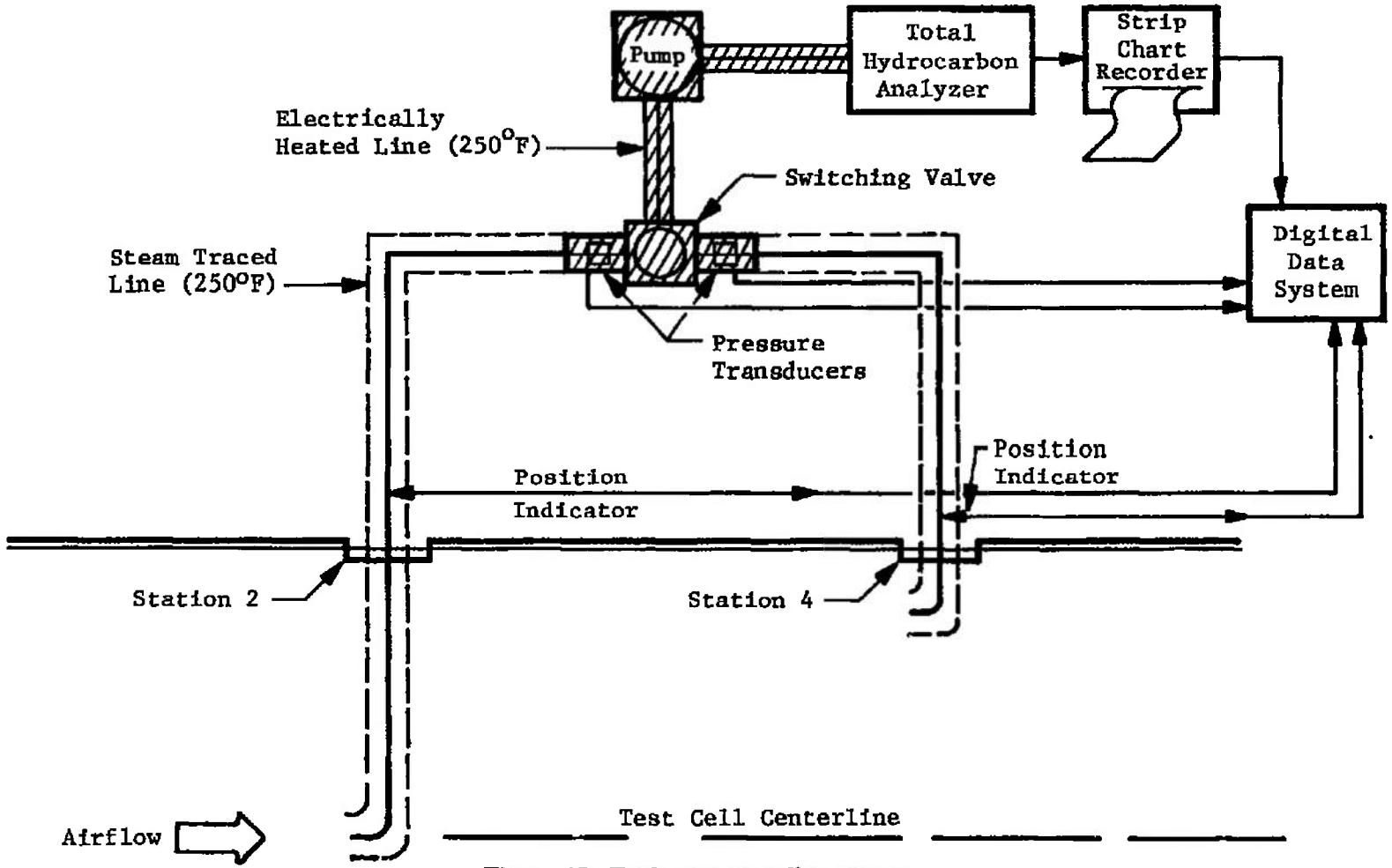

Figure 15. Fuel mass sampling system.

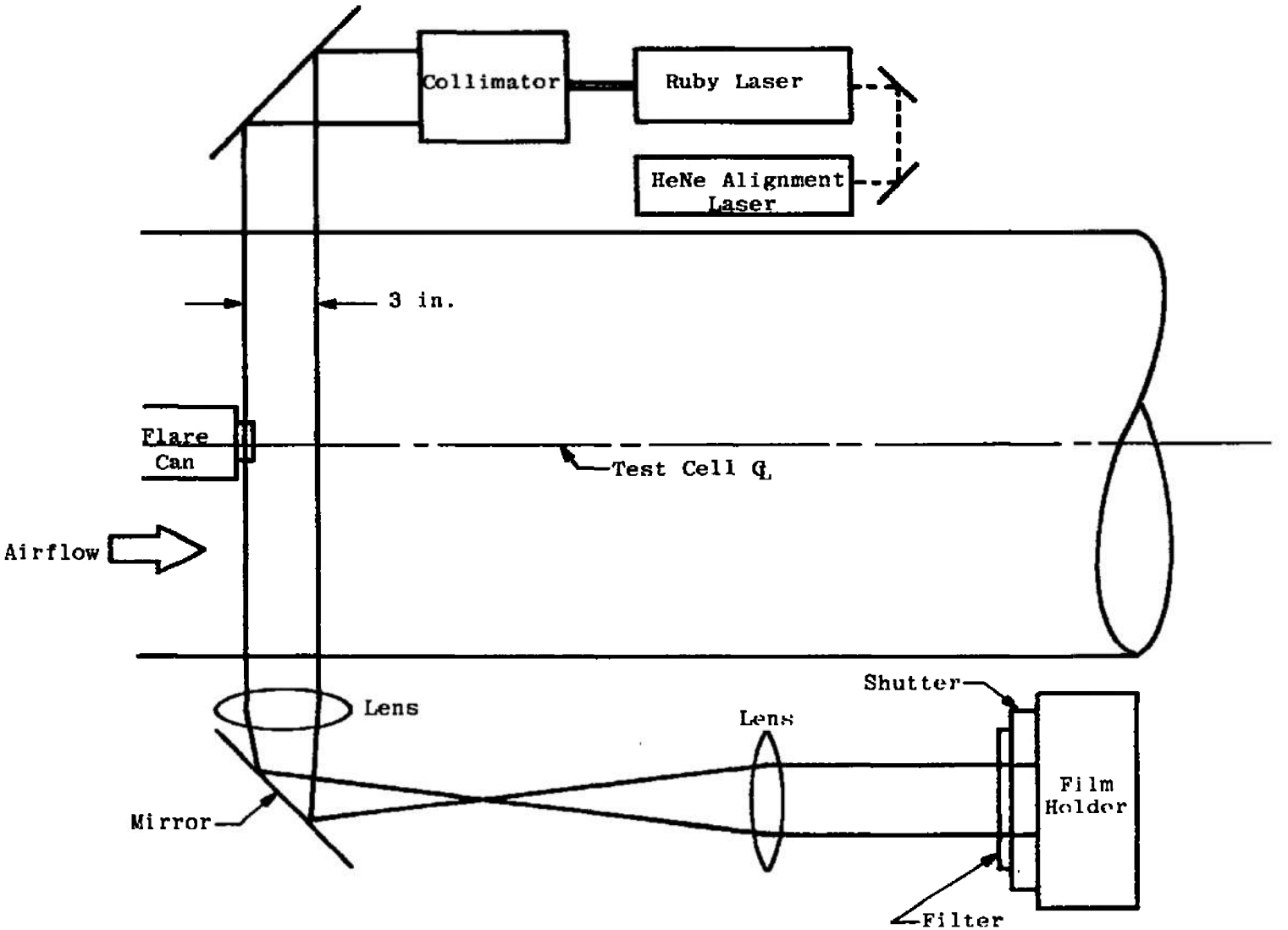

Figure 16. Pulsed laser camera system.

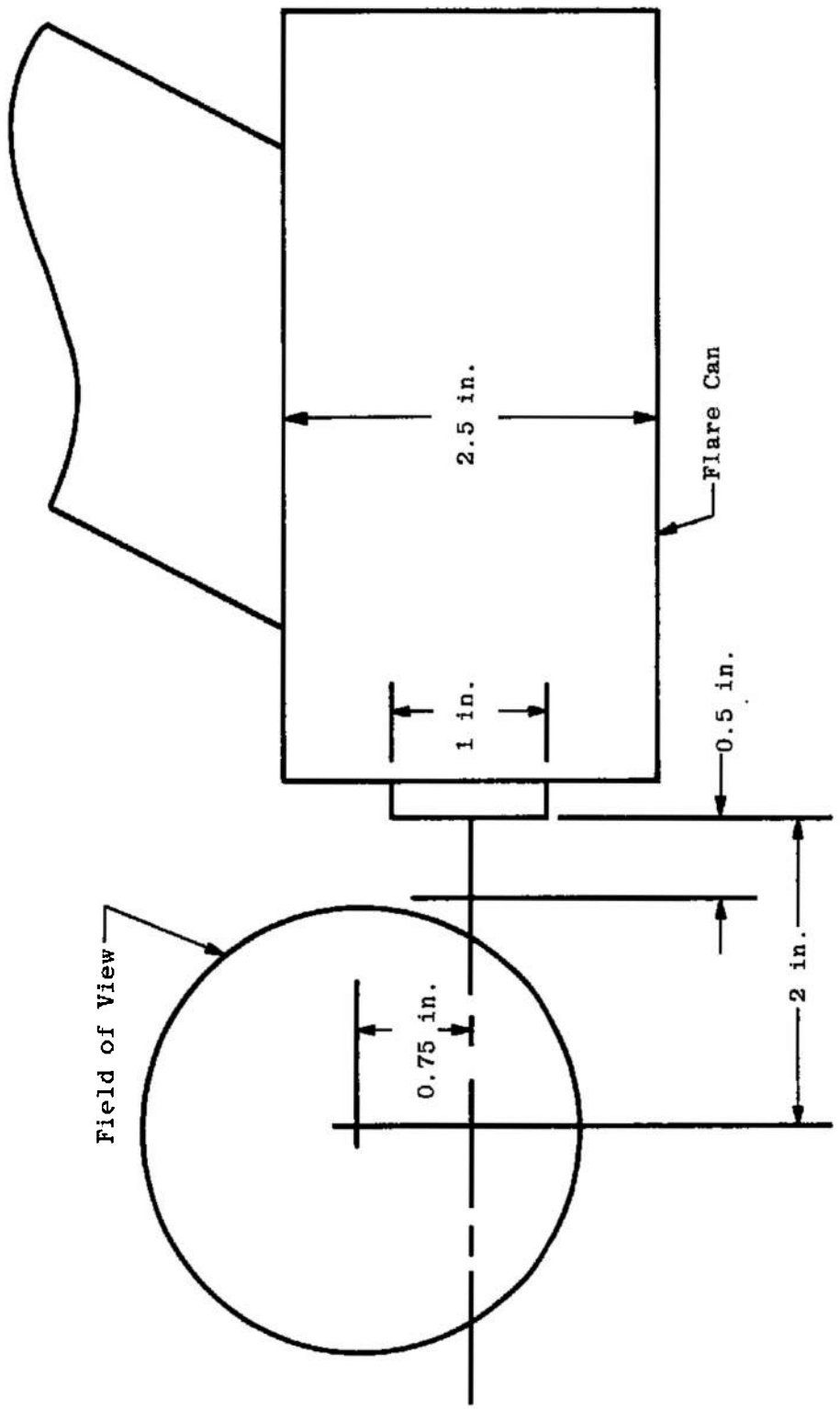

Figure 17. Laser camera field-of-view, Test 2.

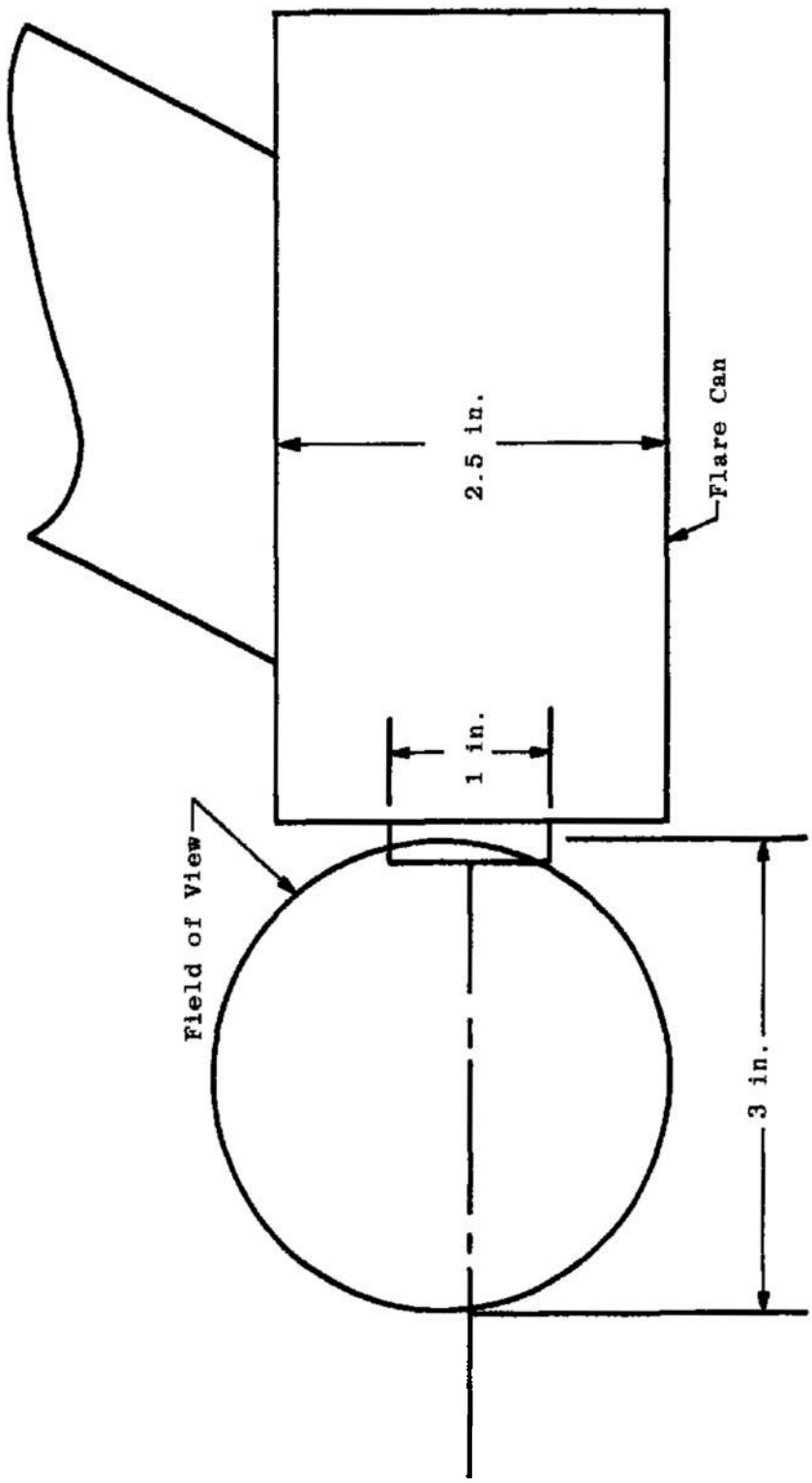

Figure 18. Laser camera field-of-view, Tests 3, 4, and 5.

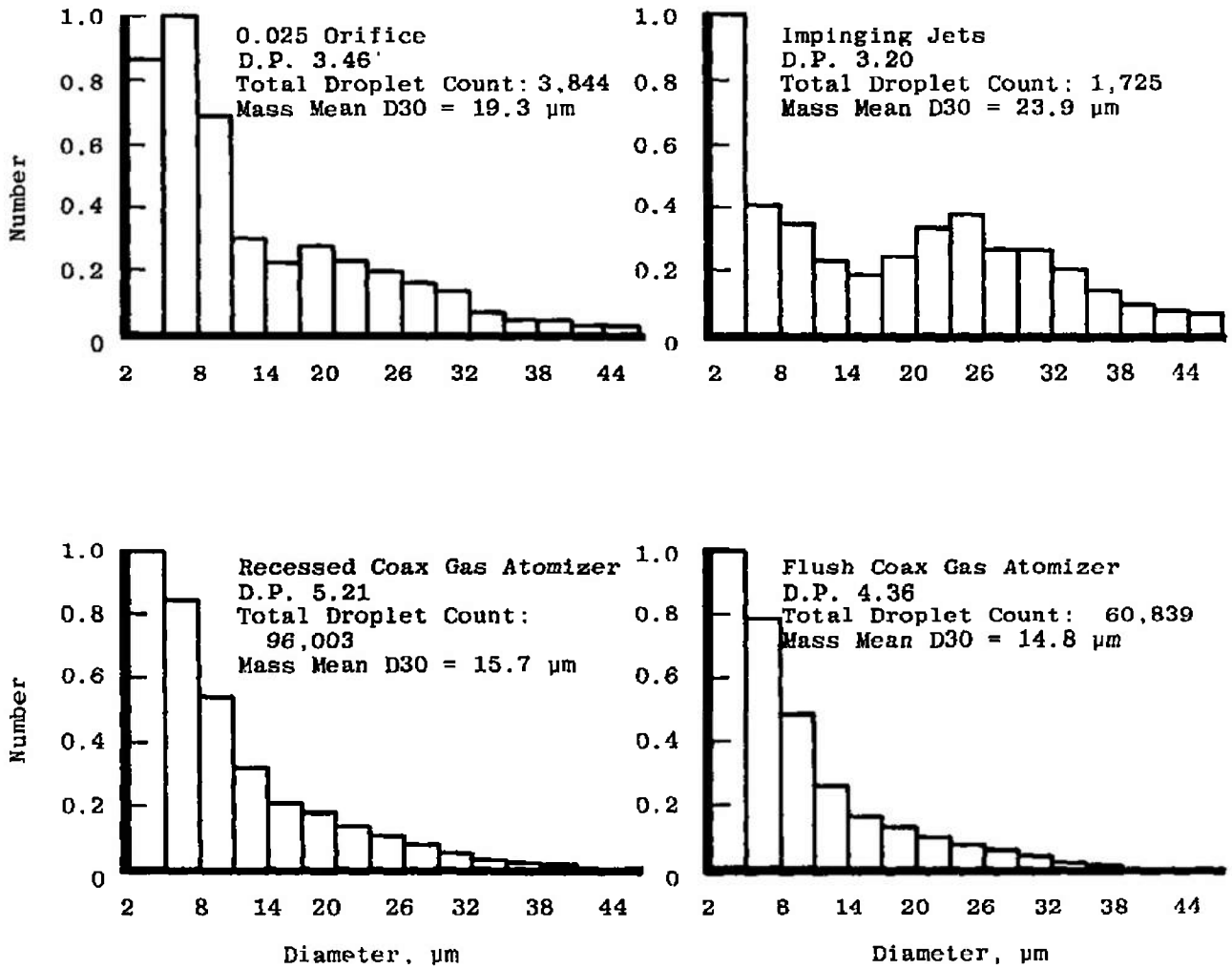

Figure 19. Size distributions recorded by Model FSSP under low tunnel velocity conditions, hydraulic versus pneumatic nozzles.

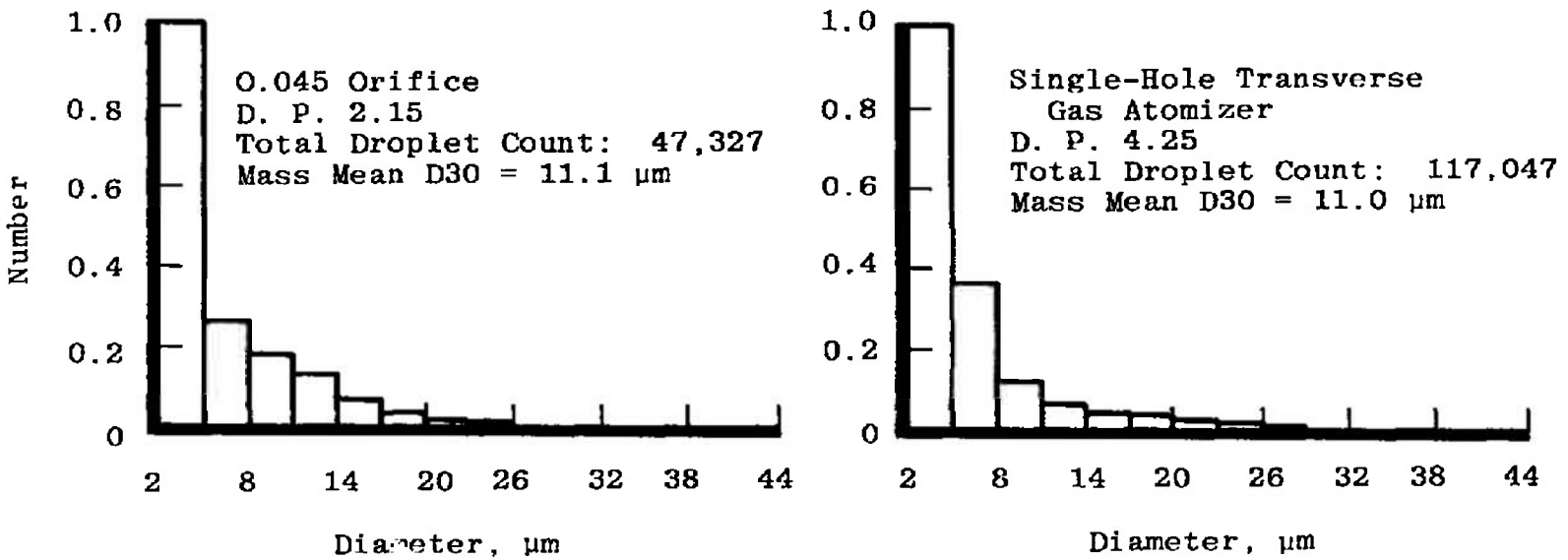

Figure 20. Size distributions recorded by Model FSSP under high tunnel velocity conditions.

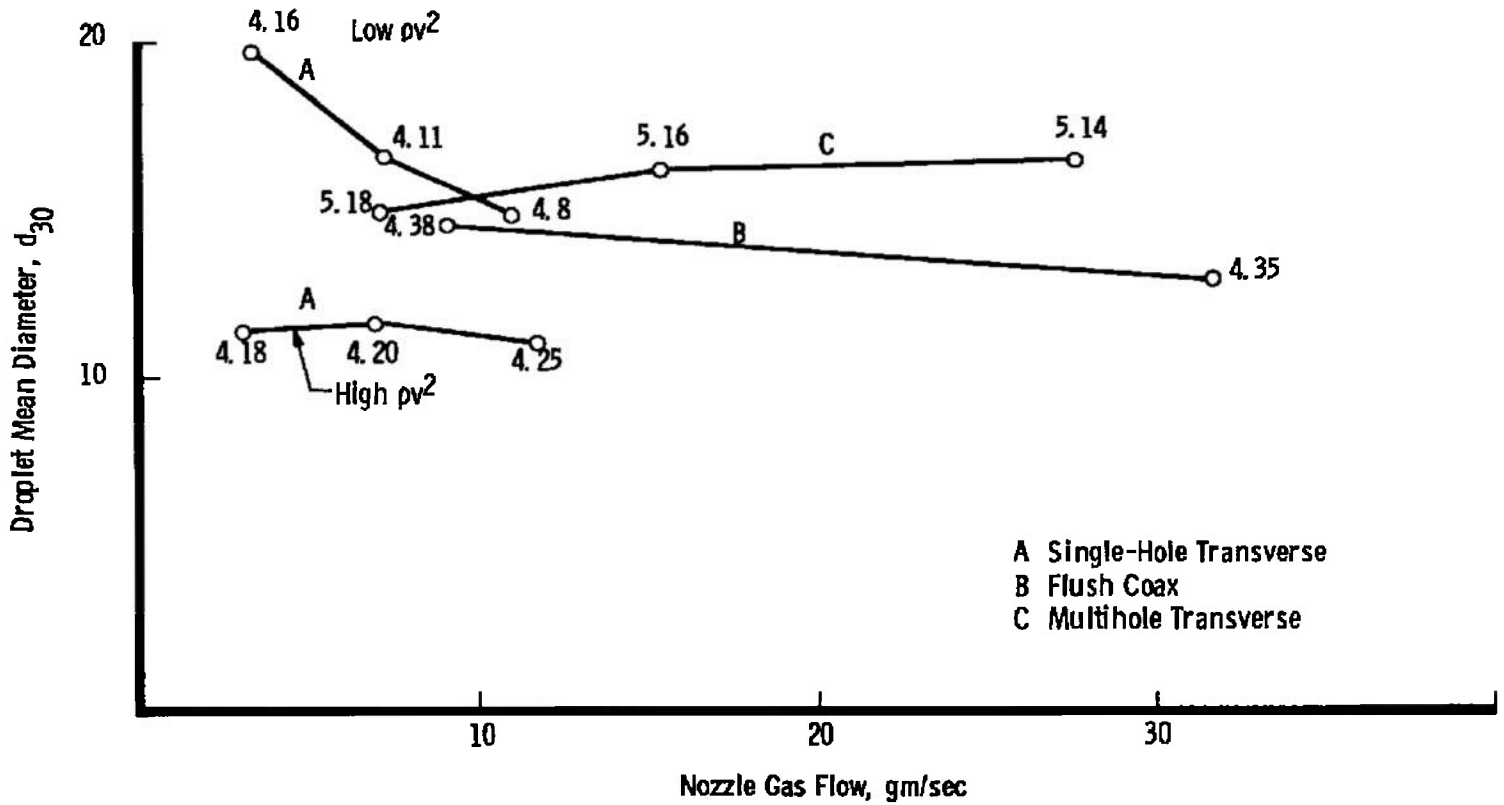

a. High fuel flow

Figure 21. Effect of nozzle gas flow rate on droplet mass mean diameter d_{30}.

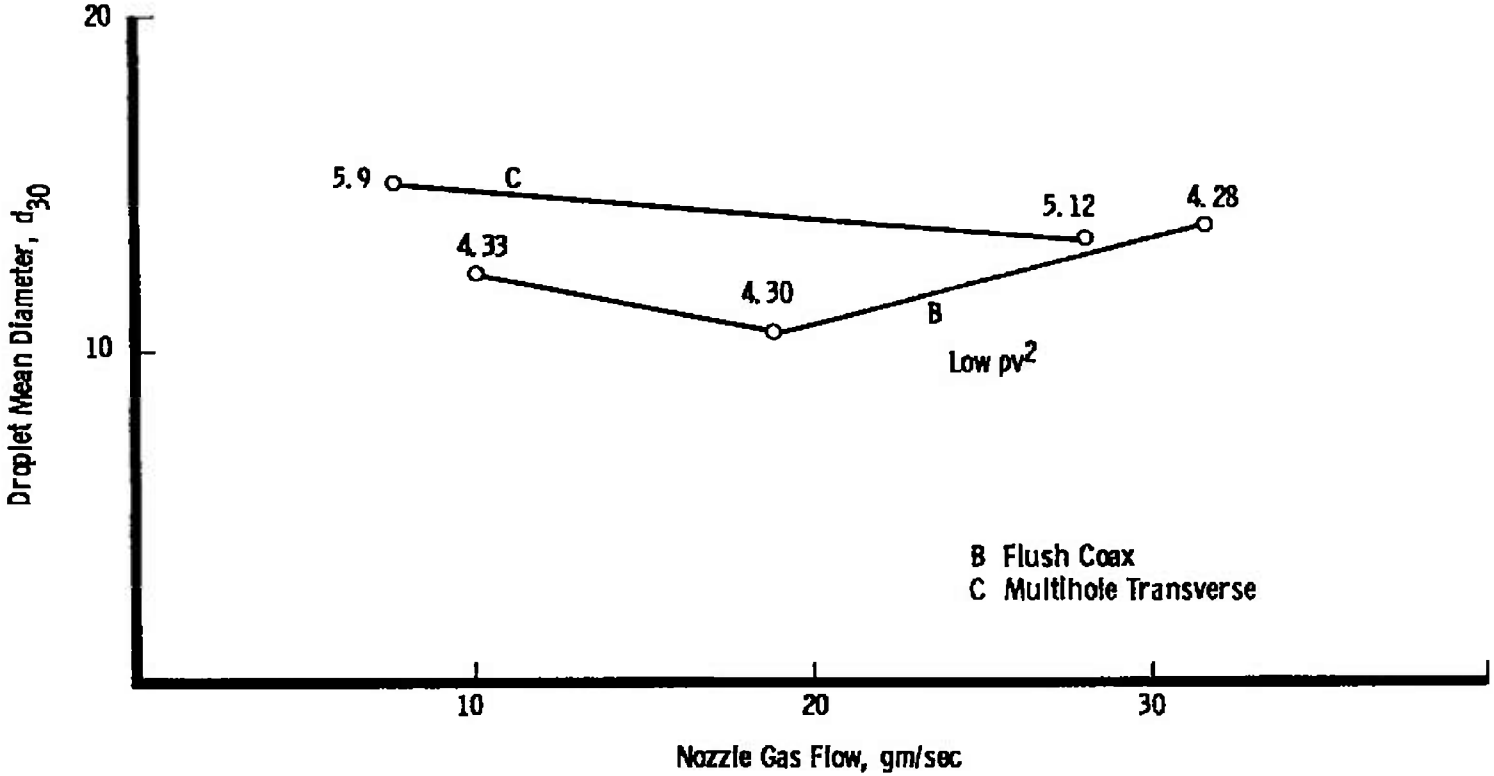

b. Low fuel flow

Figure 21. Concluded.

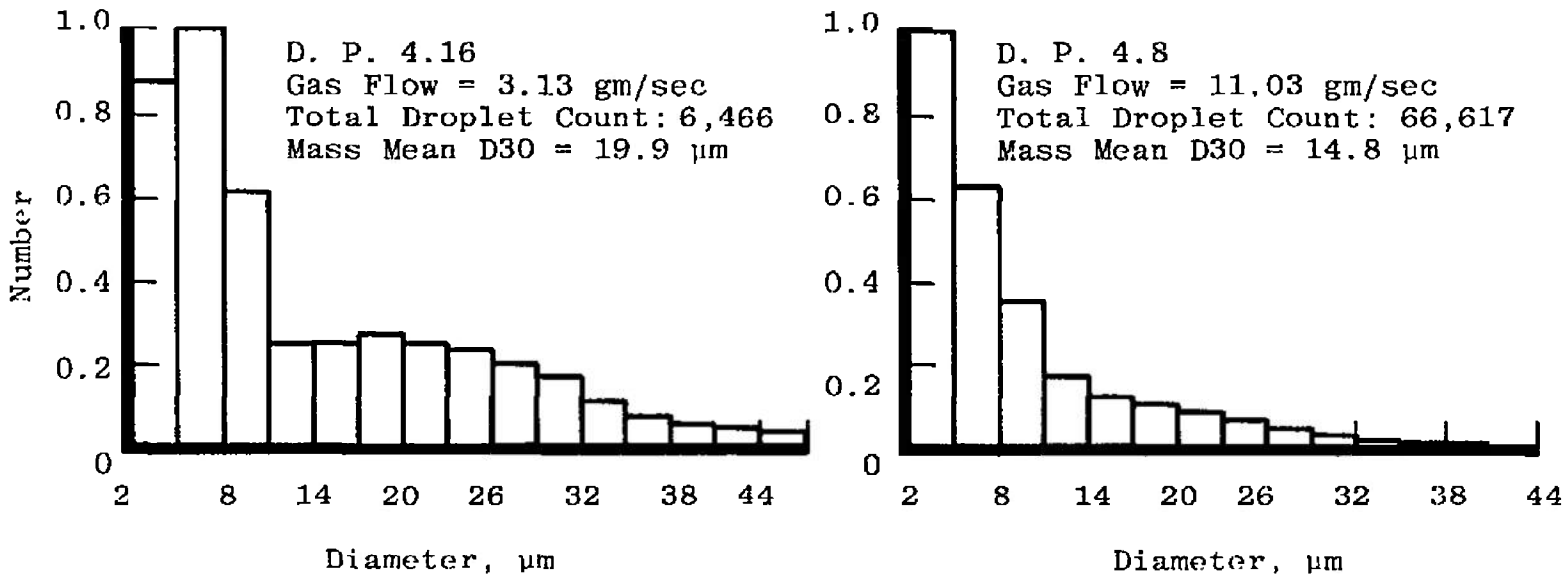

a. Inadequate gas flow **b. Adequate gas flow**

Figure 22. Effect of nozzle gas flow to single-hole transverse gas atomizer nozzle, low tunnel velocity conditions.

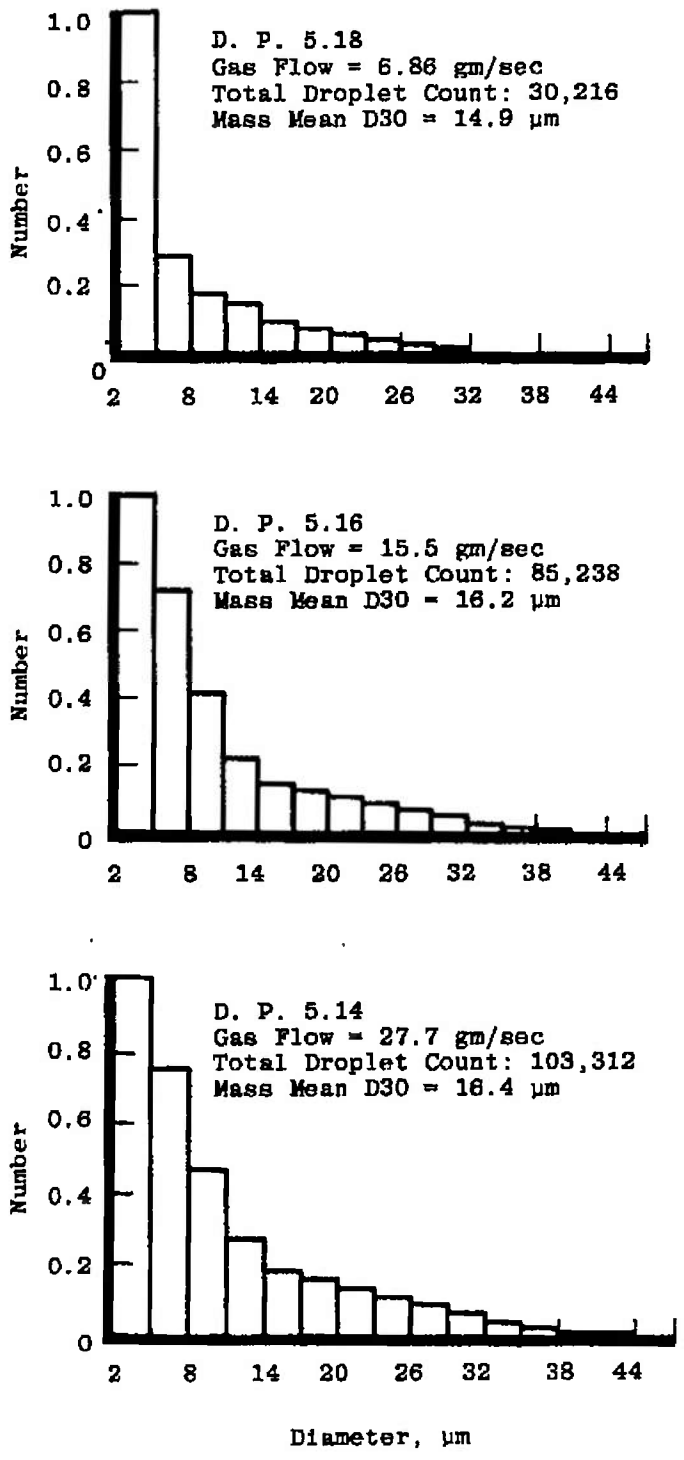

Figure 23. Effect of nozzle gas flow to multihole transverse nozzle, recorded by Model FSSP.

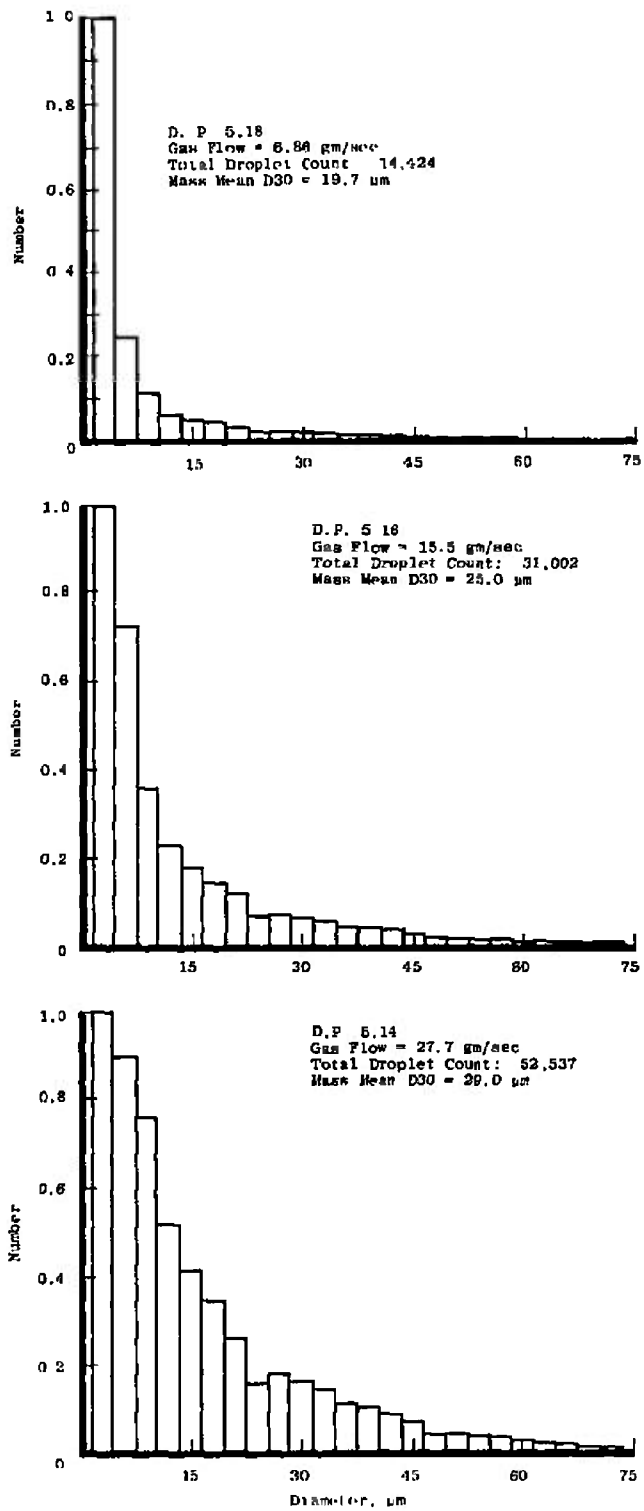

Figure 24. Effect of nozzle gas flow to multihole transverse nozzle, recorded by FOS sizer.

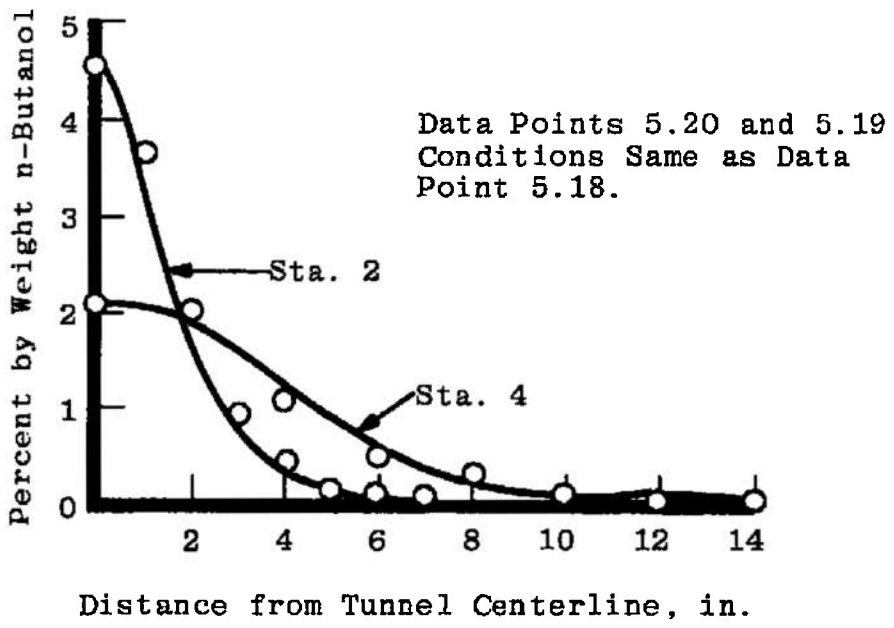

Figure 25. Dispersion of spray from Station 2 to Station 4: n-butyl alcohol mass concentration radial profiles.

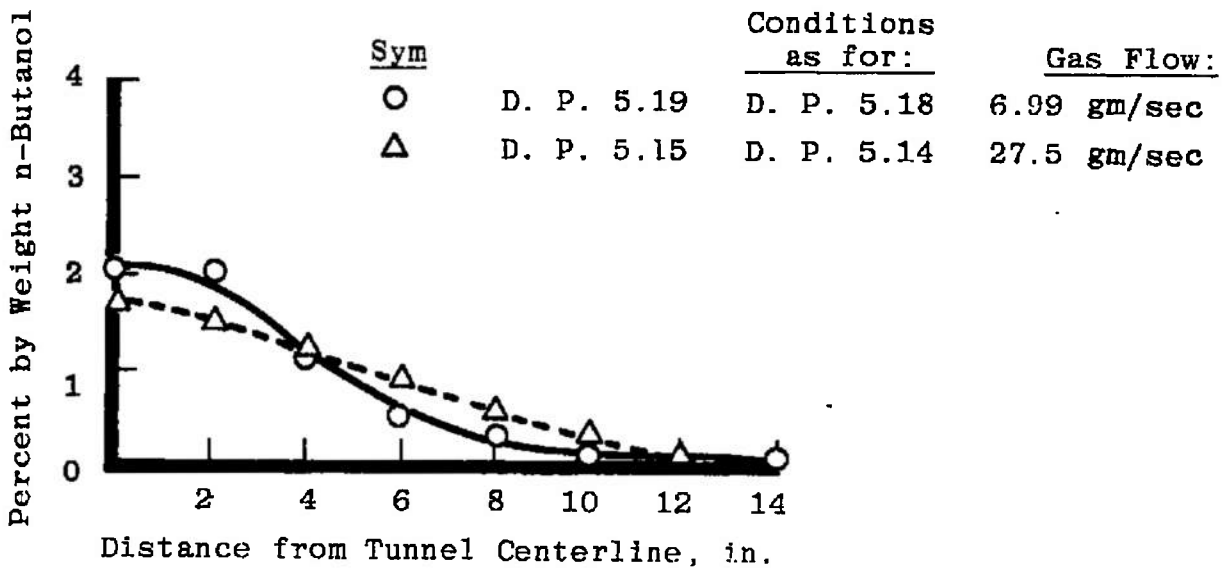

Figure 26. Dispersion of spray for different nozzle gas flows, Station 4.

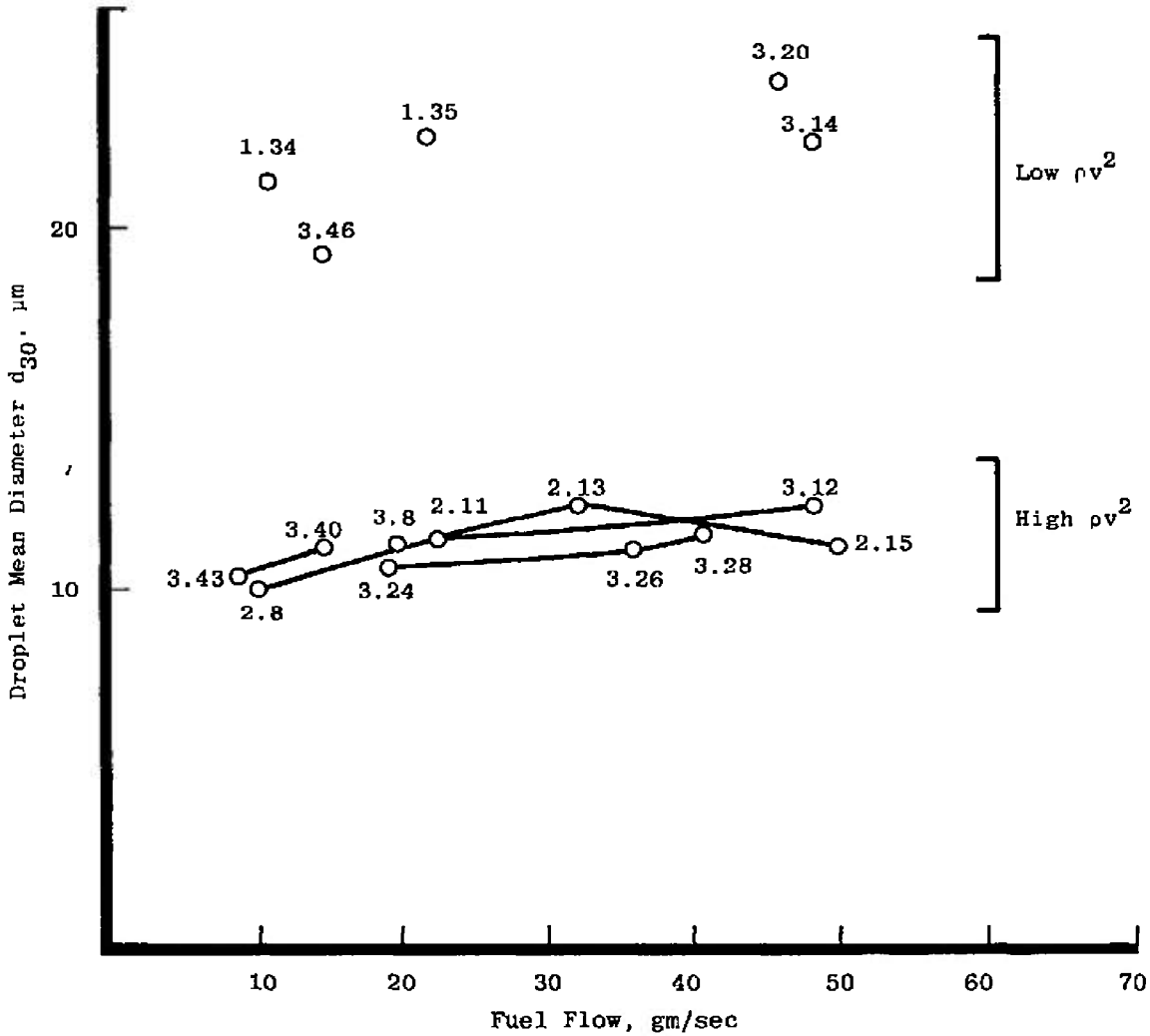

a. Hydraulic nozzles

Figure 27. Effect of nozzle fuel flow rate on droplet mass mean diameter d_{30}.

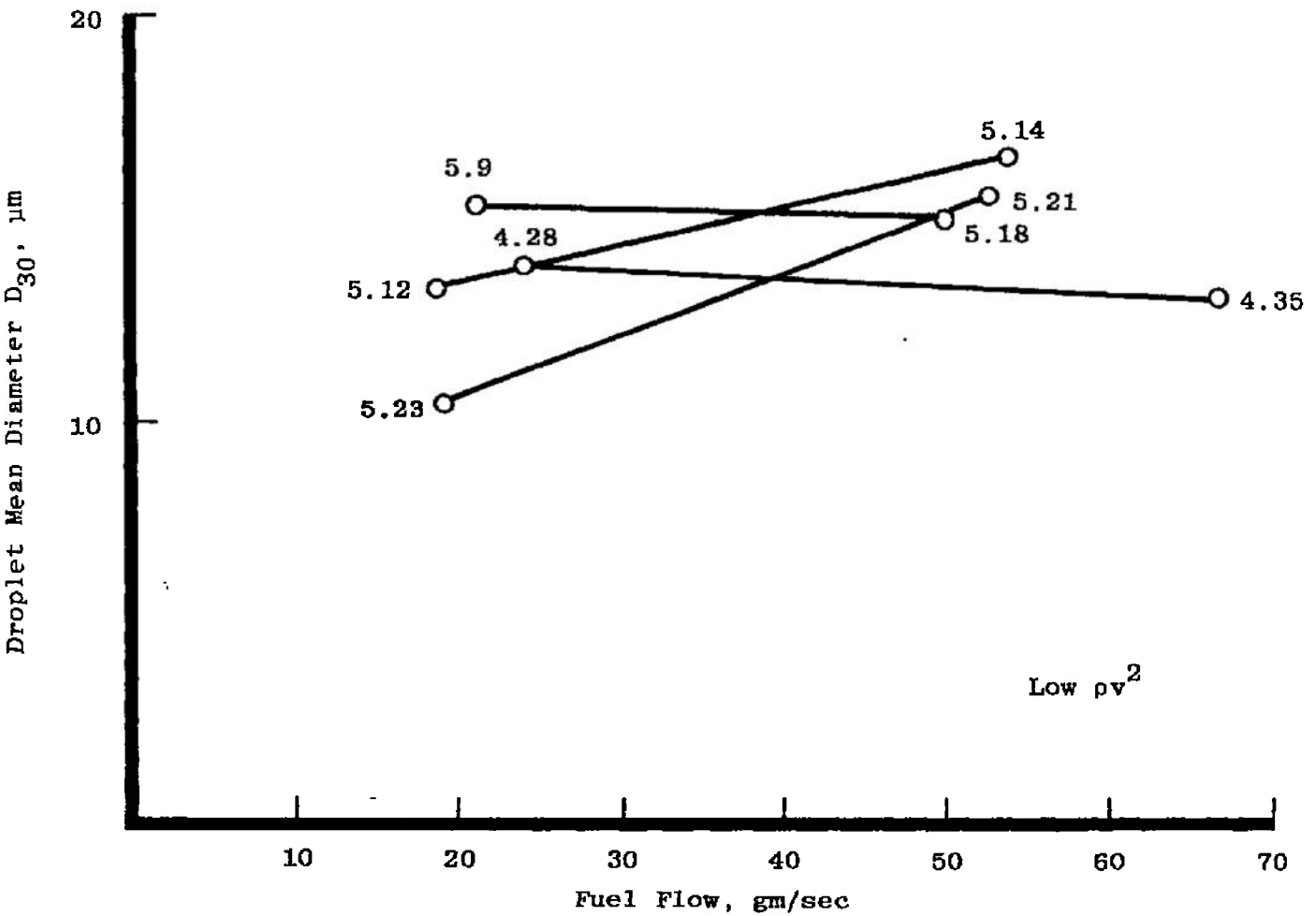

b. Pneumatic nozzles

Figure 27. Concluded.

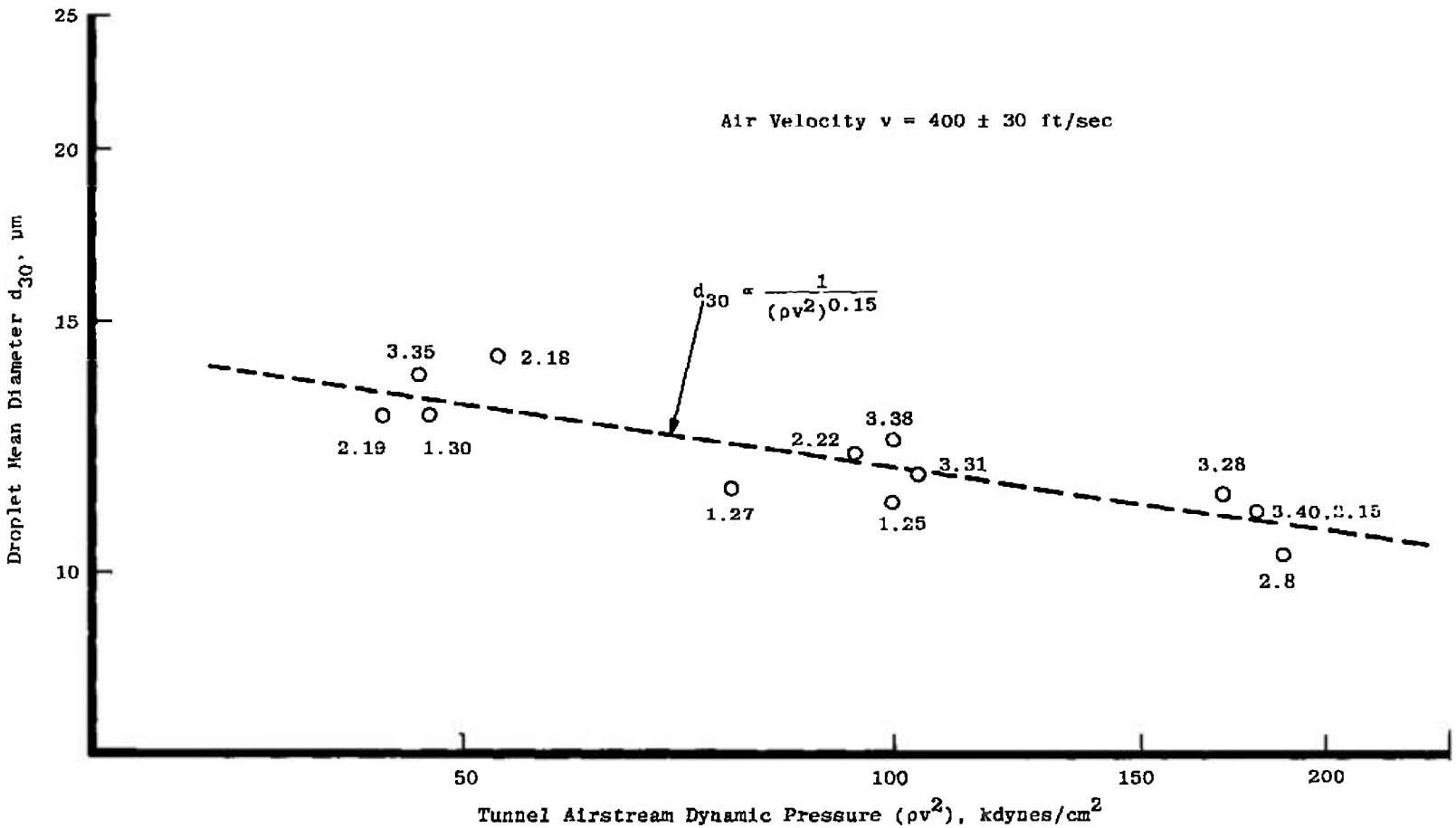

Figure 28. Effect of tunnel airstream dynamic pressure on droplet mass mean diameter d_{30}, constant velocity.

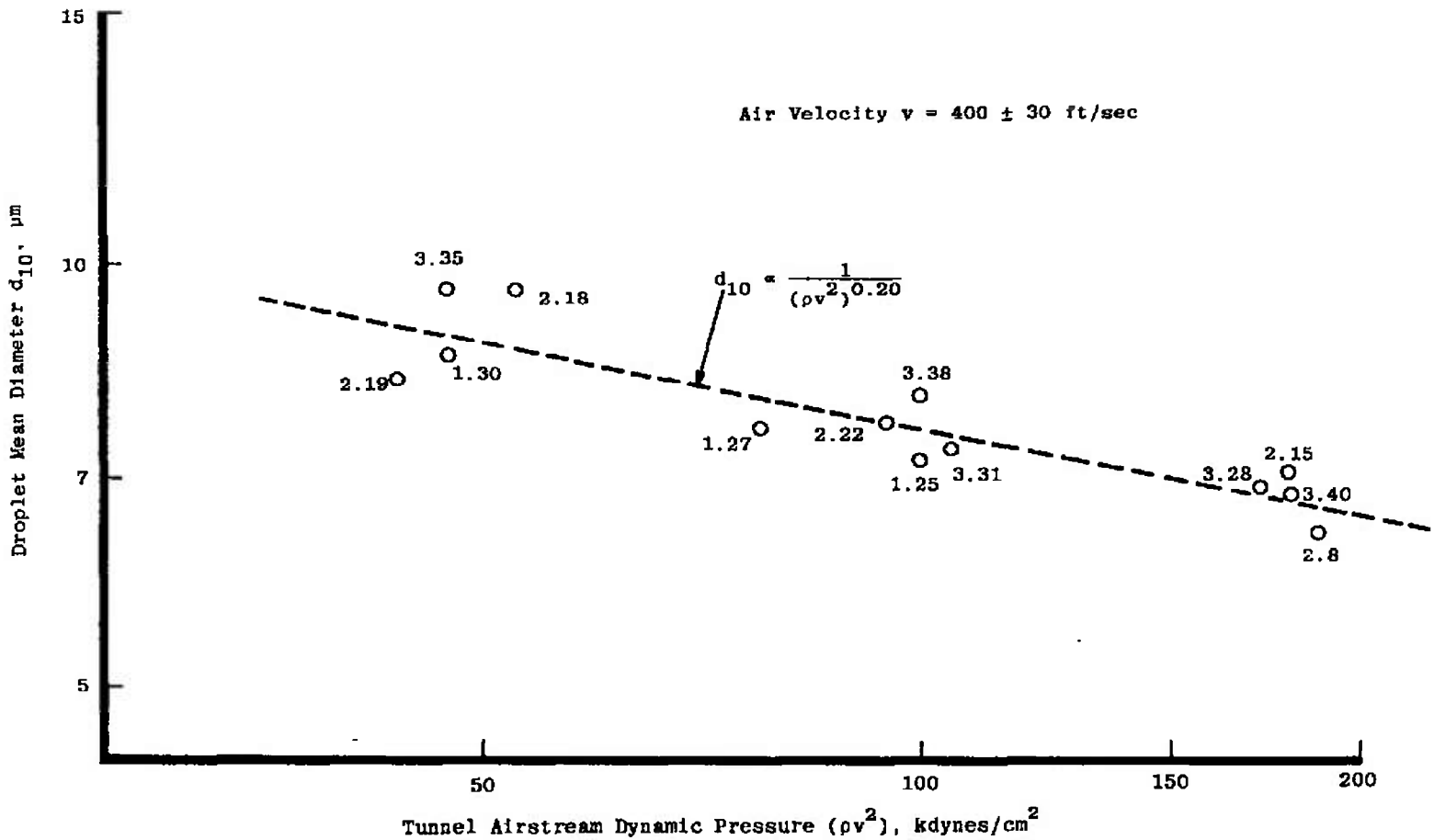

Figure 29. Effect of tunnel airstream dynamic pressure on droplet arithmetic mean diameter d_{10}, constant velocity.

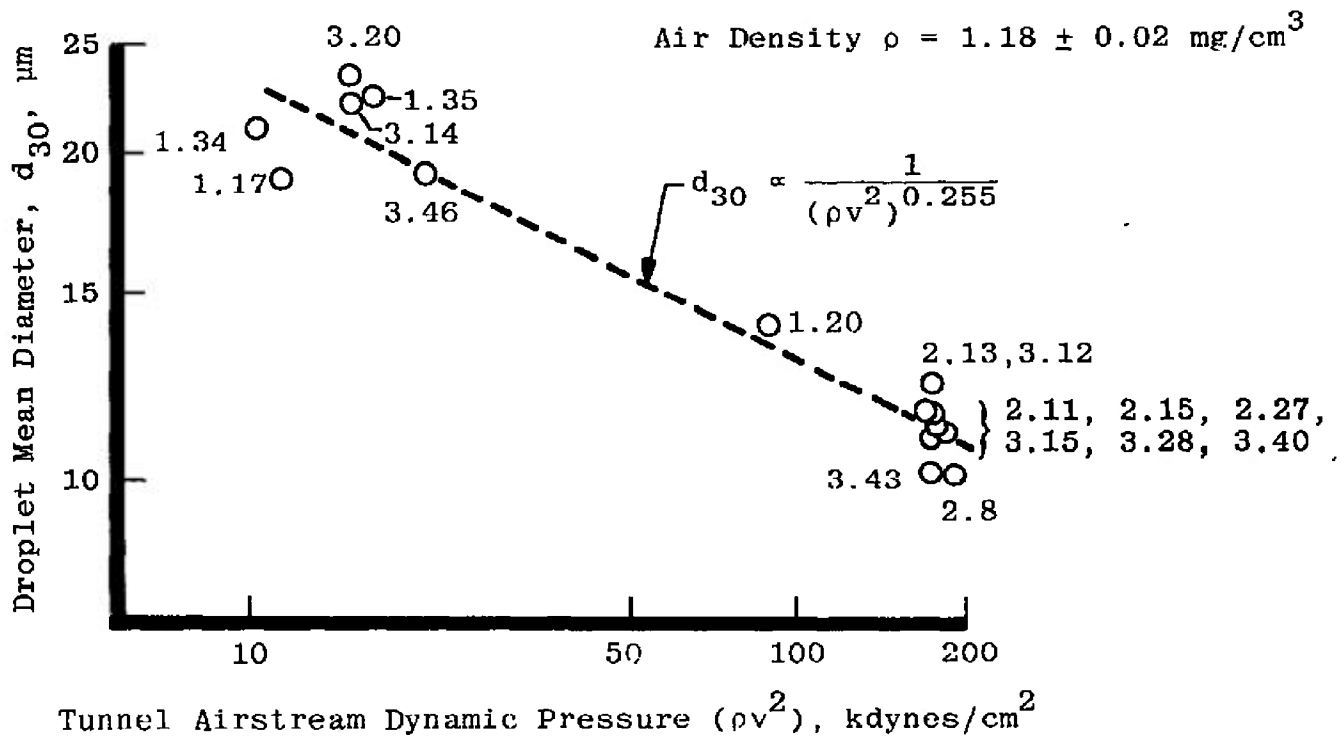

Figure 30. Effect of tunnel airstream dynamic pressure on droplet mass mean diameter d_{30}, constant air density.

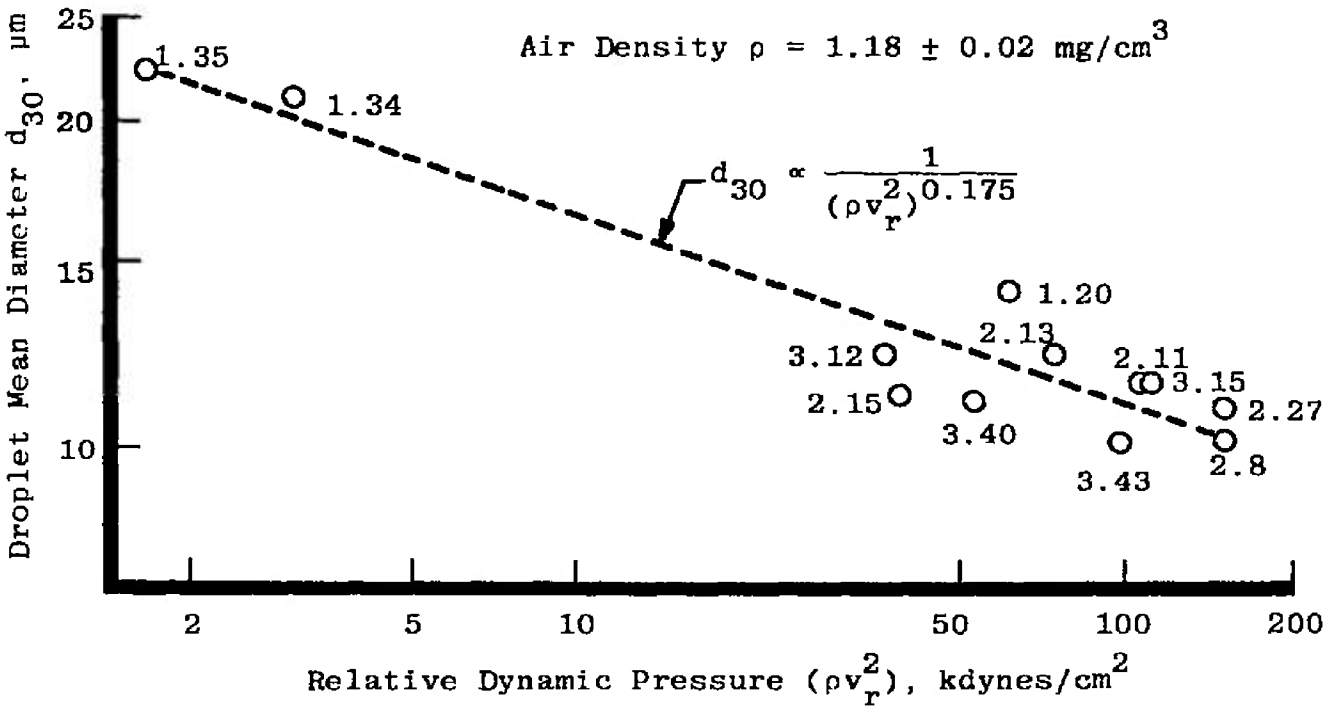

Figure 31. Effect of tunnel airstream dynamic pressure relative to fuel injection velocity on droplet mass mean diameter d_{30}, constant air density.

Table 1. Comparison of Physical Properties of N-Butyl Alcohol and TMA/TEA Mixtures at 20°C

	Density, gm/cm^3	Surface Tension, dynes/cm	Viscosity, centipoise
60/40 TMA/TEA	0.799	24.7	1.40
50/50 TMA/TEA	0.796	25.0	1.45
N-Butyl Alcohol	0.810	24.6	2.95

Table 2. Instrumentation Locations

Instrument	Station	Axial Location, ft
PMS, Inc. FSSP Single Particle Sizer	6	15
AEDC Fiber Optics System (FOS) Single Particle Sizer	5	12
Laser Extinction (Attenuation) Measurement and Orthogonal Photography	2,4	2.5,8.5
Fuel Mass Sampling System	2,4	2.5,8.5
Pulsed Laser Photography	1	At nozzle

Table 3. Data Point Summary

Type Nozzle	Test Data Pt.	Air Velocity, ft/sec	Altitude, ft	Total Air Temp., °F	Dyn. Air Press. qv^2, kdynes/cm^2	Fuel Flow, gm/sec	Fuel Temp. °F	Fuel Press., psi	Nozzle Gas Flow, gm/sec	Nozzle Gas Press., psi	Spray Droplet Mean Diam., Microns d_{30}	Spray Droplet Mean Diam., Microns d_{32}	Spray Width*, in. Stn 2	Spray Width*, in. Stn 4
0.025-in. Orifice	1.14	113	4,953	60	12.2	9.08	−3	422			21.5	28.5	—	
	1.15	112	4,958	61	11.9	9.08	−6	422			—	—	—	7.1
	1.16	111	4,955	61	11.9	9.08	−9	423			—	—	1.4	—
	1.17	103	4,954	−1	11.5	8.63	−12	423			18.9	26.9	—	—
	1.18	108	4,967	0	12.5	8.17	−5	423			—	—	—	11.2
0.045-in. Orifice	1.20	281	5,022	5	84.3	11.3	6	29			13.9	21.0	—	—
	1.21	275	4,960	0	82.1	11.3	6	29			—	—	2.9	—
	1.22	275	4,982	0	82.0	11.3	4	29			—	—	—	11.1
	1.23	438	20,274	61	102.7	10.9	6	30			12.8	18.1	—	—
	1.24	435	20,174	61	101.4	11.3	10	30			—	—	—	10.8
	1.25	407	20,036	0	100.4	11.3	2	30			11.3	17.4	—	—
	1.26	410	20,112	0	101.7	11.3	−2	30			—	—	—	10.9
	1.27	430	28,971	2	76.3	12.3	0	30			11.7	17.5	—	—
	1.28	426	28,813	0	75.6	11.8	−4	30			—	—	—	8.8
	1.29	425	28,818	2	74.8	12.3	0	30			—	—	2.2	—
	1.30	388	34,945	2	46.5	12.3	3	30			12.8	18.3	—	—
	1.31	384	34,916	0	45.8	12.7	2	30			—	—	—	8.8
	1.32	406	5,047	1	181.1	11.3	−1	30			—	—	—	14.7
	1.33	404	5,014	−2	180.5	11.3	−5	30			—	—	—	—
	1.34	98	5,029	4	10.1	11.3	4	30			21.3	28.4	—	—

*Full width at half-maximum.

Table 3. Continued

Type Nozzle	Test Data Pt.	Air Velocity, ft/sec	Altitude, ft	Total Air Temp., °F	Dyn. Air Press. ρv^2, kdynes/cm^2	Fuel Flow, gm/sec	Fuel Temp. °F	Fuel Press., psi	Nozzle Gas Flow, gm/sec	Nozzle Gas Press., psi	Spray Droplet Mean Diam., Microns d_{30}	Spray Droplet Mean Diam., Microns d_{32}	Spray Width*, in. Stn 2	Spray Width*, in. Stn 4
0.045-in. Orifice	1.35	124	5,024	−1	16.6	21.8	0	88			22.4	26.4	—	—
	2.8	415	5,045	8	186.8	10.0	4	28			10.1	15.5	—	—
	2.9	403	5,008	0	179.6	10.0	0	28			—	—	—	13.6
	2.10	390	5,047	−3	168.8	9.5	−4	28			—	—	4.3	—
	2.11	393	5,045	−1	170.7	21.8	−10	88			11.5	17.6	—	—
	2.12	394	4,987	−6	174.0	21.8	−10	88			—	—	—	11.0
	2.13	397	5,058	1	172.9	31.8	−9	167			12.2	18.6	—	—
	2.14	392	4,913	−2	170.5	31.8	−10	167			—	—	—	10.3
	2.15	402	5,051	−2	179.6	49.9	−2	392			11.1	16.6	—	—
	2.17	399	5,013	−1	176.4	49.9	−3	391			—	—	—	7.7
	2.18	412	35,301	0	52.2	51.2	1	405			14.4	20.4	—	—
0.089-in. Orifice	2.19	370	34,816	−2	43.2	48.6	0	38			13.0	19.4	—	—
	2.20	369	34,815	−2	42.9	49.2	−2	38			—	—	—	7.2
	2.21	370	34,803	−3	43.3	49.5	−1	38			—	—	4.5	—
	2.22	393	19,941	1	94.2	50.9	−3	43			12.3	18.8	—	—
	2.23	394	20,042	−1	95.2	49.5	−9	43			—	—	—	10.5
	2.24	398	5,004	3	173.3	49.5	−19	53			—	—	—	—
	2.25	395	4,960	−3	173.3	51.8	−14	53			—	—	—	12.4
	2.26	395	5,000	0	172.2	51.3	−13	53			—	—	4.9	—
	2.27	399	4,978	1	175.0	30.4	−17	32			10.9	17.1	—	—
	2.28	397	5,064	−7	176.5	31.0	−16	32			—	—	—	13.3
	2.29	387	5,079	−6	167.3	31.9	−12	31			—	—	4.4	—
	2.30	456	28,145	−1	90.2	41.4	−1	30			11.4	17.7	—	—

*Full width at half-maximum.

Table 3. Continued

Type Nozzle	Test Data Pt.	Air Velocity, ft/sec	Altitude, ft	Total Air Temp., °F	Dyn. Air Press. qv^2, kdynes/cm^2	Fuel Flow, gm/sec	Fuel Temp. °F	Fuel Press., psi	Nozzle Gas Flow, gm/sec	Nozzle Gas Press., psi	Spray Droplet Mean Diam., Microns d_{30}	Spray Droplet Mean Diam., Microns d_{32}	Spray Width*, in. Stn 2	Spray Width*, in. Stn 4
0.045-in. Orifice,	3.7	437	5,003	76	180.4	19.9	30	98			12.9	18.5	—	—
Sharp edge	3.8	402	4,994	14	173.4	19.7	14	99			11.2	17.4	—	—
	3.9	389	4,998	0	166.2	19.8	15	98			—	—	—	—
	3.10	380	5,000	0	159.0	19.8	13	97			—	—	3.3	—
	3.11	377	4,995	0	155.9	19.9	12	98			—	—	—	12.6
	3.12	392	5,001	−1	169.5	48.1	7	468			12.2	17.6	—	—
	3.13	102	5,020	1	11.1	48.1	3	468			—	—	—	7.7
	3.14	118	5,043	5	14.7	48.1	−1	468			22.3	29.0	—	—
	3.15	398	5,065	−1	174.9	19.4	−8	95			11.5	17.8	—	—
	3.16	386	5,079	0	163.9	19.1	6	92			—	—	—	10.1
	3.17	373	5,099	4	150.5	48.1	−7	465			14.9	21.2	—	—
	3.18	381	5,077	−2	159.9	48.1	−9	465			—	—	—	8.4
	3.19	388	4,976	0	165.4	46.3	−19	465			—	—	—	—
Impinging Jets	3.20	117	5,074	17	14.2	45.9	−11	141			23.9	30.5	—	—
	3.21	117	5,071	7	14.5	48.6	−26	149			—	—	—	—
	3.22	112	5,067	1	13.4	48.6	−2	149			—	—	—	10.4
	3.23	81	4,980	21	6.8	19.0	−8	40			—	—	3.8	—
	3.24	397	5,071	3	172.4	18.7	−3	38			10.7	16.9	—	—
	3.25	395	5,021	0	171.8	17.7	−6	37			—	—	—	16.0
	3.26	407	5,086	9	178.7	36.2	−8	86			11.2	17.6	—	—
	3.27	404	5,062	2	178.3	35.7	−12	86			—	—	—	13.4

*Full width at half-maximum.

Table 3. Continued

Type Nozzle	Test Data Pt.	Air Velocity, ft/sec	Altitude, ft	Total Air Temp., °F	Dyn. Air Press. ρv^2, kdynes/cm^2	Fuel Flow, gm/sec	Fuel Temp. °F	Fuel Press., psi	Nozzle Gas Flow, gm/sec	Nozzle Gas Press., psi	Spray Droplet Mean Diam., Microns d_{30}	Spray Droplet Mean Diam., Microns d_{32}	Spray Width*, in. Stn 2	Spray Width*, in. Stn 4
Impinging Jets	3.28	395	5,057	4	170.3	40.6	−5	148			11.4	18.0	—	—
	3.29	396	5,058	2	172.3	40.6	−4	147			—	—	—	13.9
	3.30	393	5,137	−5	172.0	48.1	−10	147			—	—	5.1	—
	3.31	416	20,310	0	104.0	48.6	−8	147			11.9	18.4	—	—
	3.32	408	20,290	0	100.3	48.6	−5	147			—	—	—	12.0
	3.33	424	35,748	6	53.8	48.6	2	147			—	—	—	—
	3.34	415	35,715	−12	53.6	48.6	0	146			—	—	—	11.6
0.025-in. Orifice	3.35	385	35,118	1	46.0	14.9	7	448			13.9	19.1	—	—
	3.36	617	37,237	−7	112.6	14.8	4	447			10.3	16.1	—	—
	3.37	641	37,691	−1	118.8	14.9	−1	447			—	—	—	—
	3.38	405	20,193	−1	99.3	14.9	4	447			12.8	19.0	—	—
	3.39	405	20,117	−2	99.7	14.9	0	447			—	—	—	—
	3.40	409	5,083	10	180.3	14.7	8	447			11.0	17.1	—	—
	3.41	401	5,004	3	175.9	14.8	6	447			—	—	—	—
	3.42	399	5,088	−1	176.0	14.8	0	447			—	—	—	—
	3.43	400	5,068	3	174.8	7.9	10	169			10.1	15.8	—	—
	3.44	389	4,980	0	167.0	8.0	3	169			—	—	—	—
	3.45	67	4,989	41	4.6	7.9	22	169			—	—	—	—
	3.46	138	4,915	5	20.4	14.7	2	445			19.3	26.7	—	—
	3.47	127	4,964	8	17.2	14.8	−1	445			—	—	—	—

*Full width at half-maximum.

Table 3. Continued

Type Nozzle	Test Data Pt.	Air Velocity, ft/sec	Altitude, ft	Total Air Temp., °F	Dyn. Air Press. qv^2, kdynes/cm^2	Fuel Flow, gm/sec	Fuel Temp. °F	Fuel Press., psi	Nozzle Gas Flow, gm/sec	Nozzle Gas Press., psi	Spray Droplet Mean Diam., Microns d_{30}	Spray Droplet Mean Diam., Microns d_{32}	Spray Width*, in. Stn 2	Spray Width*, in. Stn 4
Gas atomizer, single-hole transverse	4.8	144	5,083	2	22.3	49.9	11	81.6	11.03	66.9	14.8	22.5	—	—
	4.10	128	5,086	3	17.5	49.9	10	81.5	11.03	66.7	—	—	—	11.6
	4.11	119	5,037	4	15.1	51.8	3	68.1	7.31	50.0	16.6	24.8	—	—
	4.12	118	5,099	−4	15.0	53.6	15	67.6	7.35	51.8	—	—	—	10.6
	4.15	118	5,043	0	15.1	51.8	3	67.9	7.26	50.0	—	—	4.5	—
	4.16	94	5,099	4	9.4	64.0	10	50.1	3.13	28.4	19.9	27.3	—	—
	4.17	121	5,078	−1	15.8	60.8	−1	50.6	3.18	27.2	—	—	—	11.1
	4.18	400	5,127	4	173.9	64.9	12	50.9	2.81	27.7	11.3	18.1	—	—
	4.19	386	5,029	−1	164.4	63.1	0	50.9	3.19	26.7	—	—	—	12.3
	4.20	383	5,078	−1	161.9	54.5	1	69.0	6.81	49.2	11.5	18.3	—	—
	4.21	369	5,107	−3	150.2	53.1	0	68.9	6.81	48.7	—	—	—	10.2
	4.22	362	5,202	−1	151.3	55.8	12	68.1	6.94	50.7	—	—	4.7	—
	4.23	445	5,008	92	181.7	45.4	1	80.8	11.35	65.9	11.7	16.9	—	—
	4.25	371	5,181	−2	153.1	47.2	16	80.3	11.80	67.6	11.0	17.4	—	—
	4.27	376	4,965	1	155.1	45.4	7	81.8	11.80	66.5	—	—	—	—
Gas atomizer, flush coaxial	4.28	122	5,063	1	16.0	24.1	8	64.9	31.78	50.2	13.8	19.5	—	—
	4.29	107	5,053	−2	12.4	21.8	16	64.9	31.78	50.0	—	—	—	—
	4.30	112	5,054	−2	13.6	19.5	22	49.2	19.07	29.7	10.5	17.2	—	—
	4.31	112	5,037	−2	13.6	21.3	13	46.7	19.07	29.6	—	—	—	13.1
	4.32	110	5,047	−2	13.2	21.8	15	46.5	19.07	29.5	—	—	4.5	—

*Full width at half-maximum.

Table 3. Continued

Type Nozzle	Test Data Pt.	Air Velocity, ft/sec	Altitude, ft	Total Air Temp., °F	Dyn. Air Press. ρv^2, kdynes/cm^2	Fuel Flow, gm/sec	Fuel Temp. °F	Fuel Press., psi	Nozzle Gas Flow, gm/sec	Nozzle Gas Press., psi	Spray Droplet Mean Diam., Microns d_{30}	Spray Droplet Mean Diam., Microns d_{32}	Spray Width*, in. Stn 2	Spray Width*, in. Stn 4
Gas atomizer, flush coaxial	4.33	112	5,055	−1	13.6	19.1	19	30.8	9.99	15.4	12.1	19.8	—	—
	4.34	101	5,053	0	13.4	16.3	12	28.3	9.99	15.3	—	—	—	11.0
	4.35	109	5,045	−2	12.8	67.2	1	145.2	31.78	50.1	13.2	21.5	—	—
	4.36	113	5,057	−1	13.7	40.9	−2	108.0	31.78	48.8	14.8	21.8	—	—
	4.37	115	5,049	−1	14.3	47.7	−2	117.2	31.78	49.7	—	—	—	16.0
	4.38	111	5,051	−2	13.3	64.5	−2	76.9	9.53	15.8	14.7	21.7	—	—
Gas atomizer, multi-hole transverse	5.7	121	4,911	6	13.9	19.0	23	116	17.21	37.7	—	—	—	—
	5.8	121	4,908	0	15.8	19.3	23	116	17.16	37.7	—	—	—	12.8
	5.9	121	4,888	3	15.7	21.4	15	95	7.54	19.7	15.2	21.6	—	—
	5.10	119	4,903	0	15.3	21.4	11	95	7.35	19.7	—	—	—	11.7
	5.11	108	4,918	−3	15.4	21.3	11	95	7.35	19.5	—	—	2.7	—
	5.12	126	4,898	3	15.7	18.3	19	142	28.14	57.0	13.2	17.5	—	—
	5.13	127	4,894	−1	17.6	17.9	18	142	28.24	57.0	—	—	—	12.8
	5.14	128	4,884	7	17.4	53.6	−1	445	27.69	69.6	16.4	23.6	—	—
	5.15	124	4,878	−5	16.9	52.5	3	445	27.47	69.4	—	—	—	12.2
	5.16	128	4,867	−7	18.1	50.8	3	410	15.48	43.5	16.2	24.1	—	—
	5.17	122	4,877	−3	16.4	52.0	2	409	15.39	43.7	—	—	—	12.6
	5.18	124	4,880	2	16.6	50.3	0	384	6.86	23.2	14.9	23.6	—	—
	5.19	128	4,902	−19	18.6	48.0	−4	385	6.99	22.8	—	—	—	8.9
	5.20	123	4,904	2	16.2	50.1	−6	384	6.99	23.0	—	—	3.2	—

*Full width at half-maximum.

Table 3. Continued

Type Nozzle	Test Data Pt.	Air Velocity, ft/sec	Altitude, ft	Total Air Temp., °F	Dyn. Air Press. qv^2, kdynes/cm^2	Fuel Flow, gm/sec	Fuel Temp. °F	Fuel Press., psi	Nozzle Gas Flow, gm/sec	Nozzle Gas Press., psi	Spray Droplet Mean Diam., Microns d_{30}	Spray Droplet Mean Diam., Microns d_{32}	Spray Width*, in. Stn 2	Spray Width*, in. Stn 4
Gas atomizer, recessed coaxial	5.21	117	5,019	12	14.4	52.6	5	141	38.95	23.6	15.7	22.5	—	—
	5.22	116	5,032	1	14.5	52.3	5	139	39.73	23.9	—	—	—	12.0
	5.23	115	5,050	0	14.3	18.9	9	47	39.45	24.0	10.3	14.4	—	—
	5.24	118	5,016	−2	15.4	16.3	10	43	39.45	24.0	—	—	—	17.7
	5.25	112	5,060	−2	13.9	18.9	6	47	39.36	23.9	—	—	5.3	—
	5.26	102	5,039	2	11.1	23.9	5	47	26.88	16.2	—	—	—	—
	5.27	110	5,048	0	13.0	24.1	8	47	26.74	16.2	—	—	—	14.7
	5.28	109	5,060	5	12.7	24.1	8	47	26.74	16.2	—	—	—	—
	5.29	113	5,058	0	13.6	51.1	−2	133	26.79	16.4	—	—	—	11.0
	5.30	109	5,061	4	12.7	50.8	−6	133	26.60	16.2	—	—	5.6	—
Impinging jets at 180-deg orientation	5.31	379	5,091	4	156.0	21.3	0	39			10.2	15.2	—	—
	5.32	367	5,067	5	149.5	20.9	−9	39			—	—	—	—
	5.33	361	5,118	−5	144.3	21.1	−6	39			—	—	—	—
	5.34	387	5,097	−1	164.9	53.1	−3	165			11.9	17.8	—	—
	5.35	375	5,058	−2	155.0	53.6	−2	165			—	—	—	—
0.045-in. orifice, sharp edge at 180-deg orientation	5.36	400	5,111	8	172.7	19.8	−17	94			9.9	14.8	—	—
	5.37	392	5,072	1	168.3	19.9	−17	94			—	—	—	—
	5.38	386	5,122	−2	164.5	19.9	−16	94			—	—	—	—
	5.39	387	4,995	2	164.1	47.9	−15	442			11.3	16.9	—	—
	5.40	372	5,161	0	151.1	47.8	−13	442			—	—	—	—

*Full width at half-maximum.

Table 3. Concluded

Type Nozzle	Test Data Pt.	Air Velocity, ft/sec	Altitude, ft	Total Air Temp., °F	Dyn. Air Press. ρv^2, kdynes/cm^2	Fuel Flow, gm/sec	Fuel Temp. °F	Fuel Press., psi	Nozzle Gas Flow, gm/sec	Nozzle Gas Press., psi	Spray Droplet Mean Diam., Microns d_{30}	Spray Droplet Mean Diam., Microns d_{32}	Spray Width*, in. Stn 2	Spray Width*, in. Stn 4
Impinging jets at 90-deg orientation	5.41	392	5,105	3	167.9	20.3	−12	36			11.0	16.9	—	—
	5.42	384	5,125	−6	164.2	20.2	−14	35			11.1	17.1	—	—
	5.43	385	5,131	−2	163.7	53.2	−9	163			12.3	18.6	—	—
	5.44	205	5,091	−5	45.8	21.9	−6	38			15.0	22.5	—	—
	5.45	411	20,407	−5	102.9	20.9	−9	33			11.2	17.0	—	—
	5.46	284	20,237	−7	39.6	21.0	−11	32			12.9	19.2	—	—
	5.47	424	37,880	−7	50.0	22.0	−8	32			10.9	16.1	—	—
0.045-in. orifice, sharp edge at 90 deg orientation	5.48	396	5,092	2	154.7	48.3	−14	450			11.1	16.9	—	—
	5.49	394	5,153	0	170.6	20.0	−13	92			11.4	17.3	—	—
	5.50	206	5,121	−5	46.3	19.9	−10	91			13.2	19.9	—	—

*Full width at half-maximum.

Table 4. Nozzle Comparisons, d_{30} and d_{32}, Low Tunnel Velocity Conditions

Conditions	Type Nozzle	Data Point	Air Velocity, ft/sec	Altitude, K ft	Fuel Flow, gm/sec	Nozzle Gas Flow gm/sec	Spray Droplet Mean Diam., Microns d_{30}	d_{32}
Low Fuel Flow	0.045 Orifice	1.34	98	5.0	11.3	—	21.3	28.4
↓	0.045 Orifice	1.35	124	5.0	21.8	—	22.4	26.4
	0.025 Orifice	3.46	138	4.9	14.7	—	19.3	26.7
	Flush Coax	4.30	112	5.1	19.5	19.1	10.5	17.2
	Recessed Coax	5.23	115	5.1	18.9	39.5	10.3	14.4
High Fuel Flow	0.045 Sharp Edge	3.14	118	5.0	48.1		22.3	29.0
↓	Impinging Jets	3.20	117	5.1	45.9		23.9	30.5
	One-Hole Transv.	4.8	144	5.1	49.9	11.0	14.8	22.5
	Flush Coax	4.36	113	5.1	40.9	31.8	14.8	21.8
	Multi-Hole Transv.	5.18	124	4.9	50.3	6.9	14.9	23.6
	Recessed Coax	5.21	117	5.0	52.6	39.0	15.7	22.5

Table 5. Nozzle Comparisons, d_{30} and d_{32}, High Tunnel Velocity Conditions

Conditions	Type Nozzle	Data Point	Air Velocity, ft/sec	Altitude, ft.	Fuel Flow, gm/sec	Nozzle Gas Flow gm/sec	Spray Droplet Mean Diam., Microns d_{30}	d_{32}
Lowest Fuel Flow	0.045 Orifice	2.8	415	5.0	10.0	—	10.1	15.5
	0.025 Orifice	3.40	409	5.1	14.7	—	11.0	17.1
	0.025 Orifice	3.43	400	5.1	7.9	—	10.1	15.8
Low Fuel Flow	0.045 Orifice	2.11	393	5.0	21.8	—	11.5	17.6
	0.045 Sharp Edge	3.8	402	5.0	19.7	—	11.2	17.4
	Impinging Jets	3.24	397	5.1	18.7	—	10.7	16.9
Med. Fuel Flow	0.045 Orifice	2.13	397	5.1	31.8	—	12.2	18.6
	0.089 Orifice	2.27	399	5.0	30.4	—	10.9	17.1
	Impinging Jets	3.26	407	5.1	36.2	—	11.2	17.6
High Fuel Flow	0.045 Orifice	2.15	402	5.1	49.9	—	11.1	16.6
	0.045 Sharp Edge	3.12	392	5.0	48.1	—	12.2	17.6
	Impinging Jets	3.28	395	5.1	40.6	—	11.4	18.0
	One-Hole Transv.	4.25	371	5.2	47.2	11.8	11.0	17.4

Table 6. Tunnel Airstream Velocity Relative to Fuel Injection Velocity for Selected Hydraulic Nozzle Data Points

Nozzle Orifice Diameter, in.	Data Point	Flow Flow, gm/sec	Air Velocity V, ft/sec	Fuel Injection Velocity, V_λ, ft/sec	$V_r = (V - V_\lambda)$, ft/sec
0.025	1.17	8.63	103	116	−13
↓	3.40	14.7	409	190	219
	3.43	7.9	400	100	300
0.025	3.46	14.7	138	190	−52
0.045	1.20	11.3	281	45	236
↓	1.34	11.3	98	45	53
	1.35	21.8	124	85	39
	2.8	10.0	415	41	374
	2.11	21.8	393	85	308
	2.13	31.8	397	137	260
0.045	2.15	49.9	402	215	187
Sharp Edge	3.12	48.1	392	210	182
↓	3.14	48.1	118	210	−92
	3.15	19.4	398	76	322
0.089	2.27	30.4	399	32	367

$\varrho_\lambda = 0.810$ gm/cm^3

Table 7. Flare Orientation Effects on Spray Droplet Mean Diameters d_{30} and d_{32}

Type Nozzle, Condition	Orientation, deg	Data Point	Air Velocity, ft/sec	Altitude, K ft	Fuel Flow, gm/sec	Spray Droplet Mean Diameter, microns	
						d_{30}	d_{32}
Impinging Jets,	0	3.24	397	5.1	18.7	10.7	16.9
Low Fuel Flow	90	5.41	392	5.1	20.3	11.0	16.9
	180	5.31	379	5.1	21.3	10.2	15.2
Impinging Jets,	0	3.28	395	5.1	40.6	11.4	18.0
High Fuel Flow	90	5.43	385	5.1	53.2	12.3	18.6
	180	5.34	387	5.1	53.1	11.9	17.8
0.045 Sharp Edge	0	3.8	402	5.0	19.7	11.2	17.4
Low Fuel Flow	90	5.49	394	5.2	20.0	11.4	17.3
	180	5.36	400	5.1	19.8	9.9	14.8
0.045 Sharp Edge	0	3.12	392	5.0	48.1	12.2	17.6
High Fuel Flow	90	5.48	396	5.1	48.3	11.1	16.9
	180	5.39	387	5.0	47.9	11.3	16.9

APPENDIX A
PULSED LASER PHOTOGRAPHY

Figs. A-1—A-4. Example nozzle sprays under low tunnel velocity conditions. Cross-references: Fig. 19; Table 4.

Fig. A-5. Example spray from 0.045-in.-orifice hydraulic nozzle under high tunnel velocity conditions. Cross-references: Fig. 20; Table 5.

Figs. A-6 and A-7. Spray from single-hole transverse pneumatic nozzle under low tunnel velocity conditions; inadequate versus adequate nozzle gas flow. Cross-references: Figs. 21a and 22.

Figs. A-8—A-10. Spray from multihole transverse pneumatic nozzle, under low tunnel velocity conditions, increasing nozzle gas flow. Cross-references: Figs. 21a, 23, 24, 25, and 26.

Figs. A-11—A-14. Example sprays from 0.025-in.-orifice hydraulic nozzle, increasing dynamic pressure ρv^2. Cross-references: Figs. 28 and 29.

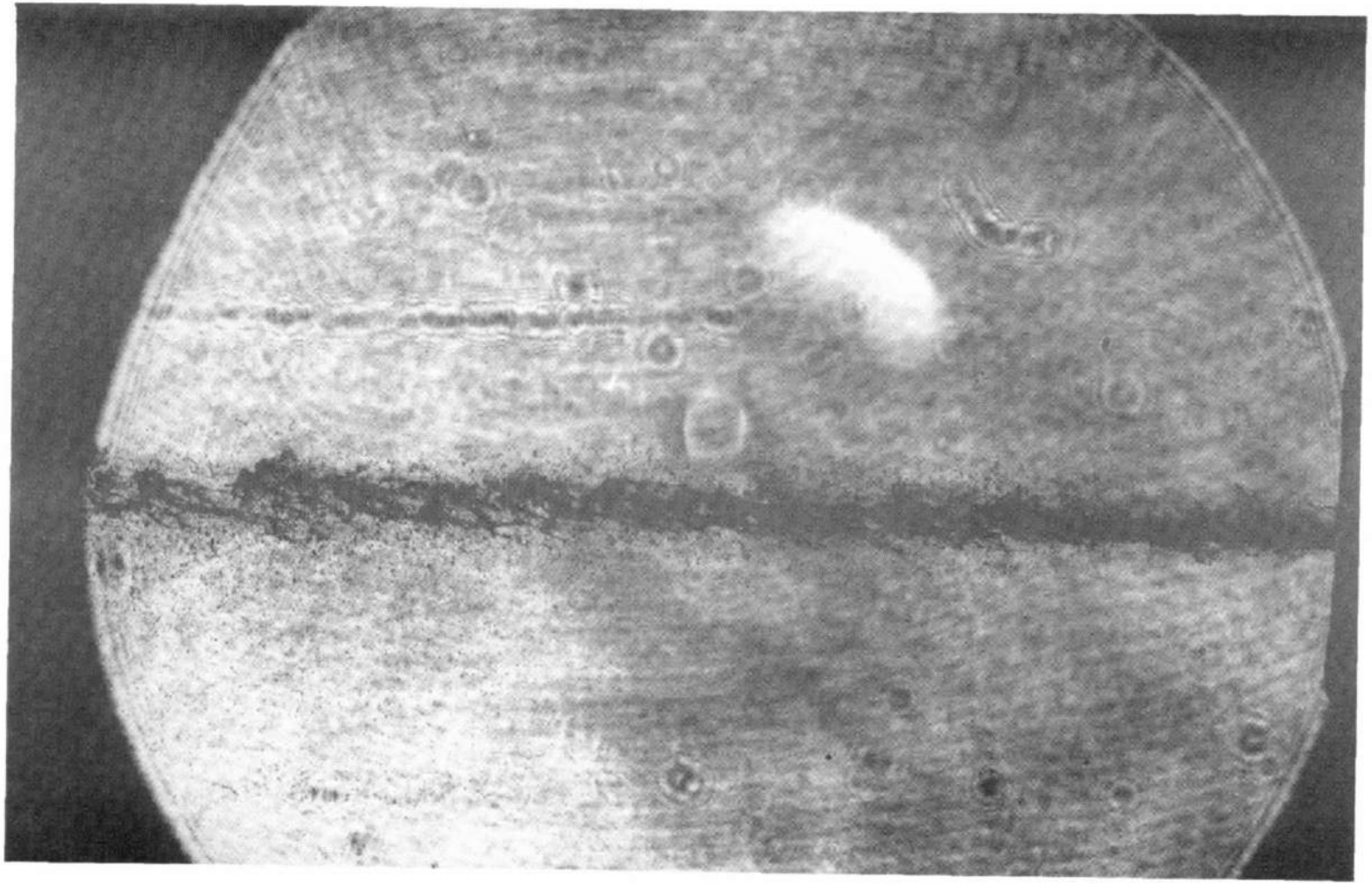

Figure A-1. D.P. 3.46, 0.025 in. orifice; $\rho v^2 = 20.4$ kdynes/cm^2.

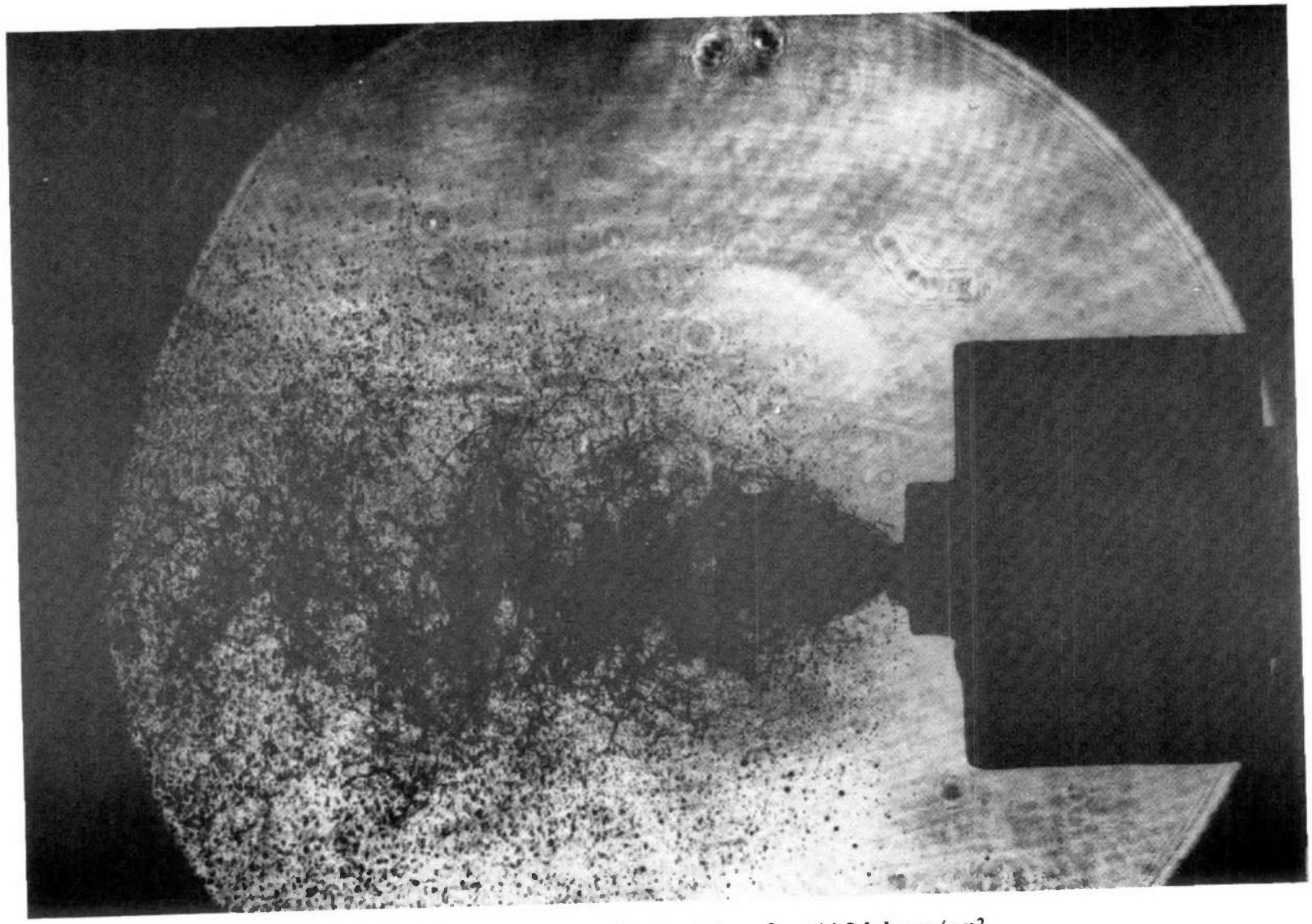

Figure A-2. D.P. 3.20, impinging jets; $\varrho v^2 = 14.2$ kdynes/cm^2.

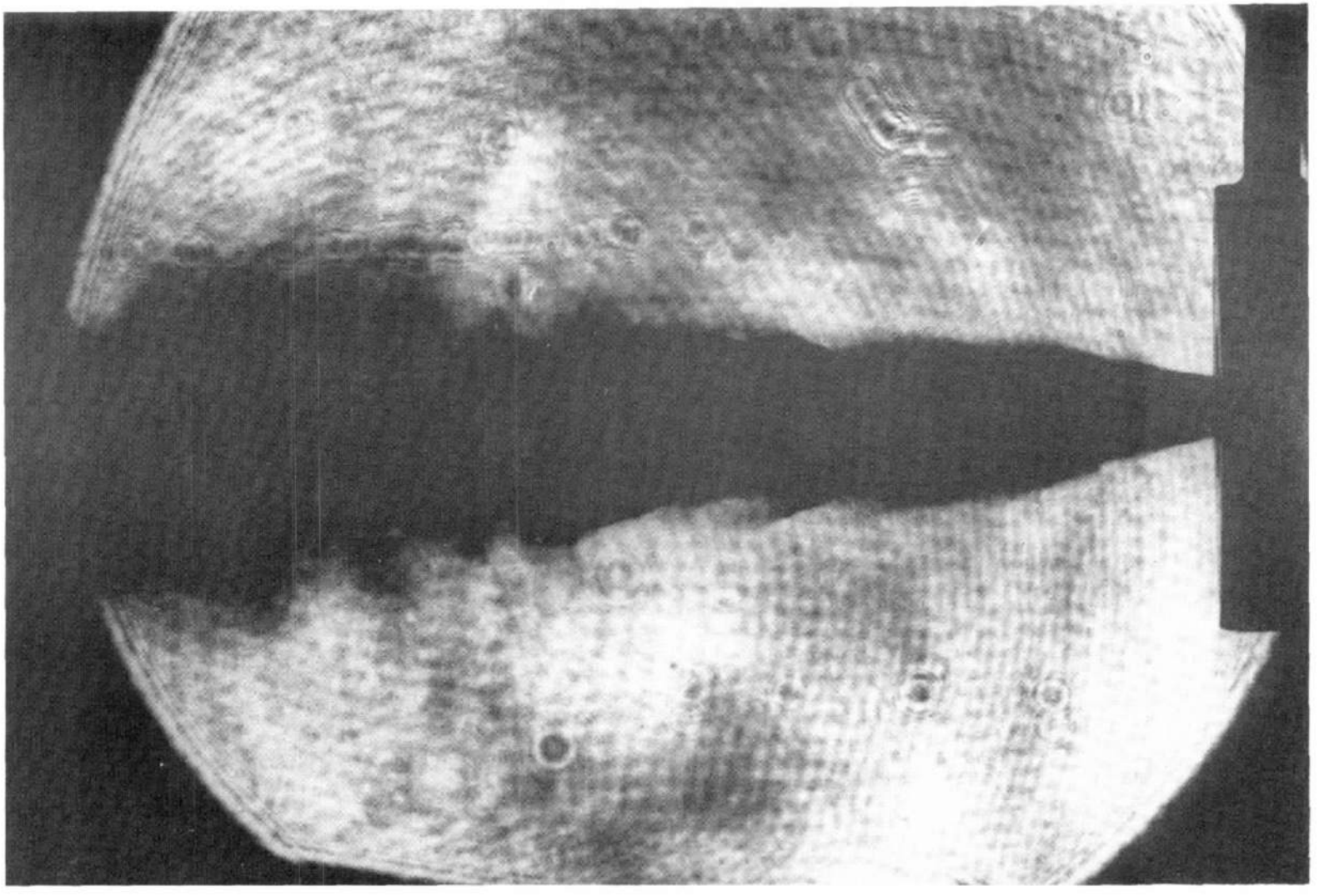

Figure A-3. D.P. 5.21, recessed coax gas atomizer; ρv^2 = 14.4 kdynes/cm^2.

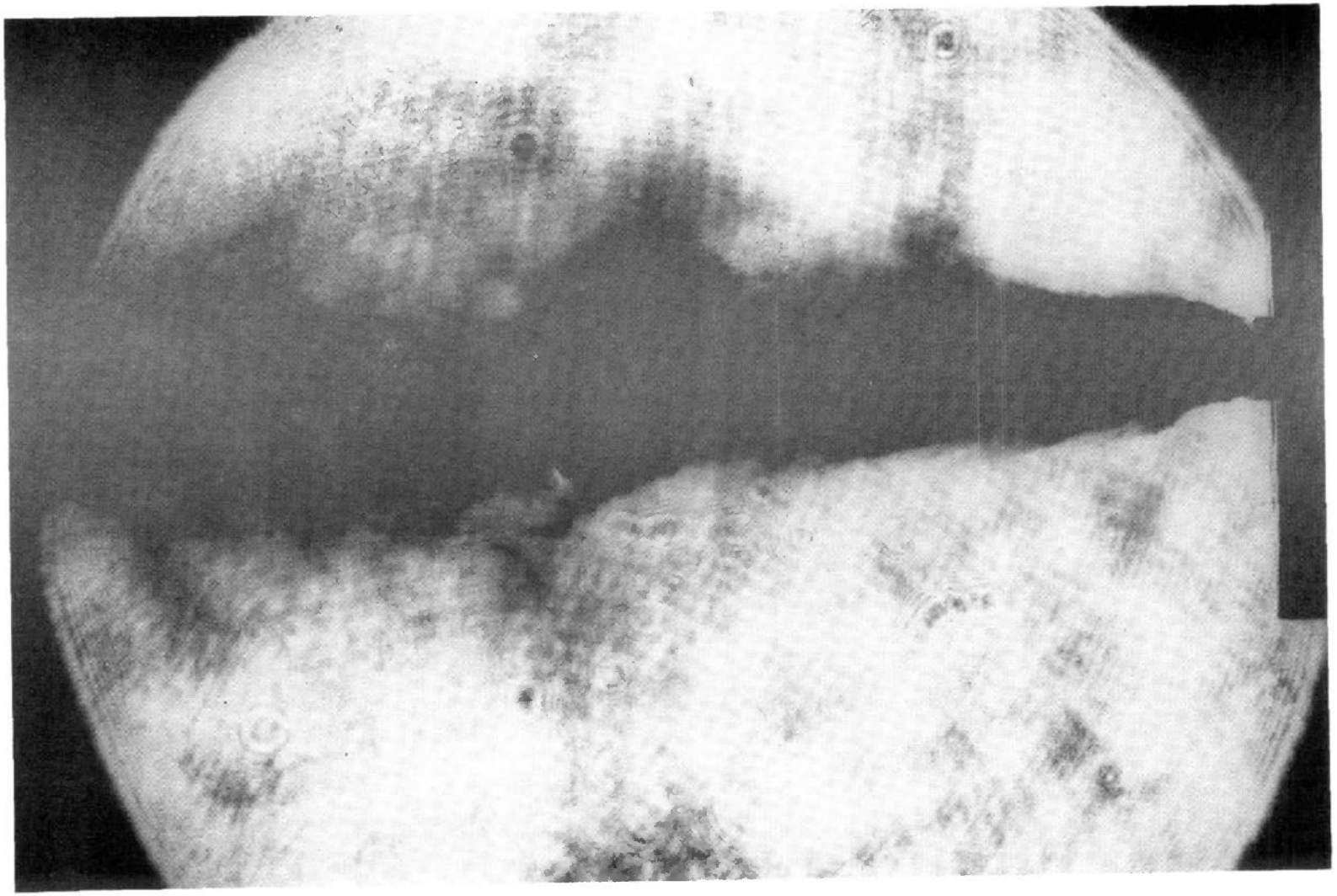

Figure A-4. D.P. 4.36, flush coax gas atomizer; ρv^2 = 13.7 kdynes/cm^2.

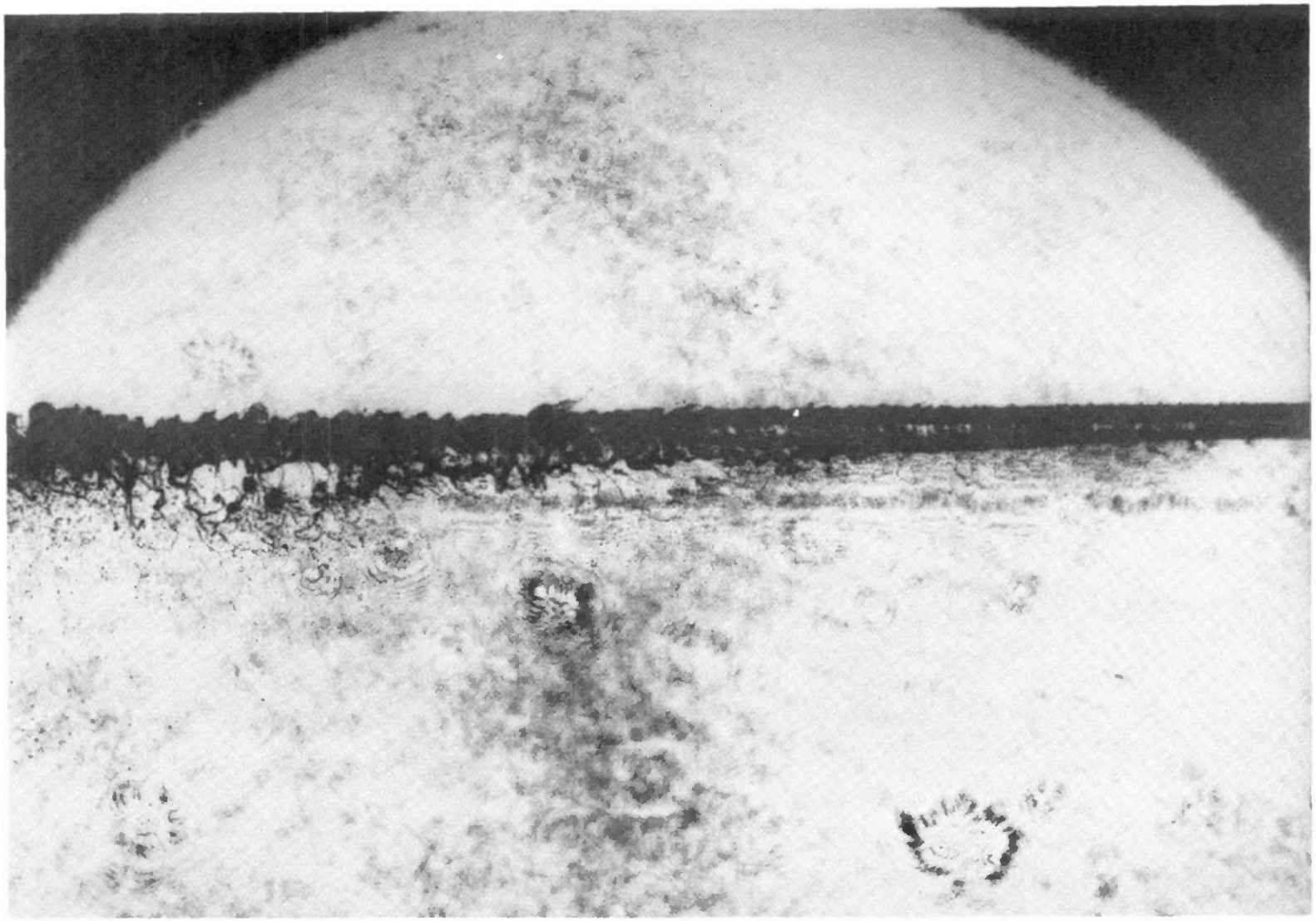

Figure A-5. D.P. 2.15, 0.045-in. orifice; ρv^2 = 180 kdynes/cm^2.

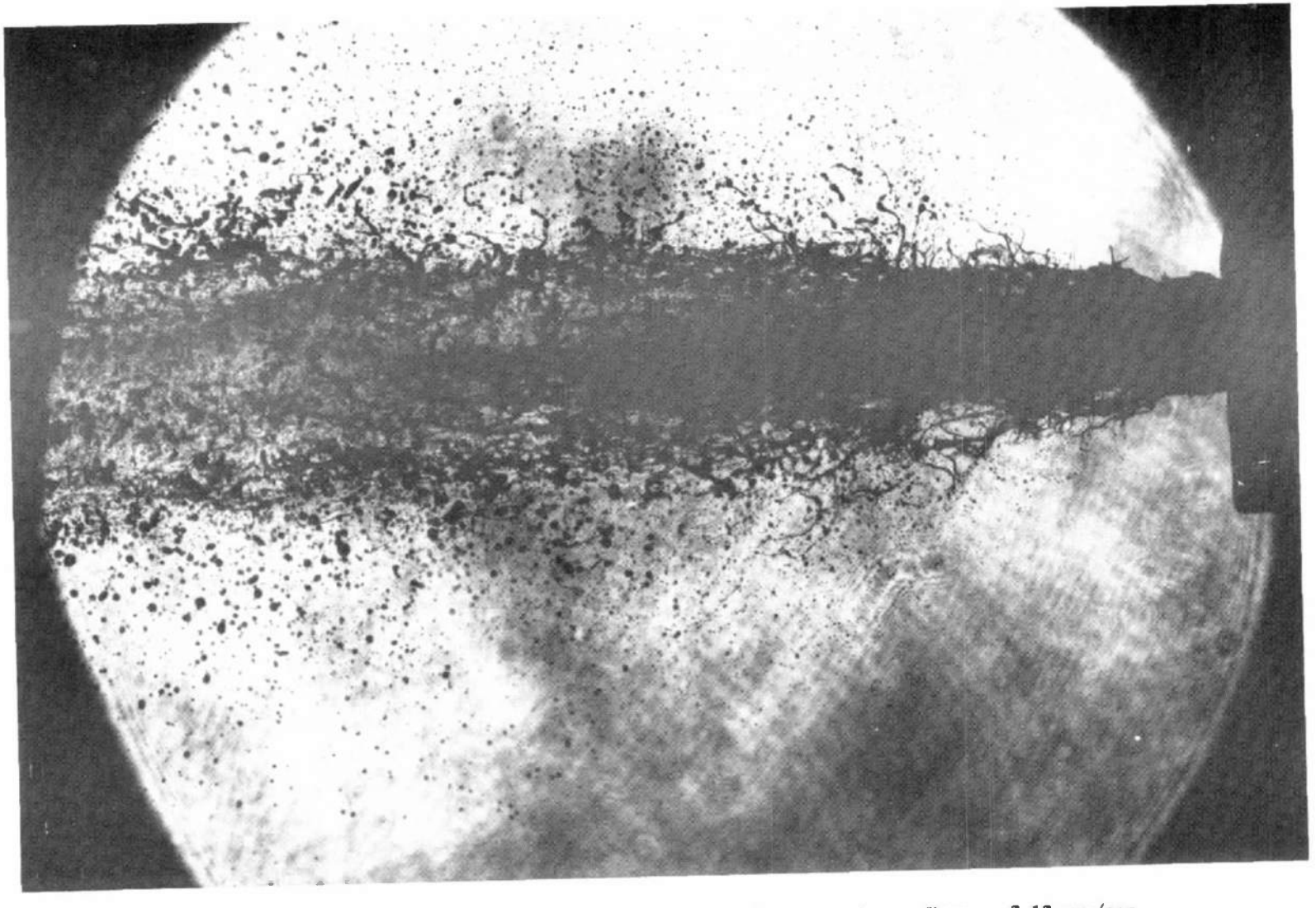

Figure A-6 D.P. 4.16, single-hole transverse gas atomizer; nozzle gas flow = 3.13 gm/sec.

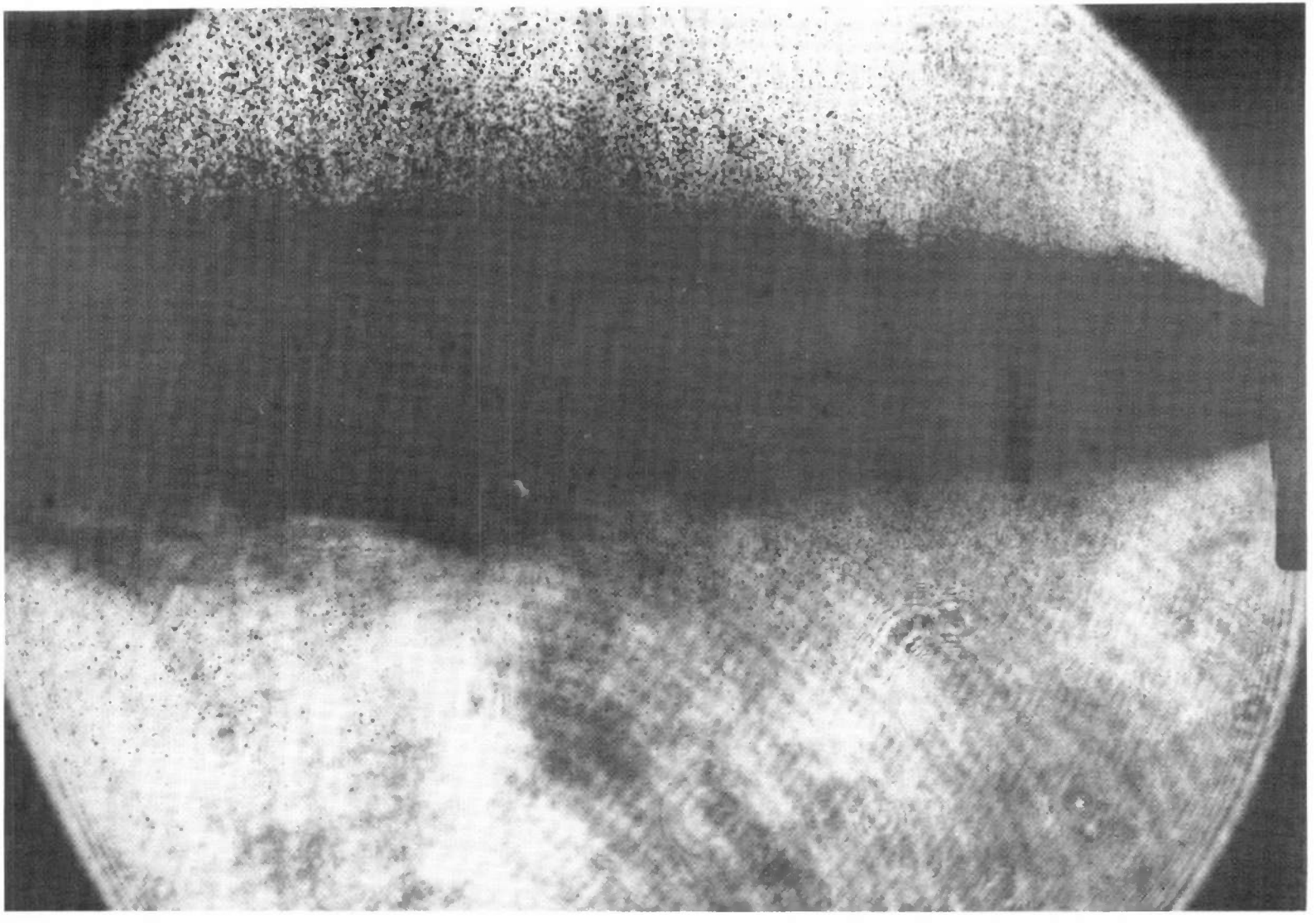

Figure A-7. D.P. 4.8, single-hole transverse gas atomizer; nozzle gas flow = 11.0 gm/sec.

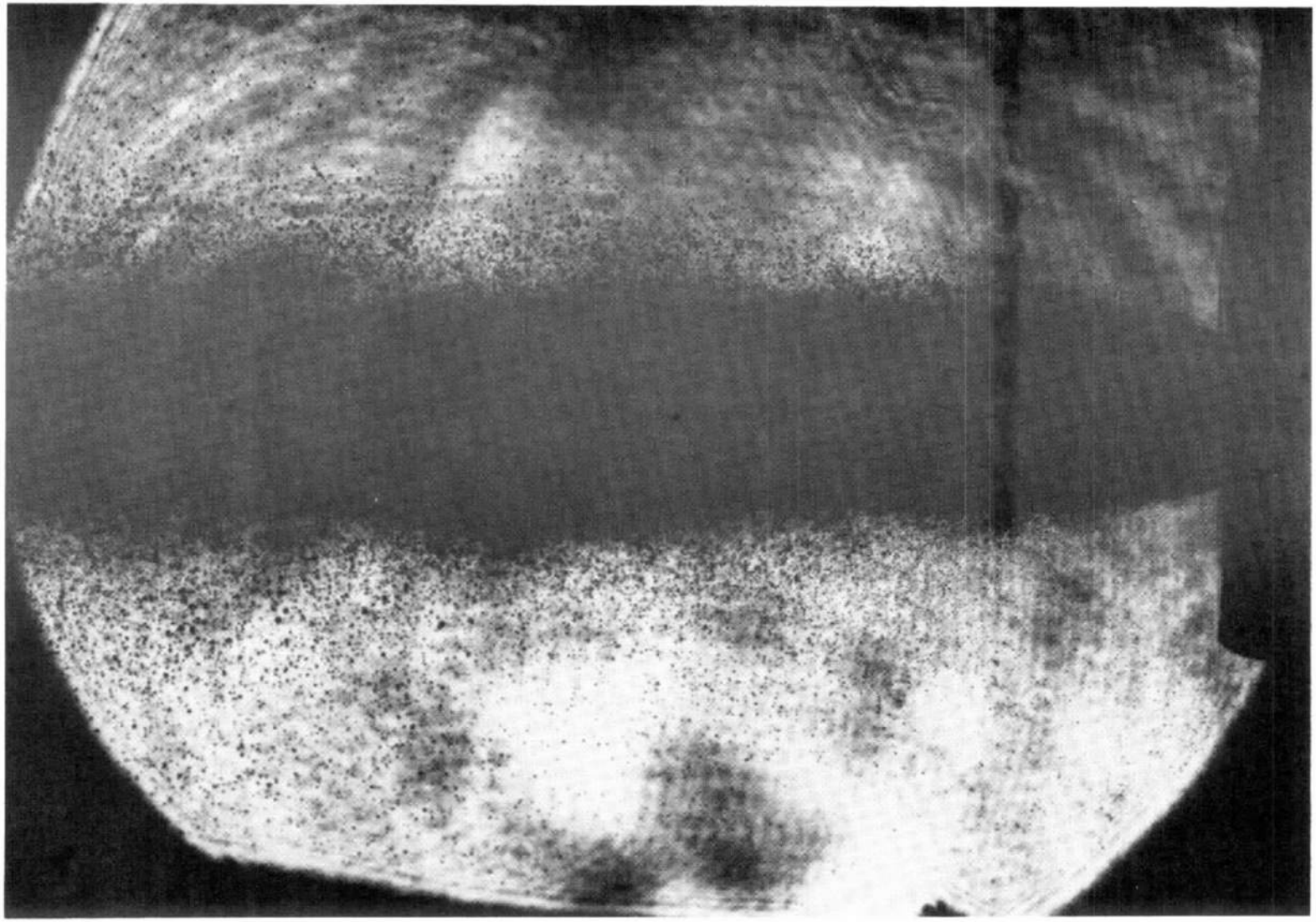

Figure A-8. D.P. 5.18, multihole transverse gas atomizer; nozzle gas flow = 6.86 gm/sec.

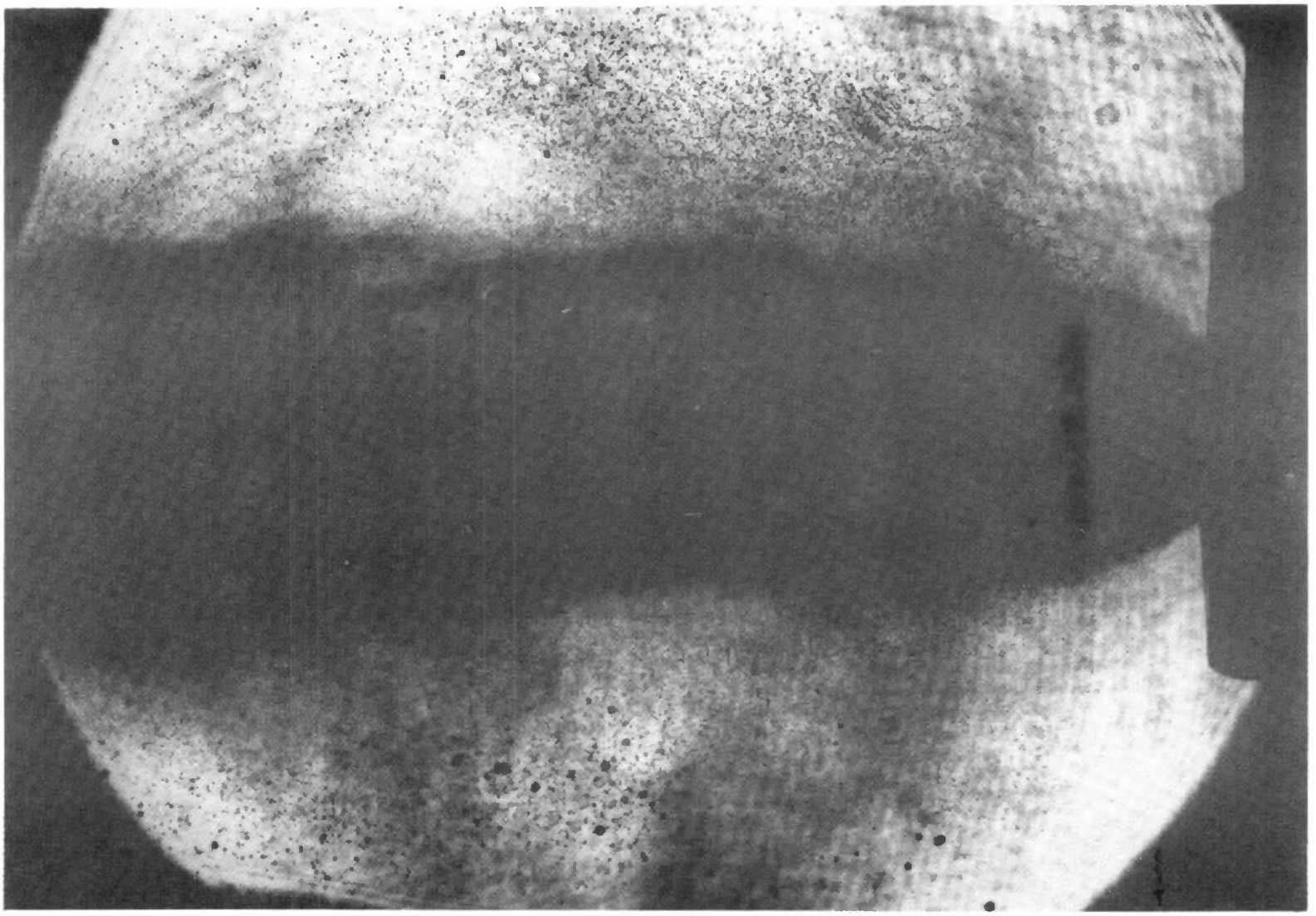

Figure A-9. D.P. 5.16, multihole transverse gas atomizer; nozzle gas flow = 15.5 gm/sec.

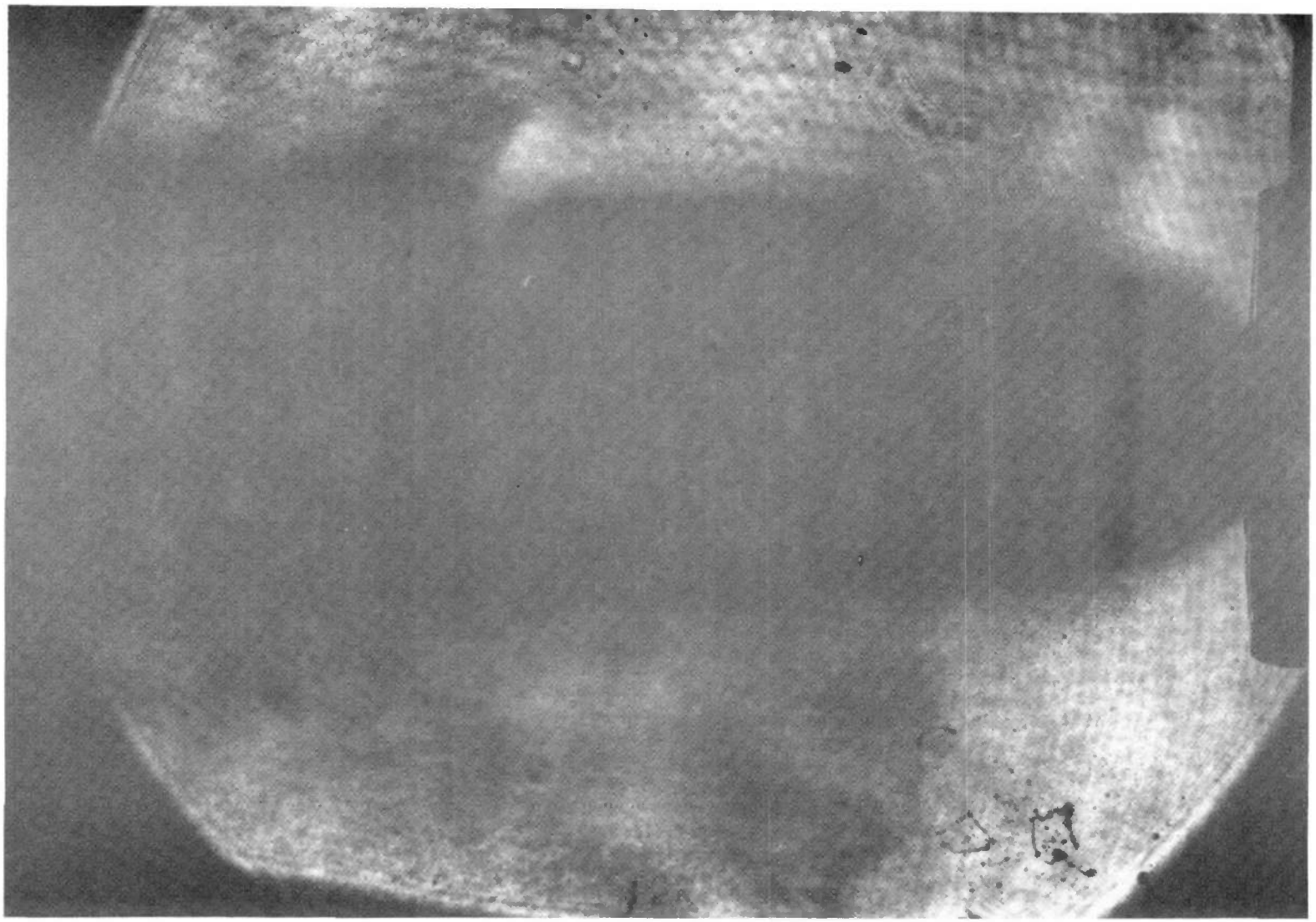

Figure A-10. D.P. 5.14, multihole transverse gas atomizer; nozzle gas flow = 27.7 gm/sec.

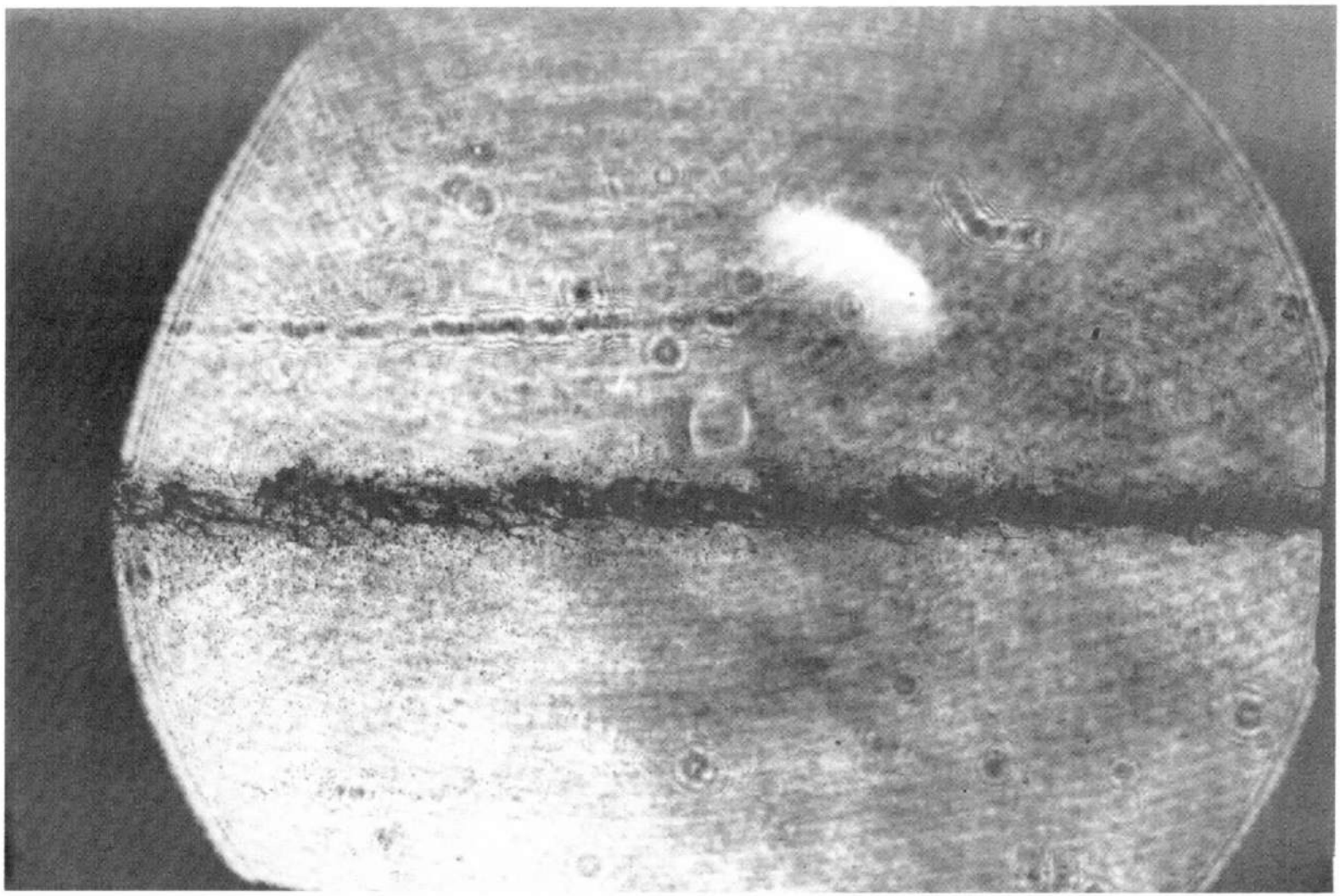

Figure A-11. D.P. 3.46, 0.025-in. orifice; air velocity = 138 ft/sec, altitude = 4.9K ft, ρv^2 20.4 kdynes/cm^2.

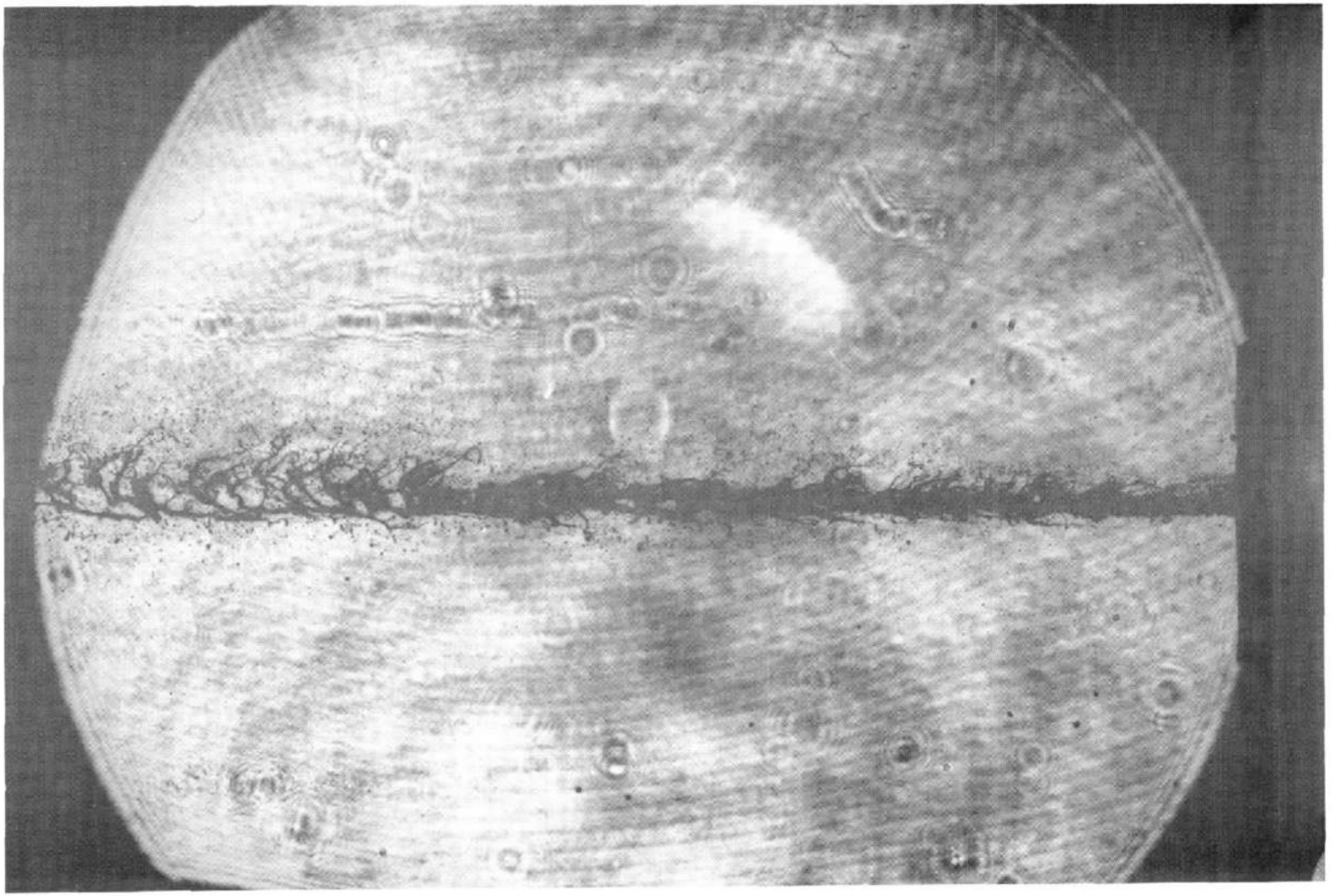

Figure A-12. D.P. 3.35, 0.025-in. orifice. Air velocity = 385 ft/sec, altitude = 35.1 Kft, ϱv^2 = 46.0 kdynes/cm^2.

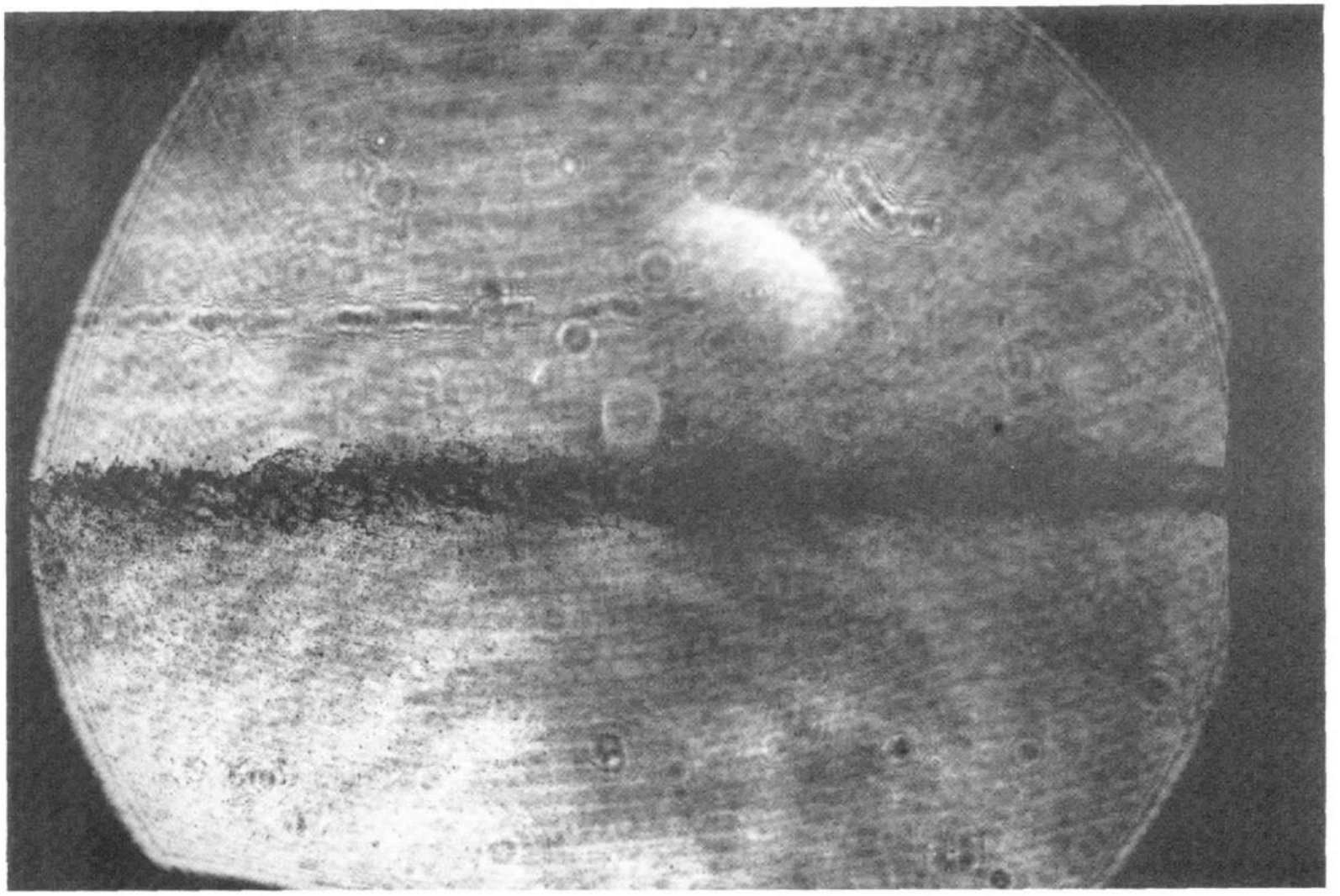

Figure A-13. D.P. 3.38, 0.025-in. orifice. Air velocity = 405 ft/sec, altitude = 20.2 Kft, ρv^2 = 99.3 kdynes/cm^2.

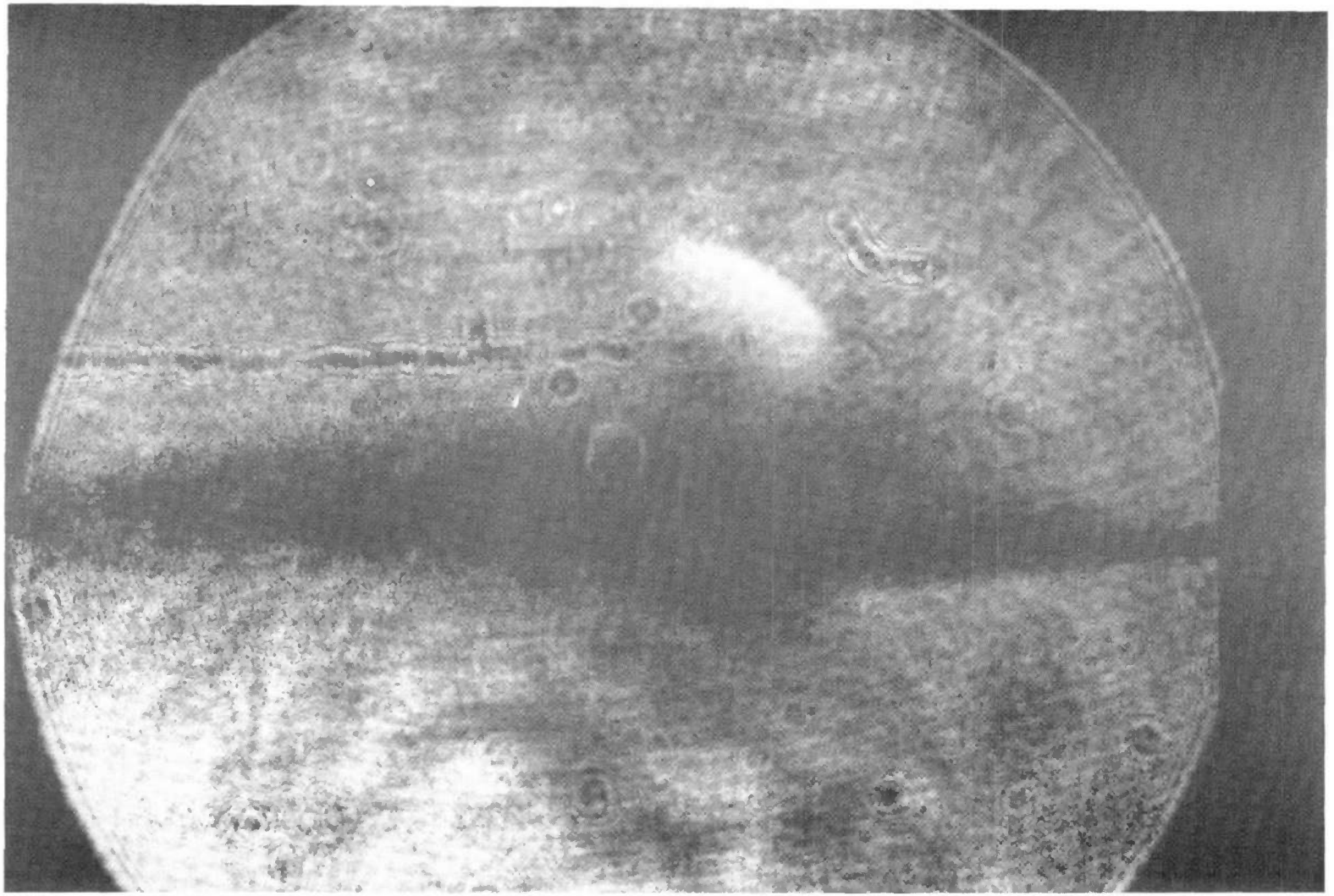

Figure A-14. D.P. 3.40, 0.025-in. orifice. Air velocity = 409 ft/sec, altitude = 5.1 Kft, ρv^2 = 180 kdynes/cm^2.